

A tunable orthosis for the suppression of involuntary tremor

Jeroen Geentjens

Thesis voorgedragen tot het behalen
van de graad van Master of Science
in de ingenieurswetenschappen:
werktuigkunde

Promotor:

Prof. dr. ir. Farid Al-Bender

Assessor:

Prof. dr. ir. Dominiek Reynaerts

Dr. Ir Claus Claeys

Begeleider:

Ir. Sven Vandenberghe

© Copyright KU Leuven

Without written permission of the thesis supervisor and the author it is forbidden to reproduce or adapt in any form or by any means any part of this publication. Requests for obtaining the right to reproduce or utilize parts of this publication should be addressed to Faculteit Ingenieurswetenschappen, Kasteelpark Arenberg 1 bus 2200, B-3001 Heverlee, +32-16-321350.

A written permission of the thesis supervisor is also required to use the methods, products, schematics and programs described in this work for industrial or commercial use, and for submitting this publication in scientific contests.

Zonder voorafgaande schriftelijke toestemming van zowel de promotor als de auteur is overnemen, kopiëren, gebruiken of realiseren van deze uitgave of gedeelten ervan verboden. Voor aanvragen tot of informatie i.v.m. het overnemen en/of gebruik en/of realisatie van gedeelten uit deze publicatie, wend u tot Faculteit Ingenieurswetenschappen, Kasteelpark Arenberg 1 bus 2200, B-3001 Heverlee, +32-16-321350.

Voorafgaande schriftelijke toestemming van de promotor is eveneens vereist voor het aanwenden van de in deze masterproef beschreven (originele) methoden, producten, schakelingen en programma's voor industrieel of commercieel nut en voor de inzending van deze publicatie ter deelname aan wetenschappelijke prijzen of wedstrijden.

Preface

I would like to thank my promotor, Prof. Dr. Ir Farid Al-Bender, for his advice and for giving me the opportunity to work on this master thesis. Next I would like to thank my mentor, Ir. Sven Vandenberghe, for his help throughout the whole master thesis. Without his knowledge of all the different thesis topics this thesis would not have been as qualitative. I would also like to thank Eddy and Gunther for making all the parts for the test set-up and the prototype. I would like to thank Raymond Wuyts who executed the tests to qualify the final prototype. At last I would like to thank all the people close to me for their support.

Jeroen Geentjens

Contents

Preface	i
Contents	ii
Abstract	iv
Samenvatting	v
List of Figures and Tables	vii
1 Introduction	1
1.1 Goal	1
1.2 Methodology	1
1.3 Result	2
2 Literature study	3
2.1 Tremor	3
2.2 Treatment of tremor	4
2.3 Wearable orthosis	7
3 Value analysis	19
3.1 Determination of the system type	19
3.2 Determination of the concept	23
4 Concept testing	31
4.1 Design of experiments	31
4.2 Test set-up	31
4.3 Results	35
5 Mathematical model	43
5.1 Transmission	43
5.2 System model	50
6 Final prototype	63
6.1 Design	63
6.2 Results	68
6.3 Improvements	71
7 Conclusion	73
Bibliography	75
Appendices	79

A	Design of experiments	81
A.1	Framework to determine the friction force	81
A.2	Framework to determine the relationship between the damping force and the height of the gap	82
B	Calibration of the sensors	83
B.1	Calibration of the force sensor	83
B.2	Calibration of the distance sensor	83
C	Simulink program to control the test set-up	86
D	Testresults at 60, 80 and 100 micron	89
D.1	Damping force at 60 micrometer	89
D.2	Damping force at 80 micrometer	89
D.3	Damping force at 100 micrometer	91
E	Technical drawings of the final damper components.	95
E.1	Technical drawings of the oil bath.	95
E.2	Technical drawing of the cover.	98
E.3	Technical drawing of the adjusting plate.	99
E.4	Technical drawing of the separation plate.	100
F	Testresults of the prototype	102
F.1	Test without the orthosis	102
F.2	Test with the orthosis at high damping tightened with the velcro strip	103
F.3	Test with the orthosis at a tuned damping without the velcro strip	104

Abstract

This thesis describes the design and the development of a tunable orthosis for the suppression of involuntary tremor. The topic has already been researched in a previous master project. Tremor is a rhythmic, uncontrollable oscillation of a body part due to involuntary contractions of the muscles. Tremor disturbs the patient's activities of daily living and decreases the quality of life. The tremor which needs to be reduced in this thesis is the tremor of the hand relative to the forearm. This phenomena occurs most of the time at elderly individuals who suffer from disorders like Parkinson's disease, brain trauma or essential tremor. The main problem is the fact that tremor occurs at different frequencies. This means the system needs to adjust itself to suppress tremor in a broad frequency range. But at the same time, the system may not suppress voluntary movements. The thesis first illustrates the most important developments of this research topic in chapter 2. These important tremor suppression methods are medication, operations and wearable orthoses. The thesis focuses on the last method, wearable orthoses. Within these wearable orthoses a distinction between three important system types can be made: a passive system, a semi-active system and an active system. A passive system only uses the energy of the tremor to suppress it. A semi-active system measures the tremor and uses this values to change the specifications of the suppression of the tremor. The tremor is still suppressed using its own energy. An active system suppresses the tremor by means of an actuator which consumes energy. A value analysis in chapter 3 determines the best system type and concept for further research. A passive system was favored by the value analysis. The final passive system concept is a flat plate damper which can change the height of the gap between the damping plates. The height can be regulated by using a screw. In chapter 4 the concept is tested on a test set-up to determine the quality of the concept. The test set-up measures the damping force in function of the height and compares this measured force to the theoretical force. These results show that the measured forces are very close to the expected theoretical values. The test set-up indicates that the concept works so the concept can be adjusted to fit an orthosis. Chapter 5 uses mathematical calculations and approximations to design the dimensions and the characteristics of the final prototype. Chapter 6 describes the final prototype that has been built from the design. The prototype has been criticized and conclusions have been made in the laster chapter.

Samenvatting

Deze thesis omschrijft het ontwerpen en het ontwikkelen van een regelbare orthese die ongewilde tremor onderdrukt. Het onderwerp werd reeds onderzocht in een master project. Tremor is een ritmische, oncontroleerbare oscillatie van een ledemaat veroorzaakt door ongewilde contracties van de spieren. Tremor hindert de dagelijkse activiteiten van de patiënt. Door tremor daalt de kwaliteit van de levensomstandigheden van de patiënt. Deze thesis zal zich voornamelijk focussen op de tremor die ontstaat in de pols. Dit komt overeen met een oscillatie van de hand ten opzichte van de onderarm. Dit fenomeen treedt meestal op bij oudere personen die lijden aan de ziekte van Parkinson, een trauma in de hersenen hebben opgelopen of essentiële tremor hebben. Het feit dat de tremor voorkomt op verschillende frequenties maakt het onderdrukken ervan moeilijker. Hierdoor moet het systeem regelbaar zijn om de onderdrukte frequentie te kunnen aanpassen. Bovendien mag het systeem de bewegingen die de persoon wel degelijk wenst te maken niet onderdrukken. In de literatuurstudie, beschreven in hoofdstuk 2, worden de huidige methoden besproken om tremor te onderdrukken. In dit hoofdstuk worden voornamelijk medicatie, operaties en orthesen besproken. Deze thesis zal zich meer focussen op deze laatste methode, orthesen. Binnen de orthesen wordt een onderscheid gemaakt tussen 3 systemen: een passief systeem, een semi-actief systeem en een actief systeem. Een passief systeem gebruikt enkel de energie van de tremor om deze te onderdrukken. Een semi-actief systeem zal eerst de tremor opmeten om vervolgens de karakteristieken van het onderdrukkingsmechanisme aan te passen. Dit mechanisme gebruikt, net zoals het passieve systeem, enkel de energie van de tremor om deze te onderdrukken. Een actief systeem zal daarentegen een actuator gebruiken om de tremor te onderdrukken. Deze actuator verbruikt externe energie en wordt gecontroleerd door metingen van de tremor. In hoofdstuk 3 wordt een waardenanalyse uitgevoerd om het juiste systeem te selecteren. Het passief systeem krijgt hierbij de voorkeur. Dit passief systeem bestaat uit een vlakke demper waarbij de hoogte tussen de demperplaten gewijzigd kan worden. Om deze hoogte te regelen, wordt gebruik gemaakt van een schroef. Hoofdstuk 4 beschrijft een testopstelling die gebruikt wordt om het finale concept te testen. Deze opstelling meet de dempingskracht in functie van de hoogte. Deze gemeten kracht wordt vergeleken met de theoretisch bepaalde kracht om zo na te gaan of het concept in werkelijkheid werkt. De gemeten waarden leunen zeer dicht aan bij de theoretische waarden en volgen dezelfde trends. Deze resultaten tonen aan dat het concept lijkt te werken en praktisch uitvoerbaar is. Vervolgens wordt in hoofdstuk 5 de finale demper volledig gedimensioneerd, gebruik makend van wiskundige benaderingen. Eerst wordt de slag van de transmissie in de demper bepaald in functie van de rotatie van de hand. Door een beredeneerde selectie van de ontwerpparameters wordt deze slag geoptimaliseerd voor de toepassing. Vervolgens wordt met een systeemmodel

de juiste stijfheid van de transmissie berekend en de ideale dempingsconstante bepaald. Met behulp van een linearisatie wordt het systeemmodel geconverteerd naar een benaderend massa-veer-demper systeem. De stijfheid en de dempingsconstante worden geselecteerd met behulp van een bodeplot van dit benaderend systeem. Uit deze bepalingen kunnen de verdere ontwerpparameters geselecteerd worden. Hoofdstuk 6 bespreekt het volledige prototype. Ten eerste wordt het finale ontwerp besproken. Hierbij wordt een duidelijke link gelegd tussen de wiskundige benaderingen en het finale ontwerp. Ten tweede worden enkele resultaten aangehaald. Het prototype heeft wel degelijk een regelbare dempende werking. Testen op een patiënt die lijdt aan de ziekte van Parkinson tonen een opmerkelijke reductie van tremor aan. De onderdrukking was het grootst bij het schrijven van zinnen. Ten derde worden enkele mogelijke verbetering toegelicht. In het laatste hoofdstuk worden de finale conclusies besproken. Uit dit werk wordt geconcludeerd dat het onderdrukken van tremor, op basis van een demper met een hoogteregeling, mogelijk is. Het prototype geeft reeds deftige resultaten. De flexibiliteit van de handschoen waarmee de demper aan de pols bevestigd is en van de huid zijn de grootste hindernissen bij het kwalitatief onderdrukken van tremor.

List of Figures and Tables

List of Figures

1.1	The top view (left) and side view (right) of the final prototype.	2
2.1	Two examples of medication used by a patient with Parkinson’s disease [5], [6].	5
2.2	The position of the thalamus within the brain [16].	5
2.3	The position of the electrode within the brain [2].	6
2.4	Different examples of wearable orthoses [23],[26],[24].	7
2.5	Summary of all the feasible concepts found in papers for the different functions of a wearable orthosis.	8
2.6	An example of needle EMG [11] and surface EMG [19] , [3].	9
2.7	The positions to attach the gyroscopes to measure relative motion of the hand [18].	9
2.8	The difference in power spectral density between tremulous motion and voluntary motion [18].	10
2.9	A block diagram of the two stage algorithm with corresponding signals [18]. . .	11
2.10	A block diagram of the two stage algorithm with the most optimal filter techniques [18].	11
2.11	A block diagram of the adaptive band pass filter [31].	12
2.12	The effect of the damping coefficient on the rotation of the hand.	13
2.13	The behaviour of a mrf when a magnetic field is applied. [15].	13
2.14	The principle of the double viscous beam suppression system [23].	14
2.15	The effect of an electrostatic field on the ERF. [34].	14
2.16	The components necessary for the suppression of tremor using FES. [24]. . . .	15
2.17	The Kotovsky and Rosen concept for passive suppression of tremor. [20]. . . .	16
2.18	The active system using actuators to counteract the tremor. [27].	17
2.19	The result of the active system using a rotary DC motor. [27].	17
3.1	Concept 1: The passive system of Kotovsky and Rosen.	24
3.2	Concept 2: A simple screw attached to the transmission.	25
3.3	Concept 3: A screw pushing down the upper plate of the damper.	26
3.4	Concept 4: A screw guiding the upper plate of the damper.	27
3.5	Concept 5: A screw pushing down the elastic upper plate of the damper.	28
4.1	The test set-up to determine the damping characteristics.	32
4.2	Graphical representation of the functionality of the distance sensor.	33

LIST OF FIGURES AND TABLES

4.3	Close up of the damper in the test set-up.	34
4.4	The upper plate of the test set-up with the 3 teflon bars.	34
4.5	Friction force at different preloads with a sinusoidal velocity.	35
4.6	Friction force in a filled bath at a certain velocity	36
4.7	Changing friction force with changing velocity	37
4.8	Velocity and damping force with a gap of 40 micron.	38
4.9	The measured force in function of the velocity at 40 micron.	39
4.10	Changing damping force with changing height.	41
5.1	All parameters of the transmission from the hand to the forearm.	44
5.2	The curvature of the transmission.	45
5.3	A graphical representation of flexion and extension of the hand.	46
5.4	The maximum flexion and extension stroke (left) and the total translation (right) in function of parameter L	47
5.5	The maximum flexion and extension stroke (left) and the total translation (right) in function of parameter x_p	48
5.6	The stroke in function of theta with all the determined parameters.	49
5.7	The behavior of the transmission at different theta.	50
5.8	A graphical summary of all the forces in the system.	51
5.9	The effect of I_{eq} on the transfer function.	55
5.10	The effect of k_{eq} on the transfer function.	56
5.11	The effect of c_{eq} on the transfer function.	56
5.12	The determination of k_{eq} and c_{eq} with the chosen boundaries.	57
5.13	The determination of k_{eq} and c_{eq} with the chosen boundaries.	59
5.14	The determination of the tremor reduction at all tremor frequencies.	60
5.15	The influence on the final system of an external mass.	61
6.1	The final design of the damper without the cover.	63
6.2	The final design of the damper with the cover.	64
6.3	The link between the oil bath design and the determined parameters.	64
6.4	The real aluminum damper components.	66
6.5	The final design of the transmission.	66
6.6	The Bota Ortho 501 wrist brace to attach the damper [11].	67
6.7	Topview and sideview of the final prototype.	67
6.8	The test without the orthosis (left) and with the orthosis (right).	68
6.9	The measured movement of the mass without the orthosis.	69
6.10	The measured movement of the mass with the orthosis.	69
6.11	Writing the name and adress without the orthosis (left), with the tightened orthosis (middle) and with the non-tightened orthosis with reduced damping (left).	70
6.12	Drawing figures without the orhosis (left) and with the orthosis (right).	70
D.1	Velocity and damping force with a gap of 80 micron.	90
D.2	The measured force in function of the velocity at 80 micron.	90
D.3	Velocity and damping force with a gap of 100 micron.	92
D.4	The measured force in function of the velocity at 100 micron.	92

List of Tables

3.1	The scores of the different system types on the functionality criterion.	20
3.2	The scores of the different system types on the aesthetics criterion.	20
3.3	The scores of the different system types on the price criterion.	21
3.4	The scores of the different system types on the ease of production criterion. . .	22
3.5	The scores of the different system types on the robustness criterion.	22
3.6	Value analysis to determine the system type.	22
3.7	Result of the value analysis.	23
3.8	Scores of concept 1 on the value analysis criteria.	24
3.9	Scores of concept 2 on the value analysis criteria.	25
3.10	Scores of concept 3 on the value analysis criteria.	26
3.11	Scores of concept 4 on the value analysis criteria.	27
3.12	Scores of concept 5 on the value analysis criteria.	28
3.13	Final results of the value analysis to determine the best passive concept.	29
4.1	Friction force at a certain velocity in a filled oil bath.	37
4.2	Measurements of the damping force at 40 micron.	39
4.3	Summary of the average results at 40,60,80 and 100 micrometer.	40
5.1	Values of the other parameters to construct figure 5.4	47
5.2	Values of the other parameters to construct figure 5.4	48
5.3	Values of all the parameters needed for the numerical calculation of maximal extension stroke.	49
5.4	Decibel boundaries for certain tremor reductions.	58
5.5	The reduced tremor amplitude at all tremor frequencies.	60
5.6	A summary of all the determined values.	61
A.1	Framework to determine the friction force.	81
A.2	Framework to determine the relationship between the damping force and the height of the gap.	82
B.1	Measurements for the calibration of the force sensor.	83
B.2	Measurements for the calibration of the distance sensor	84
D.1	Measurements of the damping force at 60 micron.	89
D.2	Measurements of the damping force at 80 micron.	91
D.3	Measurements of the damping force at 100 micron.	93

Chapter 1

Introduction

This chapter represents a general introduction to the master thesis. Section 1.1 describes the goal of the master thesis. Section 1.2 illustrates which methodology is used to achieve the goal. At last, section 1.3 describes and criticizes the final result of the master thesis.

1.1 Goal

The goal of this master thesis is to design and develop a tunable orthosis for the suppression of involuntary tremor. An orthosis is "an externally applied device used to modify the structural and functional characteristics of the neuromuscular and skeletal system" [4]. Or simply, an applied device which enforces the human limbs. Involuntary tremor is a rhythmic oscillating movement of a human limb due to involuntary contractions of the muscles. This thesis focuses on the suppression of the tremor of the hand relative to the forearm. The main goal is to have a working prototype which indicates that the theoretical foundations created to develop the prototype are correct.

1.2 Methodology

Following methodology will be followed to achieve the master thesis goal:

1. literature study
2. conceptualize suppression concept
3. proof the concept works
4. design the concept to the application
5. build prototype for evaluation

At first knowledge of all the current researched suppression systems needs to be collected in a literature study. The researched topics should form a basis to develop a concept to suppress the tremor. Before an application can be built, the concept needs to be tested. A decent test set-up needs to be developed to indicate that the concept works. When a concept has

qualitative results, the concept can be adjusted to fit for the thesis application. The design of the concept should be supported with mathematical calculations and decent approximation. All chosen parameters should be clarified. When the design is finished, the prototype can be constructed. The prototype should be evaluated and criticized.

1.3 Result

The suppression concept is a passive flat plate damper which regulates its damping characteristics using a height regulation. The concept was fully tested on a test set-up and the results indicated that the concept works. The design of the damper is fully determined mathematically. First the translation inside the damper is calculated in function of the angle of the hand. With this knowledge a lot of design parameters could be selected. The system was approached by a mass-damper-spring model to determine the optimal functionality of the prototype. By using a linearization around the starting position, the equivalent spring constant, damping constant and moment of inertia could be written in function of the design parameters. Next the equivalent constants could be determined graphically using a bode plot of the system. In this procedure the system needed to be tuned to an optimal functionality for the tremor range. When the optimal equivalent constants were determined, the missing design parameters could be calculated. Next the product prototype was built. The damper and the transmission were designed to be manufactured out of aluminum or steel using a milling machine and an electrical discharge machine. The damper was attached to a wrist brace in order to keep it at a calculated position at the forearm. Figure 1.1 shows the final prototype of this master's thesis.



Figure 1.1: The top view (left) and side view (right) of the final prototype.

The final prototype was first tested with a simplified test set-up. The test consisted out of the suppression of a spring and a mass that replicated oscillating tremor movements. This test indicated that the prototype is able to suppress rotating oscillations. The prototype was also tested by Raymond Wuyts. Raymond Wuyts is a Parkinson's disease patient. He had to execute a writing test with and without the prototype. The prototype was able to reduce the tremor. The patient could write small sentences without tremor and the speed at which he wrote increased.

Chapter 2

Literature study

2.1 Tremor

Tremor is a movement disorder in the human limbs. This movement disorder can be defined as a rhythmic, uncontrollable oscillation of a body part. The oscillation appears due to an involuntary contraction of muscles. Tremor can affect various body parts such as the head, tongue, hands and legs. The occurrence of a tremor increases with aging. More than 4 percent of the elderly are affected with tremor [19]. Tremor complicates the activities of daily living (ADL). Examples of these activities are drinking, eating, shaving, writing, driving, dressing, etc. This thesis describes the development of an orthosis to suppress tremor of the hands so patients can again execute these activities of daily living. Several types of tremor occur at a human being, the most common are physiological tremor and pathological tremor. Neurological patients can suffer from pathological tremor. Neurological disorders that cause pathological tremor are for example Parkinson's disease, Multiple sclerosis, brain trauma or essential tremor. Pathological tremor is categorized in three different categories: rest tremor, postural tremor and kinematic or intention tremor. Rest tremor appears when the limb affected by tremor is resting. For example the forearm oscillating while resting on the lap. The frequency of rest tremor ranges from 3 - 6 Hz. Postural tremor can appear by holding the limb, affected by tremor, in a position against gravity. For example stretching your arms and holding this position. The frequency of postural tremor ranges from 4 - 12 Hz. Kinematic or intention tremor appears while executing a voluntary movement. An example is the finger-to-nose test. In this test, the patient needs to touch his nose slowly with his or her finger. The frequency of intention tremor ranges from 2 - 7 Hz. Physiological tremor occurs in every normal, healthy individual. This tremor can be a postural or a kinetic action tremor, particularly in the hands, fingers and legs. Physiological tremor is more intense in situations of stress or anxiety, but also after the ingestion of stimulants like caffeine or alcohol. The frequency of physiological tremor ranges from 8 - 13 Hz. Summarizing the different types of tremor concludes that tremor frequencies range from 2 Hz - 13 Hz. Bioengineering Group CSIS determined all these frequency ranges of different tremors [18]. The fact that tremor doesn't always occur at the same frequency and amplitude makes the suppression of the tremor more difficult. In order to suppress the tremor at all of these frequencies, the suppression system needs to be adjustable. While suppressing the tremor at the different

tremor frequencies, the orthosis may not suppress the voluntary movements. This means the frequency range of the voluntary movement needs to be known too. To study the voluntary frequency range a group of approximately 20 people can be used. The group consist of young and older healthy people. The group needs to execute about 24 activities of daily living while the frequency is being measured. This study determined that the voluntary frequency range changes around 1 Hz with predominant frequency components between 0.48 and 2.47 Hz [25]. This study revealed an important aspect in the suppression of tremor, namely that voluntary movement only occurs in a frequency range under 2 Hz and tremor movement only occurs in a frequency range higher than 2 Hz. The 2 Hz boundary can be used as an important parameter to separate voluntary movement from tremor movement in the orthosis design.

2.2 Treatment of tremor

There are several treatments on the market to suppress tremor. The most commonly used treatment is medication. Other important treatments are surgeries as thalamotomy, pallidotomy and deep brain stimulation or wearable orthoses. This section describes these treatments, the advantages and the disadvantages.

2.2.1 Medication

The most commonly used treatment against tremor is pharmaceutical medication. This medication always contains dopamine. Dopamine is an organic chemical produced in the brain and functions as a neurotransmitter. A neurotransmitter is a chemical released by nerve cells to send signals to other nerve cells. The neurotransmitters not only regulate the movement of body parts, but also the emotions of an individual. Neurological patients do not produce enough dopamine. Figure 2.1 shows two examples of medication containing dopamine, namely Prolopa and Requip-Modutab. Another medication used by patients with Parkinson's disease is Azilect. The advantage of the medication is that it works very efficiently. The tremor disappears entirely at many of the patients. But there are a lot of disadvantages too [5], [6]. Not every individual can take this medication. For example women who are pregnant may not take the medication for the sake of the baby. Individuals who are depressed may not take the medication for addiction purposes. And at last people under the age of 25 may not take this medication because it interferes with the growth of their bones. Other disadvantages of medication are the many side effects. The side effects include allergic reactions, nausea, heart problems, reduction of white blood cells, etc. This means only a small group of tremor patients can take medication without any complaints.

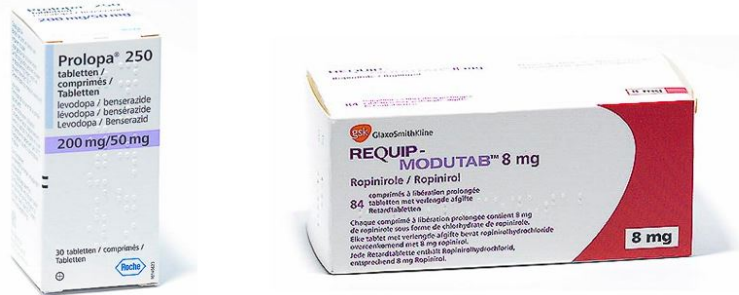


Figure 2.1: Two examples of medication used by a patient with Parkinson’s disease [5], [6].

2.2.2 Surgery

Three types of surgeries will be discussed in this section: thalamotomy, pallidotomy and Deep Brain Stimulation (DBS). Thalamotomy and pallidotomy destroys the thalamus or the globus pallidus while DBS only controls the thalamus using electrodes. DBS is safer and, most of the cases, more effective than thalamotomy and pallidotomy.

Thalamotomy

Thalamotomy destroys a small part of the thalamus. The thalamus is a symmetrical structure of two halves within the brain. It functions as a station for sensory and motor signals. Figure 2.2 shows the position of the thalamus within the brain. The procedure is typically performed on only one side of the brain, decreasing any risks of complications. The advantage of thalamotomy is that approximately 90 percent of the patients are relieved from any tremor activity [17]. The most important disadvantage of this surgery is the permanent destruction of a small part of the brain. This makes the surgery only available under rare circumstances. Other disadvantages are confusion, weakness, disturbed speech and balance problems. [10]



Figure 2.2: The position of the thalamus within the brain [16].

Pallidotomy

Pallidotomy is performed when the globus pallidus is overactive, this causes tremor. The globus pallidus is involved in the regulation of voluntary movement [8]. The surgeon reduces brain activity in the overactive globus pallidus by creating a scar. This destroys part of the globus pallidus and the functionality decreases. The advantage of the surgery is particularly the reduction of tremor. Disadvantages are a small chance to have a stroke by brain bleedings, loss of thought and memory and surgery infections. [9]

Deep Brain Stimulation (DBS)

Deep brain stimulation inactivates the thalamus without destroying it. DBS uses electric shocks to hinder the functionality of the thalamus. To deliver electric shocks to the thalamus, an electrode is inserted into the brain. The frequency of the electric shocks are tuned by a pacemaker connected to the electrode with a wire. Figure 2.3 shows the electrode within the brain ending at the thalamus. The pacemaker is mostly implanted close to the collarbone. There are many advantages of DBS. It does not destroy brain tissue, the device can be removed at any time and the pacemaker makes the device tunable for frequency changes. There are also a lot of disadvantages of DBS. Permanent brain damage when the surgery goes wrong, a battery in the pacemaker which needs to be changed every three to five years and a 1 - 3% chance of infections or a stroke after the surgery. [22]

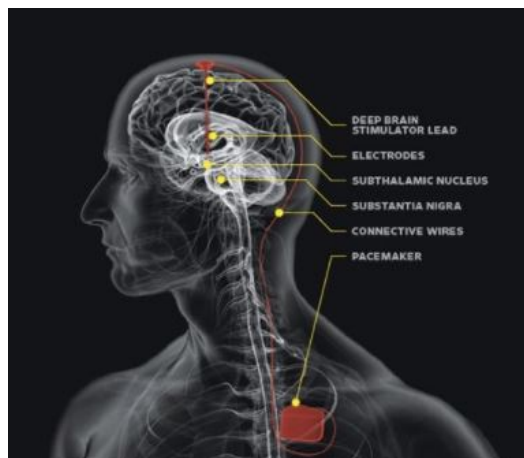


Figure 2.3: The position of the electrode within the brain [2].

2.2.3 Wearable orthosis

The last tremor suppression treatment is the use of a wearable suppression. A wearable orthosis is some kind of exoskeleton around the limb affected by tremor. The orthosis suppresses this tremor locally. There are two different possibilities to suppress the tremor. The first is to suppress the tremor with electrical stimulations counteracting the neurosignal of the brain. The second possibility is to suppress the tremor by means of biomechanical loading. Biomechanical loading systems are categorized into three categories: passive

systems, semi-active systems and active systems. A passive system only uses the energy of the tremor to suppress it. A semi-active system measures the tremor and uses this information to change the specifications to suppress the tremor. The tremor is still suppressed by using its own energy. As in the semi-active system, the active system first measures the tremor. With this information it suppresses the tremor by means of an actuator which consumes energy. Figure 2.4 shows different types of wearable orthoses. A wearable orthosis is the core subject of this master thesis so this will be described more detailed in the next section.

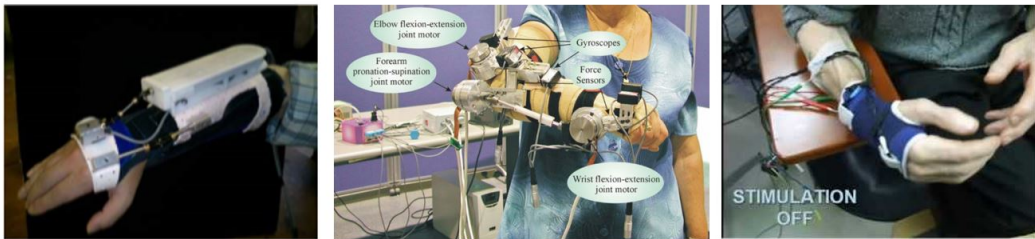


Figure 2.4: Different examples of wearable orthoses [23],[26],[24].

2.3 Wearable orthosis

As said in 2.2.3 there are three different categories of biomechanical loading suppression systems. A passive system, a semi-active system and an active system. Another method to suppress tremor is electrical stimulation. Figure 2.5 shows a functional decomposition of a wearable orthosis for tremor suppression. The concepts found in subject-related papers are listed underneath every project function. A passive system only suppresses the tremor. A semi-active system first measures the total movement of the hands. Then it filters out the tremor frequency and tremor amplitude from the total measured movement. Afterwards it calibrates the tremor frequency and tremor amplitude into operational values for the suppression of the tremor. And finally it uses a controllable damper to suppress the tremor. The active system and electric stimulation fulfill the same functions as a semi-active system. The difference between these systems is the way in which they suppress the tremor. An active system suppresses the tremor using an actuator, an actuator applies a force or a torque on the hands and uses external energy to do so. Electric stimulation suppresses the tremor with electric shocks counteracting the neurosignals of the brain. This section describes the most important concepts in detail.

2. LITERATURE STUDY

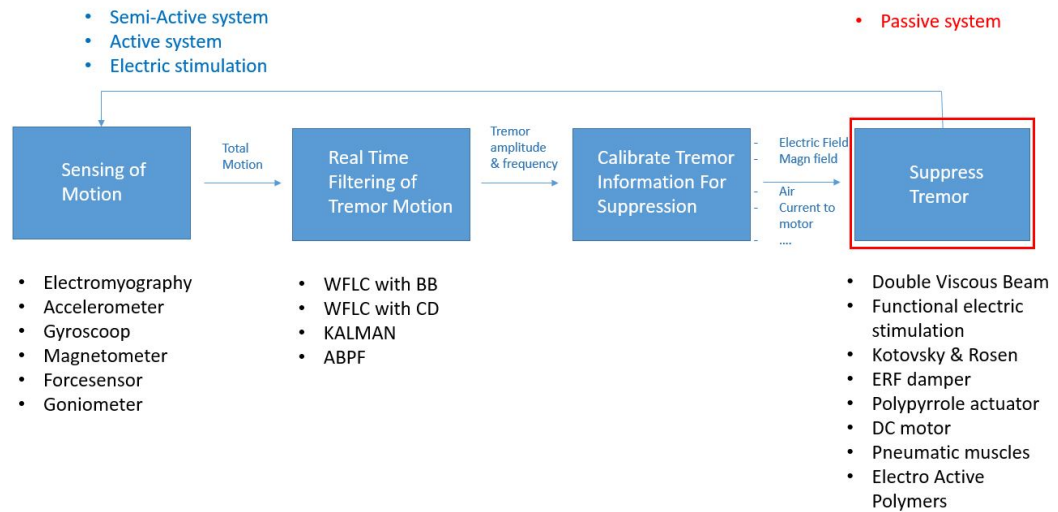


Figure 2.5: Summary of all the feasible concepts found in papers for the different functions of a wearable orthosis.

2.3.1 Sensing of motion

Measurements of the total motion of the hands need to be accurate. If wrong measurements have been sent to the system, the system will not suppress the tremor efficiently. An accurate measurement is possible using electromyography, accelerometers, gyroscopes or force sensors.

Electromyography

When muscles flex, they generate electrical potential. Electromyography or EMG measures the electrical potential of this muscle fibers. There are two types of EMG sensors, namely surface EMG and needle EMG. Surface EMG measures the electrical potential using electrodes attached to the skin. Needle EMG measures the electrical potential through a needle inserted in the muscle. Figure 2.6 on the right shows how needle EMG works. The middle and left picture show examples of the use of surface EMG. The measurement of the electrical potential of the muscles can not be used to determine the tremor amplitude but the tremor frequency can be determined. Using EMG, patterns of motoneural discharges can be measured. The amount of discharges within a certain time interval can be converted to the tremor frequency. The advantages of EMG are the efficiency of the measurement, the extra control-time because the contraction of the muscle happens before the movement of the hand and, at last, the dimensions of the sensor. The disadvantages of EMG are its price and its inability to measure the tremor amplitude. [19]

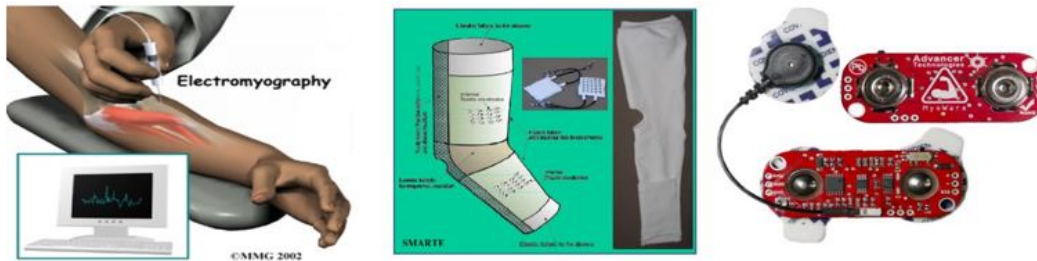


Figure 2.6: An example of needle EMG [11] and surface EMG [19] , [3].

Accelerometer

Accelerometers measure the linear acceleration based on Newton's second law. A mass is force-loaded in a mass-spring-damper system. The acceleration is then determined with Newton's second law formula ($\text{Force} = \text{mass} \times \text{acceleration}$). To determine the acceleration of the hand relative to the forearm, one accelerometer needs to be attached to the hand and another sensor needs to be attached to the forearm. Subtracting the two measurements gives the relative linear acceleration in three directions. The advantages of an accelerometer are its reliability, its ease of use and its price. The accelerometer also has some disadvantages. First you need a second integration to determine the position of the hand. Second the measurements are linear while the rotational measurements are of greater importance. At last gravity interferes with the measurements.

Gyroscope

A gyroscope provides a direct measurement of the angular velocity, uninfluenced by gravity. In order to determine the angular position, the measurements need to be integrated. The angular acceleration can be determined by taking the derivative. No second integration is needed, contrary to the accelerometer. Again two gyroscopes are needed to measure the motion of the hand relative to the forearm. Figure 2.7 shows where to position the gyroscopes in order to measure the motion of the hand relative to the forearm. The advantages of the gyroscope are its efficiency, its direct measurement of angular velocity, its price and its low energy consumption. Gyroscopes do have a major disadvantage. Temperature affects the measurements of the gyroscope non-linearly. This means a non-linear compensation system is needed to obtain good results. Decent gyroscopes do have such compensation system.

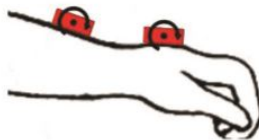


Figure 2.7: The positions to attach the gyroscopes to measure relative motion of the hand [18].

Force sensor

A force-sensor is a piezoelectric sensor which voltage increases when force is applied. This type of sensor are used in active systems to directly measure the tremor force which needs to be countered by the actuator.

2.3.2 Real time filtering of tremor motion

The sensors measure the total motion of the hand. The total motion includes the voluntary motion and the tremor motion. In order to suppress the tremor, the tremor motion needs to be known. This section describes how to filter this tremor motion from the total motion. The most important aspect for filtering tremor motion is the difference in the frequency contents of voluntary and tremulous motion. Tremor occurs, as said in 2.1, at frequencies higher than 2 Hz. More particular in the 2-13 Hz frequency range. Voluntary movement only occurs at frequencies lower than 2 Hz, mostly close to 1 Hz. This means that the frequency of 2 Hz is an important parameter for the different filter techniques. Another important characteristic to differentiate tremor motion from voluntary motion is the power spectral density. Figure 2.8 shows the difference in power spectral density between tremulous and voluntary motion. Voluntary motion has considerably more energy than tremulous motion. [18]

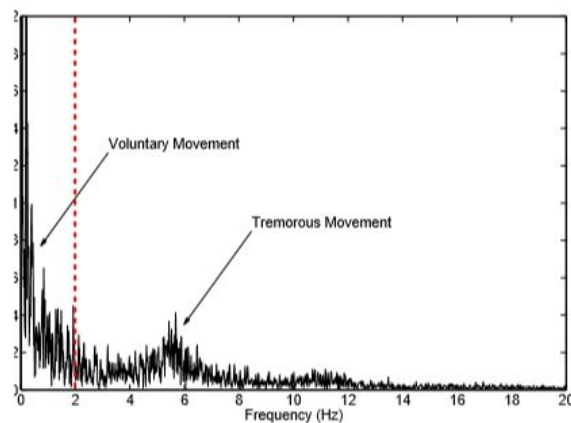


Figure 2.8: The difference in power spectral density between tremulous motion and voluntary motion [18].

Two stage algorithm

This subsection describes the two stage algorithm. The first stage isolates the voluntary movement and subtracts it from the total movement. The second stage estimates the frequency and the amplitude of the remaining signal. Figure 2.9 shows a block diagram of the two stage algorithm with the corresponding signals. Two real-time voluntary movement estimation algorithms are already developed for the first stage. The first algorithm is based on a g-h filter which uses a Benedict-Bordner filter or a critically dampened filter to estimate the values of g and h. The second algorithm uses a Kalman filter to estimate the voluntary movements. Three algorithms are developed to estimate the frequency and the amplitude of the tremor

in stage 2. The first algorithm uses a weighted frequency fourier linear combiner. This algorithm is mostly used in the research of tremor modeling. The second algorithm uses a bandlimited multiple fourier linear combiner. The third and last algorithm uses a Kalman filter. These filter techniques are fully explained in paper [18].

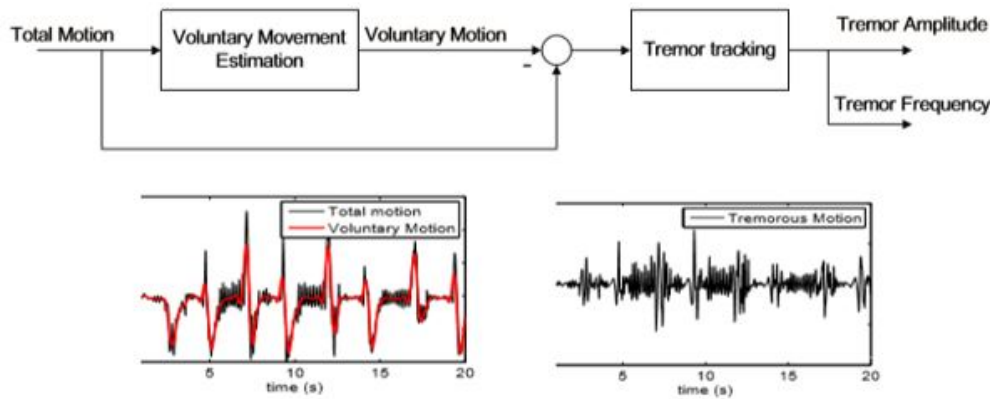


Figure 2.9: A block diagram of the two stage algorithm with corresponding signals [18].

Figure 2.10 shows the block diagram with the most optimal filter techniques for tremor estimation. All the algorithms are compared and this configuration gives the most optimal results for the two stage algorithm. The voluntary motion is estimated with a g-h filter using a critically dampened filter to estimate g and h. The tremor frequency is estimated with a weighted frequency linear combiner. This frequency is fed, together with the tremor signal, to the Kalman filter to estimate the tremor amplitude. [18]

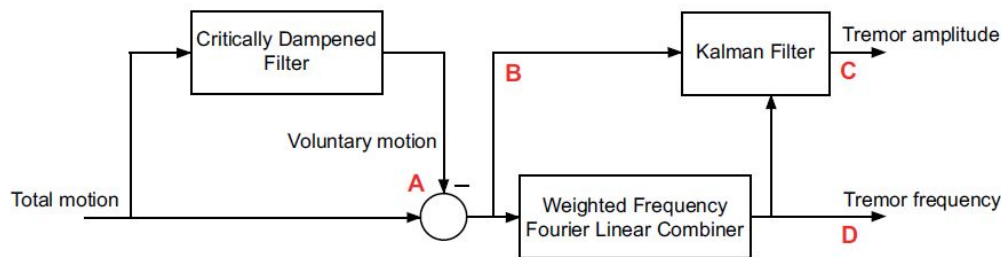


Figure 2.10: A block diagram of the two stage algorithm with the most optimal filter techniques [18].

Adaptive band pass filter (ABPF)

The adaptive band pass filter shown in 2.11 extracts information around a certain center frequency. The filter starts with an estimated tremor frequency. In the next step the system measures the interval between two zero points of the motion sine wave. This interval is equal to a half period T . With this information a new tremor frequency equal to $\omega = \frac{2*\pi}{T}$ is fed to

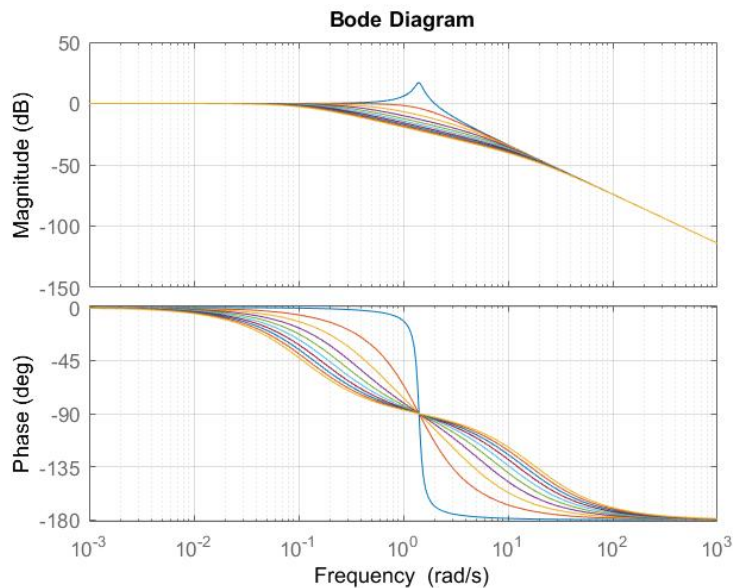


Figure 2.12: The effect of the damping coefficient on the rotation of the hand.

Double viscous beam - MRF damper

The double viscous beam is developed by a Spanish research group. The suppression system is based on a controllable damper. The damper uses a magnetorheological fluid which can change its viscosity when a magnetic field is applied. A magnetorheological fluid (MRF) is a fluid with micro magnetizable particles in a nonmagnetic medium. The magnetizable particles align in the direction of the magnetic flux when the magnetic field is applied. The stronger the magnetic field, the harder the particles align. Due to this alignment, the viscosity of the fluid increases. So summarized, the viscosity of a MRF increases when the applied magnetic field increases. [15] Figure 2.13 shows a magnetorheological fluid without a magnetic field on the left and the same MRF with a magnetic field.

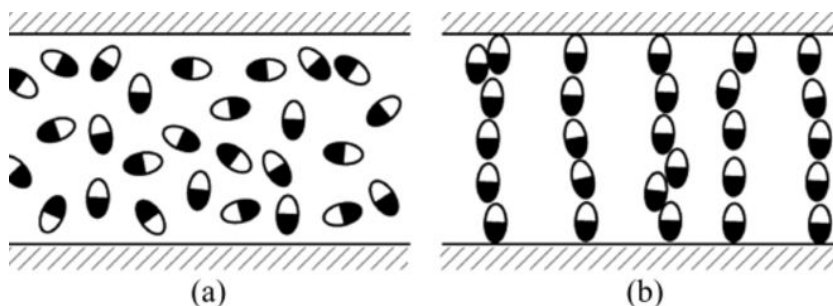


Figure 2.13: The behaviour of a mrf when a magnetic field is applied. [15].

Figure 2.14 illustrates a prototype using a MRF. A transmission, which converts the rotational movement of the hand to a translating movement inside the damper, translates into a MRF filled chamber. The translation is partially blocked by the MRF due to its viscosity. A sensor and a control algorithm estimate the tremor. The strength of the magnetic field can be adjusted in order to block the movement of the transmission more if needed. By adjusting the magnetic field properly, the high velocities of tremor movement are blocked, but the small velocities at voluntary movement will not be blocked. [23]

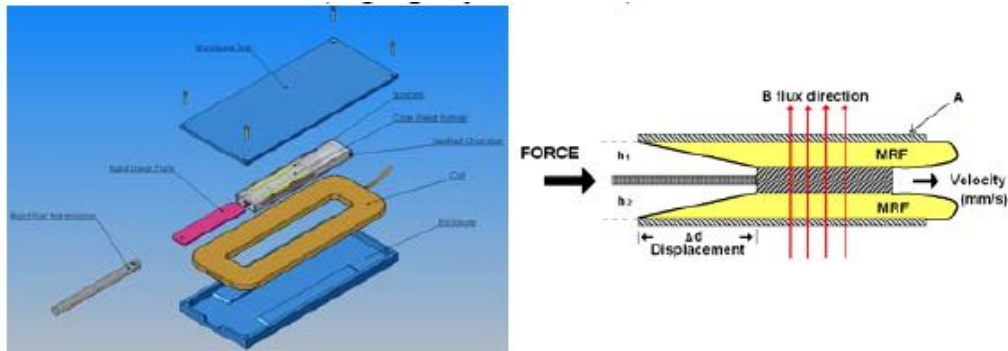


Figure 2.14: The principle of the double viscous beam suppression system [23].

ERF damper

An Electro-Rheological Fluid is a fluid with solid particles which have a different dielectric constant as the medium. The solid particles polarize when an electrostatic field is applied. This causes a dipole moment. The dipole-dipole interaction causes a formation of columns of the solid particles along the electrostatic field [34]. Figure 2.15 shows the erf with no field applied (a), with a field of 500 V/mm (b) and with a field of 900V/mm (c). It is clear that the solid particles align more with increasing electrostatic field. This causes the static yield stress to change linearly with the applied electrostatic field. The dynamic yield stress increases quadratically with the increase of the electrostatic field [7]. The response time of an electrorheological fluid is only a few milliseconds [34]. But research has shown that the response time is a lot longer in switching applications [30].

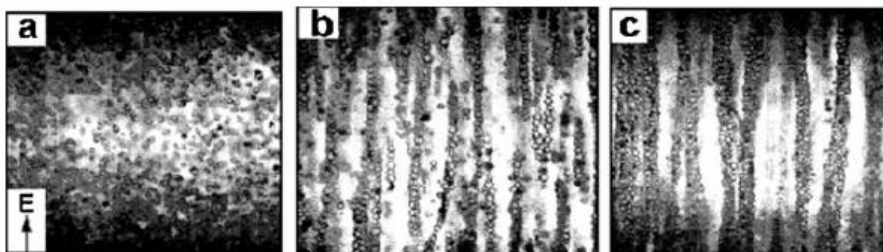


Figure 2.15: The effect of an electrostatic field on the ERF. [34].

Functional electric stimulation

Functional electric stimulation (FES) uses low voltage electrical pulses to control tremor. The electrical pulses are passed along to the muscles using electrodes. This electric "shock" generates muscle activity. This muscle activity should counteract the tremor contractions. First the tremulous motion needs to be measured using decent sensors. An adaptive band pass filter can be used to determine the tremor frequency and tremor amplitude. With this tremor information following electrical stimulation parameters can be adjusted: pulse intensity, pulse duration, stimulation frequency, etc. [24]

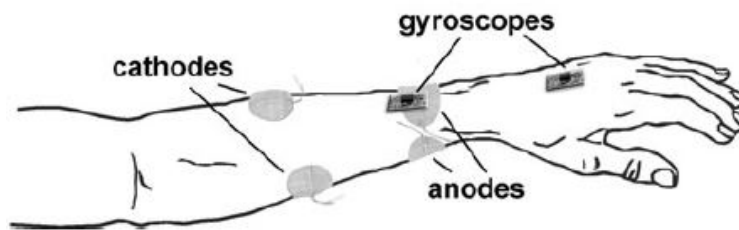


Figure 2.16: The components necessary for the suppression of tremor using FES. [24].

Kotovskiy and Rosen

Kotovskiy and Rosen created a passive suppression system. The system does not use a transmission. A beam filled with viscous silicone oil is attached from the hand to the forearm. The beam housing is made from flexible material which can bend along with the hand. When the hand rotates a small motion d of the upper plate relative to the bottom plate appears as can be seen in figure 2.17. This occurs due to the different bending radius r and R . This small movement can be used to create damping. Because the movement is so small, the viscous oil needs to have a viscosity in the order of millions of centistokes. Figure 2.17 shows the system developed in 1998. [20]

Electroactive polymers (EAPs)

Research has shown the potential of EAP-actuators. EAPs are plastic materials which shape and size can change when voltage or current is applied. When subjected to an electric field, an EAP can have an actuating strain of over 300 percent. For this reason, EAPs can be used as artificial muscles in robots due to their functional similarity to natural muscles. Another advantage of EAP is the weight of the polymer. A polymer is a plastic, so it has a negligible weight. The drive voltage to obtain strains of 300 percent however can be as big as $150\text{V}/\mu\text{m}$, which is enormous [12]. Another disadvantage of the EAPs is the workable frequency range. The frequencies in which to EAPs could contract are much lower than tremor frequencies. To speed up the EAPs new research has been done. Instead of changing the size, the EAPs could change their stiffness when they get redox cycled. The paper describes polypyrrole actuators working in a frequency range of 2 to 16 Hz. [33]

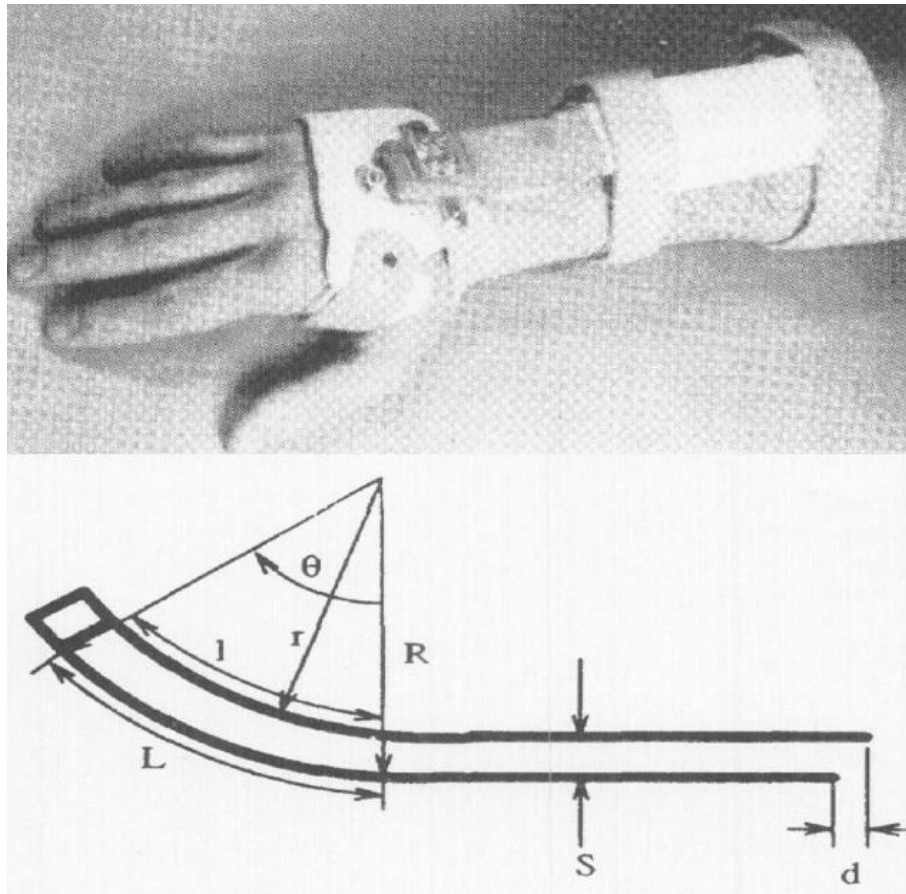


Figure 2.17: The Kotovsky and Rosen concept for passive suppression of tremor. [20].

Active actuators

Active systems use sensors, mostly gyroscopes and force sensors, to measure the motion and the forces of the oscillating limb. This information is used to estimate the tremor frequency and tremor amplitude with a decent control algorithm. This frequency and amplitude can be used to properly suppress the tremor using actuators. Figure 2.18 uses rotary DC motors and harmonic pancake transmission to suppress the tremor [27].

Pneumatic muscles are another possibility to suppress tremor actively. This however generates bad results due to following facts [14]. Pneumatic muscles are not easy to control accurately and the response time of pneumatic muscles is a lot slower than the response time of DC motors. Rotary DC motors are currently by far the best active suppression tools. Figure 2.19 shows the results of the active system shown in figure 2.18. The results are good, both the angular velocity as the tremor power is decreased significantly but the system is very bombastic.

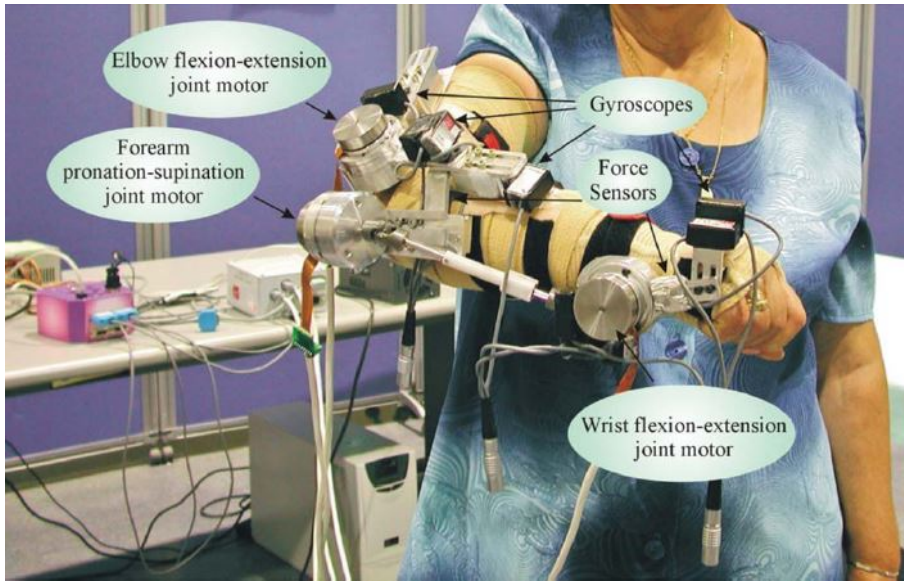


Figure 2.18: The active system using actuators to counteract the tremor. [27].

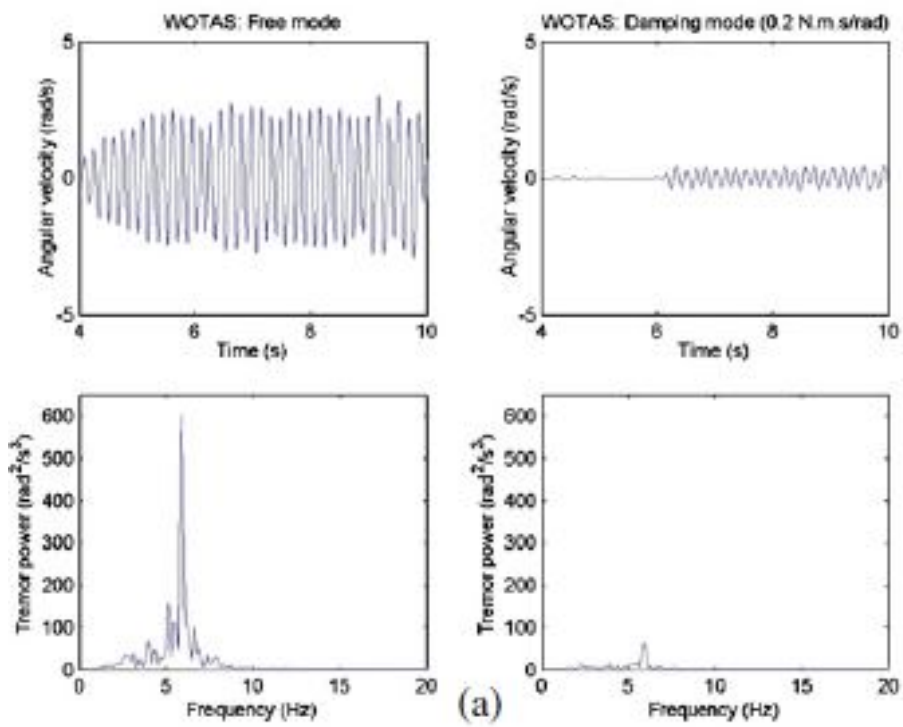


Figure 2.19: The result of the active system using a rotary DC motor. [27].

Chapter 3

Value analysis

Section 2.3 described the different functions of the thesis project using a functional decomposition. All the functions can be executed by many different concepts. A value analysis is the perfect system to select the best concept for every function. It compares the different concepts using criteria. Each criteria receives a fractional value corresponding to its importance. Afterwards the concepts receive a score on a scale from one to five for every criteria. One, meaning the concept does not meet the standards of the criteria at all. Five, meaning the concept is perfect for that criteria. The criteria concept score is the fractional value of the criteria multiplied with the score of the concept for that criteria. The overall concept score is the sum of all these criteria concept scores. The concept with the highest score gets selected to fulfill the functionality.

3.1 Determination of the system type

The system type is determined using following criteria: functionality, size, price, ease of production and robustness. Each criteria receives a fractional value. Next the system types are valuated for each criteria. The system type with the highest end score will be selected to develop in the thesis.

Functionality

Functionality evaluates how good the system type works. Functionality receives the highest score of 0,4. A product needs to work well before the production starts, before it will be sold at a decent price and before aesthetics matter. For this reason, the criteria is valuated with the maximum score. Table 3.1 shows the score of each system type on the functionality criterion.

Aesthetics

Aesthetics describe how appealing the product looks. The most important factor in the aesthetics criterion is the size of the product. The consumer needs to wear the product a lot and he or she would prefer the system as small as possible. The criterion is valuated at a score of 0,15, this valuation is less than 0,4 for functionality and 0,25 for robustness. A good

3. VALUE ANALYSIS

System	Score	Explanation
Active	5	An active system is able to generate a movement in opposite phase to the movement of the hand. This means theoretically the active system is able to fully suppress the tremor. For this reason the active system receives the maximum score of 5 points.
Semi-active	4	The semi-active system adjusts the damping constant consistently to achieve optimal damping at every time instance. A disadvantage of a damping system instead of an active system is the settling time. Every time a damping parameter changes, the system needs a small time instance to recover the damping state. For this reason the semi-active system loses a point in comparison to the active system and receives a score of 4 points.
Passive	2	The passive system needs to be tuned manually. This means the damping state is rarely optimal and needs to be adjusted every time a tremor parameter changes. For this reason it only receives a score of 2 points.

Table 3.1: The scores of the different system types on the functionality criterion.

working system is better than a bad working system that looks good. The system needs to be resistant against daily activity impacts. A strong material is more likely to be used as a good looking material. Table 3.2 shows the score of every system type on the aesthetics criterion.

System	Score	Explanation
Active	1	The active system receives the worst aesthetics score of 1. The reason of this bad valuation is the bigger size of the system due to the actuators, sensors, batteries and a controller.
Semi-active	3	A semi-active system receives a better score, namely 3. The higher score is a result of the size of the damper being smaller than the actuators.
Passive	5	In contrary to the passive system, the semi-active system still needs sensors, batteries and a controller. This is why the passive system receives the highest score of 5.

Table 3.2: The scores of the different system types on the aesthetics criterion.

Price

The price of the system is along with the ease of production the worst valued criterion. The price criterion only received an importance factor of 0,1. This is due to the fact that the system is in a research phase. When a decent working prototype is developed, the price could become more important. Because this type of system can increase the quality of living, it is more important that it works decently. Many individuals would also pay a little more for a decently looking, qualitative product. Table 3.3 shows the score of every system type on the price criterion.

System	Score	Explanation
Active	1	The active system receives the worst price score of 1. This is due to the many components needed for this system type like the components to sense and control the tremor motion and actuators to suppress it.
Semi-active	1	The semi-active system, together with the active system, receives a score of only 1. It also needs extra components to sense the tremor. The semi-active dampers can be expensive due to the rheological fluids.
Passive	5	The passive system receives the highest score of 5. No expensive electrical or actuating components are needed. The damper can be made from cheap viscous silicone oils.

Table 3.3: The scores of the different system types on the price criterion.

Ease of production

The ease of production is the worst valued criterion and receives a score of only 0,1. It is important that the system can be made. But it is not important how difficult it is to make. A good working system that is difficult to make, but doable, is better than an easy to make bad product. A product that is easy to make can reduce the price, but the price is also a criterion of less importance. Table 3.4 shows the score of every system type on the ease of production criterion.

Robustness

The robustness criterion is very important and receives the second highest score of 0.25. The system needs to be resistant against the impacts of daily activities. The system can't break down when the individual for example bumps his arm against any kind of object. But it is more important to have a working system before it can be made robust. Table 3.5 illustrates the score of every system type on the robustness criterion.

3. VALUE ANALYSIS

System	Score	Explanation
Active	1	The active system receives the worst ease of production score of 1. The actuating systems can be very complex to build accurately and a decent control program needs to be made.
Semi-active	3	The semi-active system receives a slightly better score of 3. The system also needs a control program but the damper is less complex to make than the actuating systems.
Passive	5	The passive system receives the highest score of 5. There is no need for a control program linked to any sensors. The passive damper is less difficult to build than the semi-active damper.

Table 3.4: The scores of the different system types on the ease of production criterion.

System	Score	Explanation
Active	1	The active system receives the worst robustness score of 1. The logic behind this valuation is simple, the less components that can break down, the higher the score. The active system has the most components, so it receives the worst score.
Semi-active	3	The semi-active system receives a score of 3. Simply because it needs less components than the active system, but more components than the passive system.
Passive	5	The passive system receives the highest score of 5. The system is very robust because it does not need any electrical components.

Table 3.5: The scores of the different system types on the robustness criterion.

Final results

This section interprets the final results of the value analysis. Table 3.6 summarizes all the scores of the system types on the different criteria.

	Functionality (0,4)	Aesthetics (0,15)	Price (0,1)	Ease of production (0,1)	Robustness (0,25)
Passive system	2	5	5	5	5
Semi-active system	4	3	1	3	3
Active system	5	1	1	1	1

Table 3.6: Value analysis to determine the system type.

Table 3.7 shows the final score of every system type calculated from the values of table

3.6. The passive system receives the highest score of 3,80. This means the final system will become a passive system. The great advantages of a passive system is its compactness and robustness. The functionality will probably be worse than a semi-active or an active system. But no individual would like to have a bombastic system full of actuators, batteries and sensors.

System type	Total score
Passive system	3.80
Semi-active system	3.20
Active system	2.60

Table 3.7: Result of the value analysis.

3.2 Determination of the concept

The passive system is selected as the best system type for this kind of application as described in 3.1. This section describes which concept of a passive system will be developed in the master thesis. Equation 2.1 showed the parameters of the damping system which can be adjusted in a passive system. The concepts are based on the adjustment of the gap height H . Changing the dynamic viscosity η is unknown for a passive system. The gap height can easily change from for example 10 micron to 1 mm, which is a regulation factor of 100. This regulation factor is a lot harder to achieve with the damping surface A .

Concept 1

The first concept is the Kotovsky and Rosen passive system described in section 2.3.3. In order to make this system tunable, a third plate is added which can go up and down to regulate the gap height. Figure 3.1 illustrates the concept graphically. The system scores on the different value analysis criteria are shown in table 3.8.

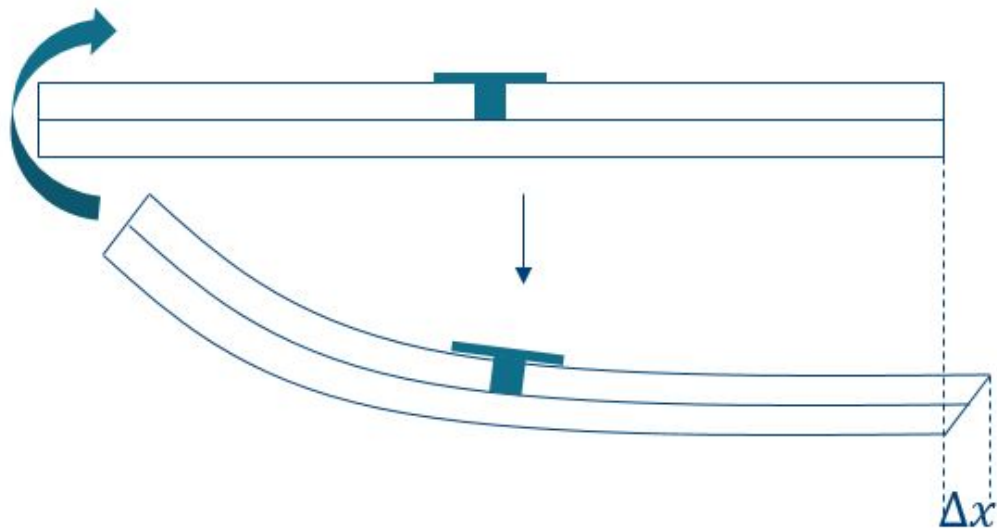


Figure 3.1: Concept 1: The passive system of Kotovsky and Rosen.

Criterion	Score	Explanation
Functionality (0,40)	1	The concept received the worst score of 1 due to the small stroke Δx . It is also difficult to keep all the plates aligned when they are bent.
Robustness (0,25)	5	The system receives the highest robustness score of 5 because there is no need of a transmission. A transmission is always a weak part in the system.
Aesthetics (0,15)	3	The aesthetics are directly linked to the size of the system. The system is less compact in height than concept 2. And the damper is much longer because it already starts at the hand.
Price (0,1)	2	Due to the small stroke, the oil of the system needs to be very viscous. Viscous oils are likely to be more expensive. All the plates need to be bendable. Elastic material can be more expensive than aluminum or steel used in the other concepts
Ease of production (0,1)	1	The system is very difficult to make due to the alignment problems of the plates when the system is bent.

Table 3.8: Scores of concept 1 on the value analysis criteria.

Concept 2

The second concept is a simple screw attached in the transmission to lower or to lift the transmission relative to the bottom plate. Figure 3.2 illustrates the concept graphically. The system scores on the different value analysis criteria are shown in table 3.9.

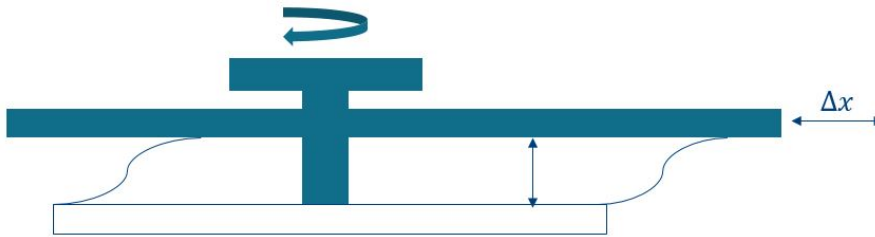


Figure 3.2: Concept 2: A simple screw attached to the transmission.

Criterion	Score	Explanation
Functionality (0,40)	2	Theoretically this system should work fine but this is not the case in practice. It's difficult to keep the transmission aligned with the bottom plate. Its not possible to build an oil chamber in this system because of the screw attached to the transmission. This means a membrane needs to be used to keep the oil in place. This membrane adds elastic forces to the system model.
Robustness (0,25)	1	The system is weak due to the membrane and the transmission. The membrane can get pierced. A transmission is always a weak point in a system.
Aesthetics (0,15)	5	The aesthetics are directly linked to the size of the system. Only two plates are needed and they can be placed very closed to each other. This can make the system very compact.
Price (0,1)	5	The system can be made very cheap. Not a lot of components are needed.
Ease of production (0,1)	3	The system itself is quite simple but the membrane is not easy to integrate properly into the system.

Table 3.9: Scores of concept 2 on the value analysis criteria.

Concept 3

The third concept uses an oil bath to contain the oil. An extra plate is added to regulate the height of the gap between the plates. This eliminates the membrane necessary in concept 2. The height is regulated using a screw which pushes a plate down. Springs are attached to push the plate back up when the screw moves back up. Figure 3.3 illustrates the concept graphically. The system scores on the different value analysis criteria are shown in table 3.10.

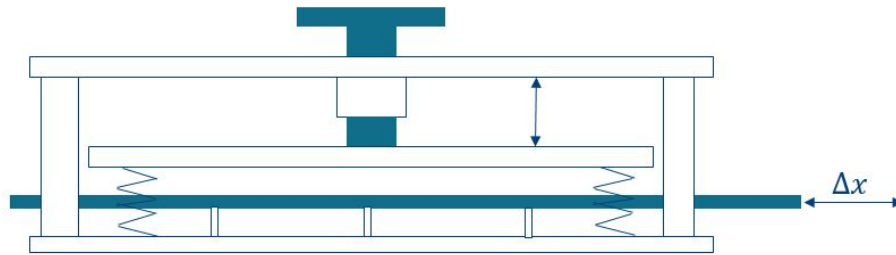


Figure 3.3: Concept 3: A screw pushing down the upper plate of the damper.

Criterion	Score	Explanation
Functionality (0,40)	5	The system receives the highest score on functionality. The membrane of concept 2 is deleted so no extra elastic forces appear. The stroke of this concept is a lot bigger than the stroke of concept 1.
Robustness (0,25)	3	The system receives a lower robustness score due to the transmission. A transmission is always a weak component.
Aesthetics (0,15)	2	The system is less compact than system 2 due to the extra adjusting plate. The screw comes out of the damper which adds height to the total system. The springs to push the adjusting plate back up add width to the system because they can not interfere with the transmission.
Price (0,1)	4	The system can be made very cheap. The entire system is made from simple aluminum plates, screws and springs.
Ease of production (0,1)	5	The system is quite simple to make. All the part can easily be milled.

Table 3.10: Scores of concept 3 on the value analysis criteria.

Concept 4

The fourth concept uses a similar system as concept 3. A screw regulates the height of an additional adjusting plate which makes it possible to contain the oil in a chamber. But in this system, the screw does not push the plate down. The adjusting plate has a threaded hole in which the screw attaches. Springs are used to align the plate parallel to the transmission. Figure 3.4 illustrates the concept graphically. The system scores on the different value analysis criteria are shown in table 3.11.

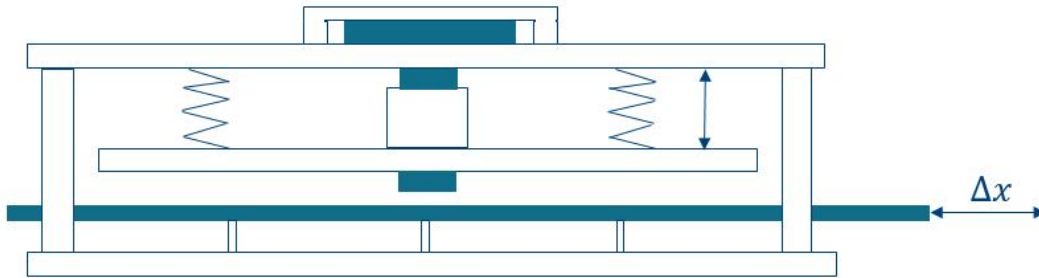


Figure 3.4: Concept 4: A screw guiding the upper plate of the damper.

Criterion	Score	Explanation
Functionality (0,40)	5	The system receives the highest score on functionality. The membrane of concept 2 is deleted so no extra elastic forces are added into the system. The stroke is much higher than the stroke of concept 1.
Robustness (0,25)	3	The system receives a lower robustness score due to the transmission. A transmission is always a weak component.
Aesthetics (0,15)	4	The system is less compact than system 2 due to the extra adjusting plate. But the screw does no longer come out of the damper, so it does not add height as in concept 3. The springs can be attached above the adjusting plate, so they do not add width. This makes the concept compacter than concept 3.
Price (0,1)	4	The system can be made very cheap. The entire system is made from simple aluminum plates, screw and springs.
Ease of production (0,1)	5	The system is quite simple to make. All the part can easily be milled.

Table 3.11: Scores of concept 4 on the value analysis criteria.

Concept 5

The fifth and last concept also uses an extra adjusting plate to contain the oil in an oil bath. This concept uses a very flexible plate which bends when the screw pushes it down. This way the gap height can be regulated. Figure 3.5 illustrates the concept graphically. The system scores on the different value analysis criteria are shown in table 3.12.

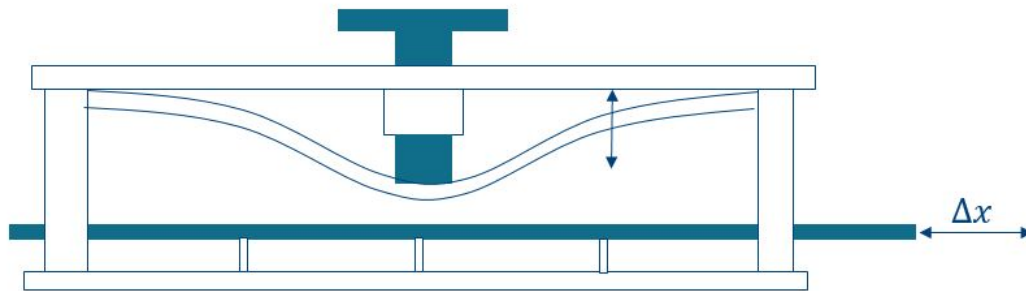


Figure 3.5: Concept 5: A screw pushing down the elastic upper plate of the damper.

Criterion	Score	Explanation
Functionality (0,40)	3	The membrane of concept 2 is deleted so no extra elastic forces are added into the system but the plate bends at a certain curvature. This means that the height-variation of the gap is limited. The adjusting plate can never come as close, with its whole surface, to the transmission as the previous concepts.
Robustness (0,25)	2	The system receives a lower robustness score due to the transmission. A transmission is always a weak component. Also the elastic plate can break down after a certain amount of height adjustments.
Aesthetics (0,15)	3	The system is less compact than system 2 due to the extra adjusting plate. No springs are necessary, so no extra width is necessary. The screw does come out of the damper which adds height.
Price (0,1)	4	The system can be made very cheap. The entire system is made from simple aluminum plates and screws.
Ease of production (0,1)	5	The system is quite simple to make. All the part can easily be milled.

Table 3.12: Scores of concept 5 on the value analysis criteria.

Final results

Table 3.13 shows the final score of every passive system concept. Concept 4 has the best final score and will be developed in this master thesis.

Concept	Total score
Concept 1	2.40
Concept 2	2.60
Concept 3	3.95
Concept 4	4.25
Concept 5	3.05

Table 3.13: Final results of the value analysis to determine the best passive concept.

Chapter 4

Concept testing

This chapter describes the test set-up and the results of the tests used to verify the final concept determined in section 3.2. The final concept is a passive flat plate damper that changes its damping constant by changing the gap height H between the plates. Formula 4.1 states that the damping coefficient is inversely proportional to the height. The height in this case is the gap between the plates. The test needs to confirm that the damping coefficient is really inversely proportional to the gap between the plates and that the height regulation of a couple micrometers works efficiently with a simple M3 screw.

$$C = \frac{\eta * L * B}{H} \quad (4.1)$$

4.1 Design of experiments

The design of experiments represents a guideline or a framework for the experiments. It should explain what an individual wants to learn from his or her experiments and which tests are necessary to do so. These experiments should determine if the damping coefficient is tunable by mechanically changing the gap height. The framework of the experiments is added in Appendix A.

4.2 Test set-up

The test set-up was previously built by KULeuven for other applications. Adjustments were made to monitor the damping characteristics. Figure 4.1 shows the complete set-up.

4. CONCEPT TESTING

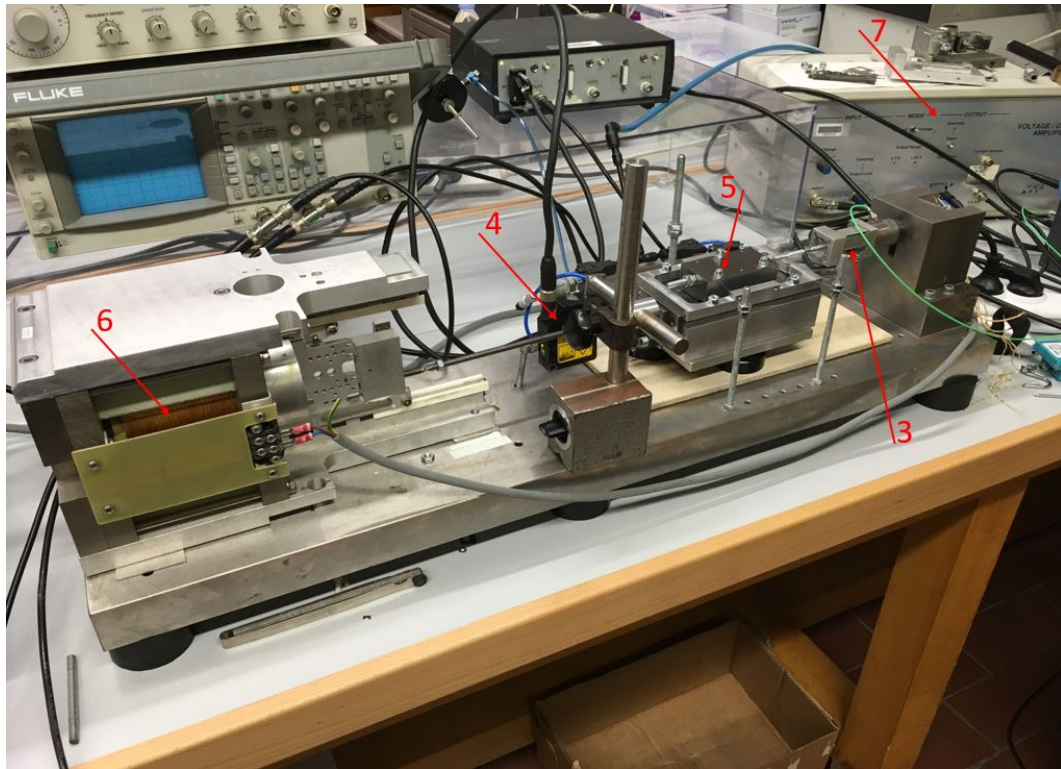


Figure 4.1: The test set-up to determine the damping characteristics.

4.2.1 Parts

The test set-up contains the parts listed below. Figure 4.1 displays most of these parts in the test set-up.

1. Computer with matlab/simulink and dSPACE controldesk
2. dSPACE controller
3. KISTLER 9031 SN143089 force sensor
4. BAUMER CH8501 distance sensor
5. Damper
6. Electromagnetic source
7. Amplifier

1: Computer with matlab/simulink

The simulink program to control and monitor the test set-up is attached in appendix C. The simulink program is linked to the dSPACE controldesk to monitor the data in real time.

2: dSPACE controller

The dSPACE controller has the control desk software which directly connects to simulink. This way mathematical models can be build within simulink using the real-time measurement signals of the controller. The control desk software has special display tools to display the results. The dSPACE controller not only reads signals but can also send signals to the test set-up using sources of simulink. This way the electromagnetic source can be controlled using dSPACE.

3: KISTLER force sensor

The KISTLER force sensor uses piezoelectricity to determine the applied forces. When piezoelectric crystals are exposed to mechanical stress, they accumulate electric discharge. This electric discharge can be measured and calibrated in order to determine the exact force.

4: BAUMER distance sensor

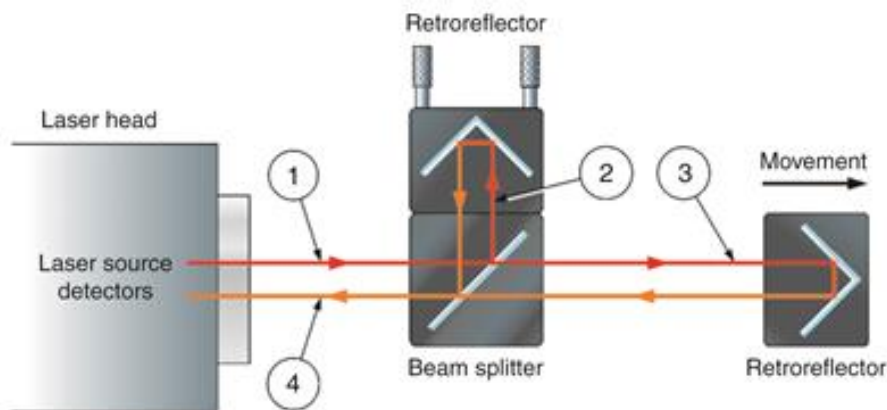


Figure 4.2: Graphical representation of the functionality of the distance sensor.

Figure 4.2 shows how the distance sensor works. The principle of the sensor is based on interferometry. First a laser source in the sensor generates a laser beam with a wavelength of 675 nanometers (1). Next the laser beam is split within the sensor creating a reference beam (2) and a traveling beam (3). The reference beam reflects due to mirrors. The other beam travels towards the oil bath and also reflects. Both laser beams come back to the same point and again form one beam due to interferometry (4). The path length of the reference beam remains constant but the path length of the traveling beam changes with the position of the oil bath. When the oil bath changes its position with distance d , the path length of the traveling beam changes with two times distance d . This change in path length can be seen in the characteristics of the interferometry.

5: Damper

Figure 4.3 shows a close up of the damper in the test set-up. The upper plate of the damper is attached to the force sensor. The bottom plate is an oil bath which is attached to the electromagnetic source. The electromagnetic source gives the oil bath a sinusoidal velocity profile equal to tremor motion. On the bottom of the upper plate three teflon bars are attached as can be seen in figure 4.4. These three small bars keep the upper plate aligned on a certain height relative to the oil bath. M3 screws regulate this height by pushing the teflon bars down. Teflon also guarantees a small friction force in the tests. Three fishing lines keep the upper plate aligned in the direction of the force sensor.

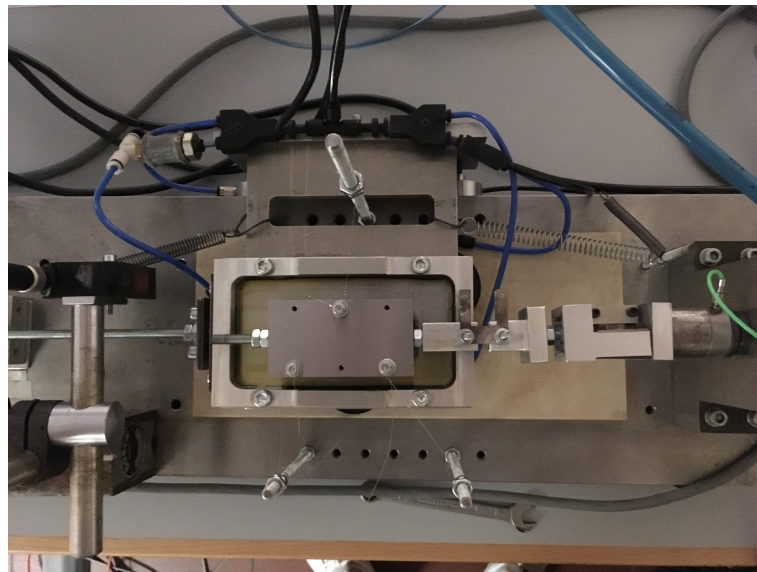


Figure 4.3: Close up of the damper in the test set-up.

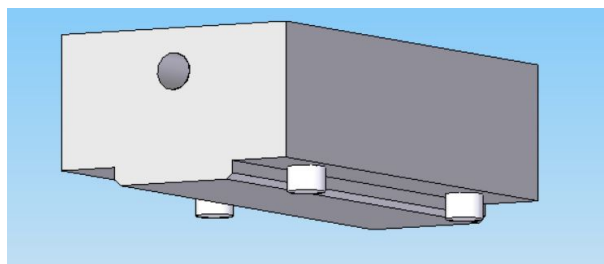


Figure 4.4: The upper plate of the test set-up with the 3 teflon bars.

6: Electromagnetic source

The electromagnetic source sends an alternating current through a copper coil. This copper coil is surrounded by a magnet. This generates a Lorentz force which creates a linear translation with the same frequency as the frequency of the alternating current. The amplitude

of the alternating current can be calibrated to the amplitude of the translation of the oil bath. This way the oil bath can translate at tremor frequencies with a determined amplitude.

7: Amplifier

The dSPACE controller can send source signals of Simulink towards the test set-up. These signals need to be amplified before they can drive the electro magnetic source.

4.3 Results

4.3.1 Test to measure friction force with greased teflonbars

This test determines if the friction is coulomb friction. Coulomb friction is independent to changing velocity. The teflon bars are greased with the viscous oil to have a better estimation of the friction. The lubrication decreases the friction. The test measures the different friction forces at different preloads. The test set-up is preloaded with 500 gram, 1000 gram and 1500 gram. The friction force needs to increase with increasing preload. The velocity profile is sinusoidal. If coulomb friction occurs, the friction force needs to have a sinusoidal profile too.

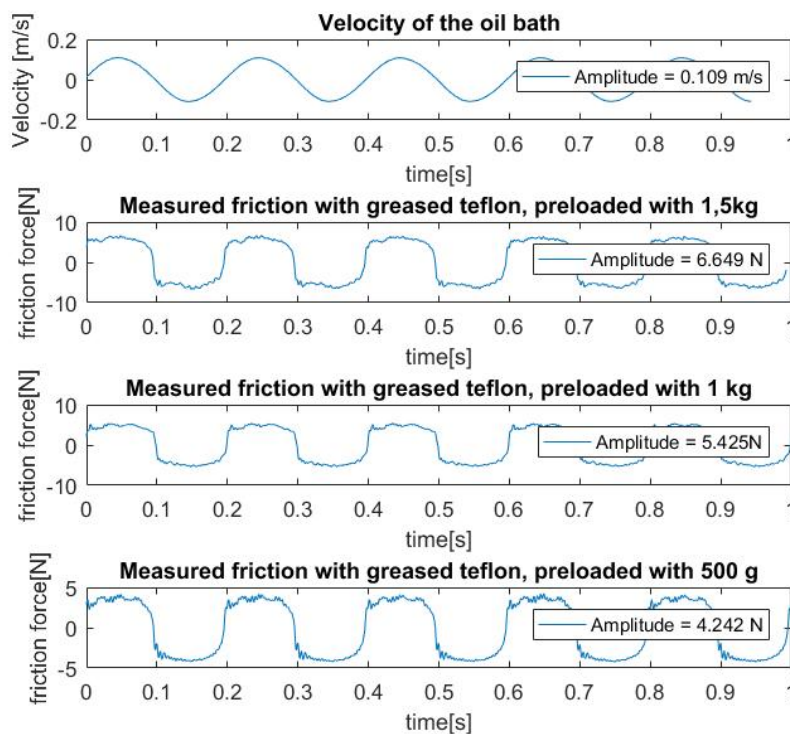


Figure 4.5: Friction force at different preloads with a sinusoidal velocity.

Results

The friction force profile is not sinusoidal as can be seen in figure 4.5. It changes between a positive and a negative value. The change occurs when the sinus of the velocity changes from sign or direction. This indicates that the friction is velocity independent. The friction also increases when the preload increases. This test indicates the occurrence of coulomb friction.

4.3.2 Test to measure friction force with filled oil bath

Measurements with a filled bath, when damping and friction occurs, show a different behavior. The sum of the friction and the damping force is, in some cases, smaller than the friction force measured in 4.3.1. This means when the bath is filled with oil, a different friction profile occurs. The friction measurements with only greased teflon bars is not representative enough. The test to determine the behavior of the friction force in section 4.3.1 needs to be repeated with a slightly filled oil bath. This gives a better approximation of the friction force in the test set-up.

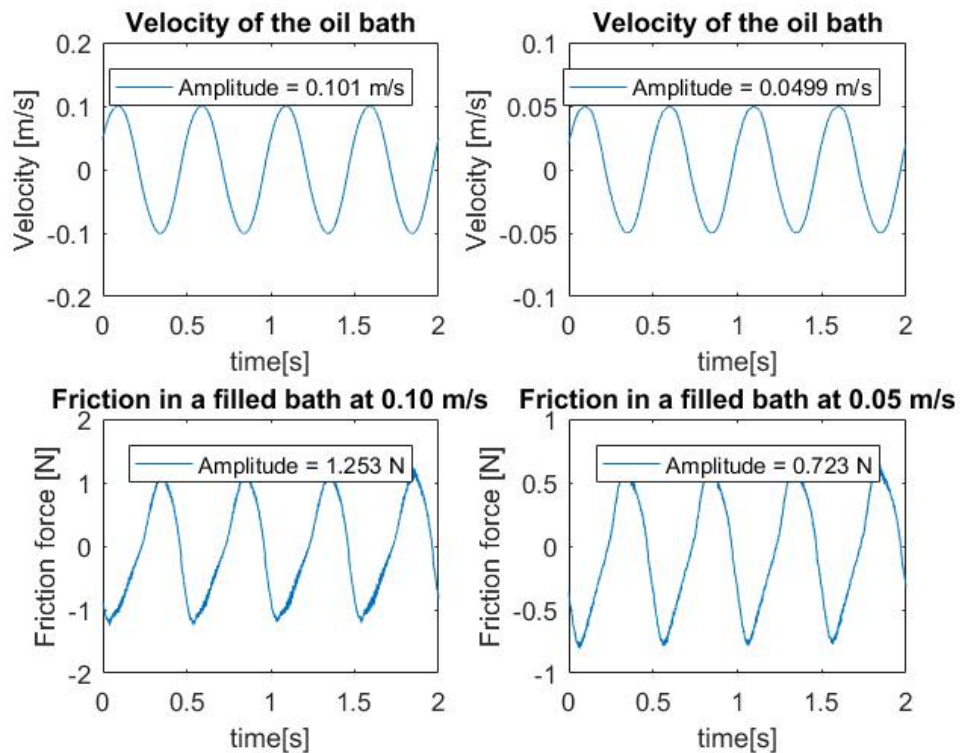


Figure 4.6: Friction force in a filled bath at a certain velocity .

Results

Figure 4.6 shows the measurement of the friction at different velocities with a constant preload of 500 gram. The friction force no longer changes between a positive and negative value but changes with increasing and decreasing velocity. The velocity dependent friction force profile can be determined with measurements at different velocities. Table 4.1 shows the occurring friction forces at certain velocities. The measured friction forces and velocities represent the amplitudes of the measured singles as shown in figure 4.6. These values are plotted in figure 4.7. The friction force seems to be linearly increasing with increasing velocity. At 0 m/s the profile approaches to a friction force of approximately 0.38 N. This force represents the velocity independent coulomb force in the system. The figure can be used to determine the friction force at a certain velocity graphically.

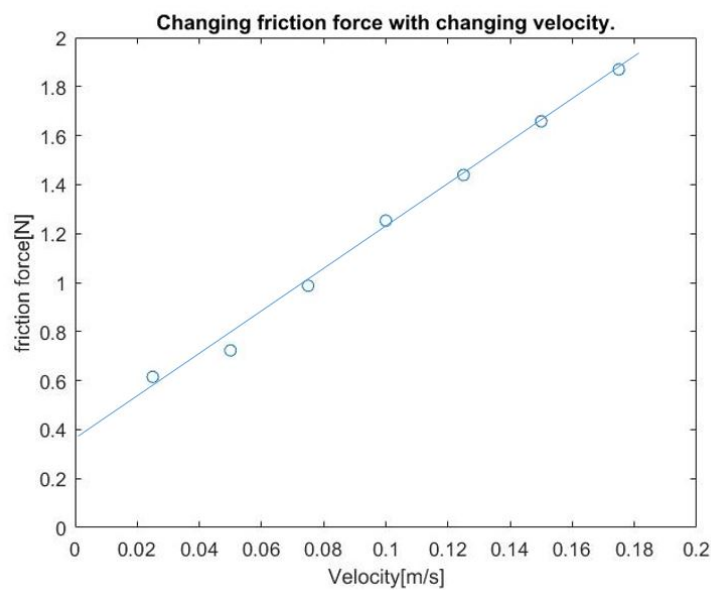


Figure 4.7: Changing friction force with changing velocity .

Velocity [m/s]	0.025	0.05	0.075	0.1	0.125	0.150	0.175
Friction force [N]	0.615	0.723	0.987	1.253	1.439	1.658	1.87

Table 4.1: Friction force at a certain velocity in a filled oil bath.

4.3.3 Dampingtests for different gap heights

The friction force of the test set-up is determined in section 4.3.2. This friction force can be subtracted from the total measured force to determine the damping force. This damping force will be determined at four different gap heights: at 40, 60, 80 and 100 micrometer. These heights will be verified using calibrated reference plates. With these measurements

4. CONCEPT TESTING

the damping force can be determined in function of the height. The damping force needs to be inversely proportional to the height as in formula 2.1.

Damping force at 40 micrometer

Figure 4.8 shows the measured force at a sinusoidal velocity with an amplitude of 0.165 m/s. The friction force can be determined using figure 4.7 and equals 1.785 newton. Formula 4.2 shows how to calculate this friction force from the measured data illustrated in figure 4.7.

$$F_{friction} = \frac{0.165 - 0.150}{0.175 - 0.150} * (1.870 - 1.658) + 1.658 = 1.785\text{N} \quad (4.2)$$

The friction force needs to be subtracted from the measured force in figure 4.8 to obtain the damping force at 40 micrometer.

$$F_{damping} = F_{measured} - F_{friction} = 7.187\text{N} \quad (4.3)$$

The real damping force obtained by equation 4.3 can be compared with the theoretical value calculated with formula 4.4.

$$F = \frac{v * \eta * A}{H} = 7.709\text{N} \quad (4.4)$$

$v = 0.165$ m/s, velocity of the oil bath.

$\eta = 1.168$ pa.s, dynamic viscosity of the omala 320 oil.

$A = 0.0016$ m², contact surface between the plates.

$H = 40$ μm , height of the gap between the plates.

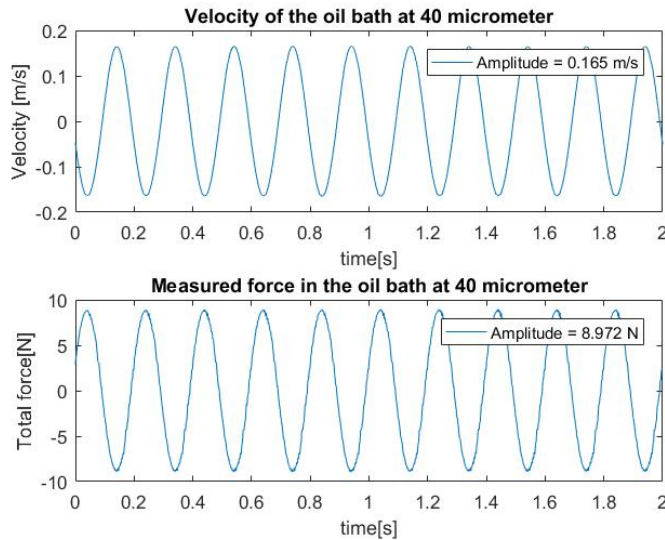


Figure 4.8: Velocity and damping force with a gap of 40 micron.

Figure 4.9 illustrates the measured force in function of the velocity. This figure indicates that the force changes linearly with changing velocity. The red curve shows the theoretical determined profile. A coulomb force of approximately 0.38 N occurs at a velocity of 0 m/s. This coulomb force was determined graphically in figure 4.7. The force changes linearly from 0.38 N to 8.97 N. The value of 8.97 N represents the force amplitude of figure 4.8. The measured profile approaches the determined profile quite good. The coulomb force of 0.38 N can not be concluded from the figure, but the measurements stay within an acceptable range.

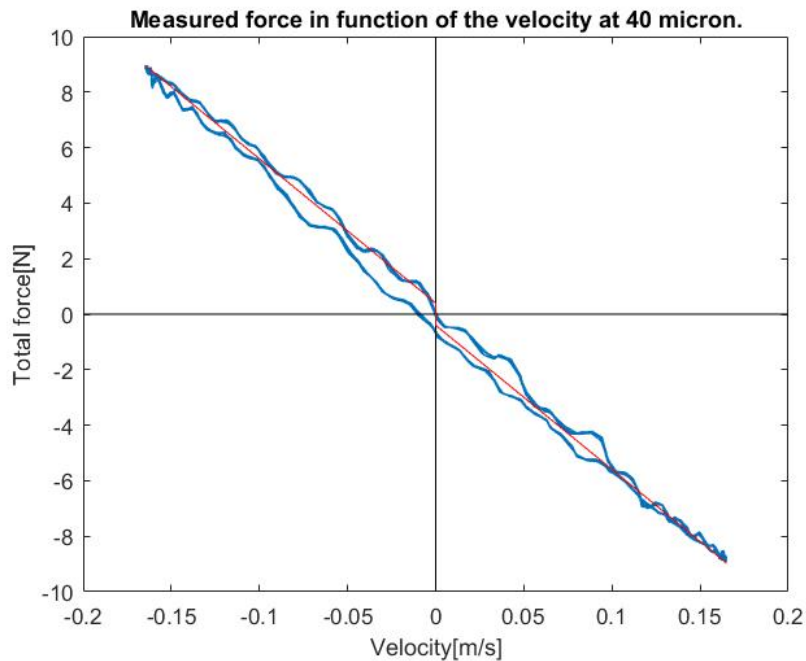


Figure 4.9: The measured force in function of the velocity at 40 micron.

The test is repeated three times to minimize the measurement errors. The average value is used to determine the relation between the damping force and the height H of the gap between the plates. Table 4.2 shows all the measurements of the three test and the average values at 40 micrometer.

	Velocity [m/s]	Theoretical force [N]	Measured force [N]
Measurement 1	0.165	7.709	7.187
Measurement 2	0.161	7.522	7.237
Measurement 3	0.160	7.475	7.410
Average	0.162	7.569	7.278

Table 4.2: Measurements of the damping force at 40 micron.

Global test results

The same procedure as in section 4.3.3 was followed at 60, 80 and 100 micrometer. All the results are attached in appendix D.

Height [μm]	Velocity [m/s]	Theoretical force [N]	Measured force [N]
40	0.162	7.569	7.278
60	0.165	5.139	5.184
80	0.161	3.761	3.886
100	0.166	3.102	3.302

Table 4.3: Summary of the average results at 40,60,80 and 100 micrometer.

Table 4.3 summarizes the average values of the tests. Figure 4.10 represents these values graphically to have a better representation of the results. The measured values are very close to the theoretical values. This indicates that the tests succeeded and the damping changes inversely proportional to the height. The small differences between the measured values and the theoretical determined values can possibly be explained by following reasons:

- Heating of the oil due to friction which slightly changes the dynamic viscosity.
- The calibrated reference plates to control the gap height H variate with 10 micrometer. This means an error of maximum 10 micrometer on the gap height H is possible.
- The calibration of the force and distance sensor can have small errors. This would not change the trends of the measurements, only the measured values themselves.
- There can be losses in the joint and the connections of the parts due to clearance.
- The occurrence of non-linear and/or non-coulomb interactions between the teflon bars and the oil bath.

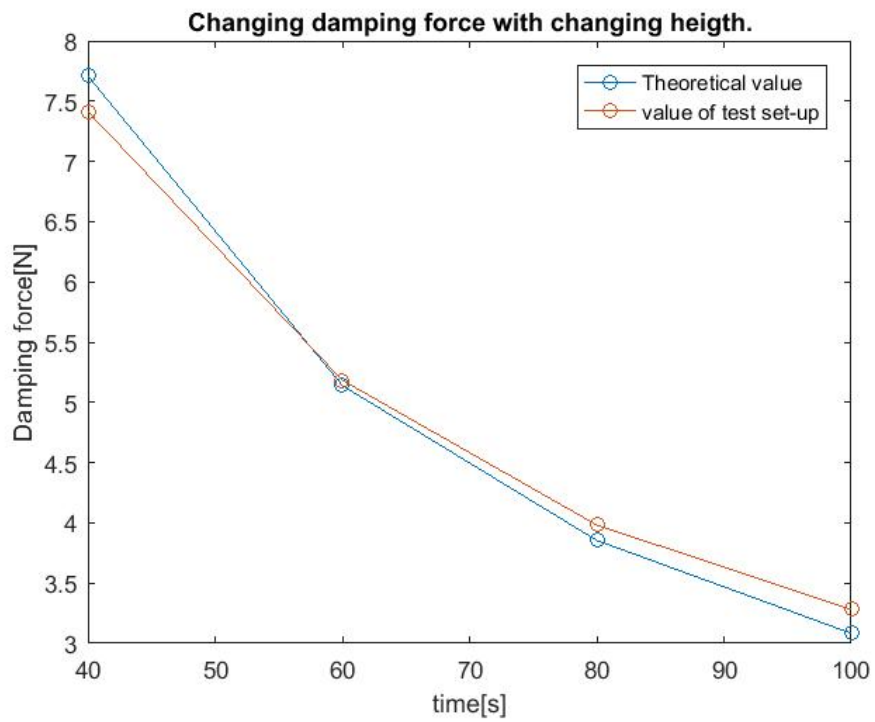


Figure 4.10: Changing damping force with changing height.

Chapter 5

Mathematical model

This chapter describes the mathematical model of the system needed to design the damper. First the stroke Δx inside the damper is calculated in function of the angle of the hand θ in section 5.1. A lot of design parameters are selected to achieve an optimal quasi linear stroke. Section 5.2 describes the determination of the system model. After linearization, the model approaches a mass - damper - spring model. The knowledge of the equivalent damping constant and the equivalent spring constant are important to optimize the functionality of the damper to the tremor frequency range. Other system parameters can be selected in function of these constants.

5.1 Transmission

This section describes the transmission between the oscillating hand and the damper. The oscillating hand needs to be dampened relative to the forearm. The damper is mounted on the forearm. This means that the rotating movement of the hand needs to be converted to a translating movement in the damper. The transmission consists of an elastic plate. Figure 5.1 visualizes this transmission for better understanding.

A much needed parameter in the calculations and the design of the damper is the stroke Δx . The stroke describes the translation of the transmission within the damper. Figure 5.1 shows two situations, one with the hand in rest at θ_0 and one with the hand under an angle $\theta = \theta_0 + \Delta\theta$. When the hand is in rest at θ_0 , the length from point A to the damper is equal to l_0 . When the hand moves up towards an angle θ , the length from point A to the damper is equal to a value l . By moving the hand towards θ part of the transmission goes into the damper. This part is called the stroke Δx and needs to be determined with equation 5.1. The length l_0 is a known design parameter but the length l needs to be calculated.

$$\Delta x = l_0 - l \tag{5.1}$$

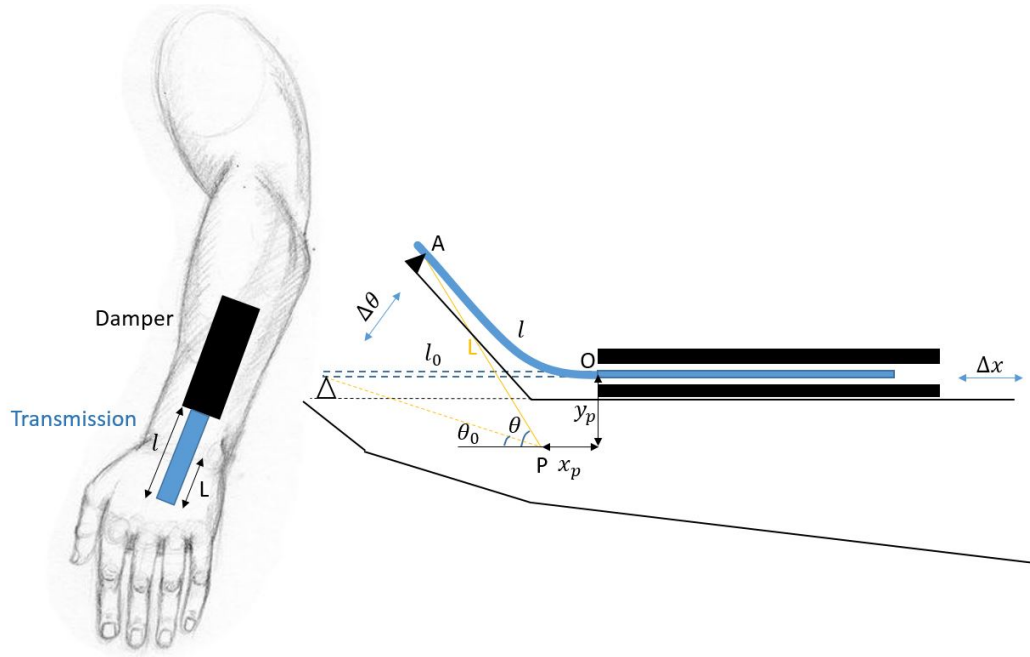


Figure 5.1: All parameters of the transmission from the hand to the forearm.

Figure 5.2 concentrates on that part of the transmission where the curvature occurs. The transmission can be separated into small segments dS . The s -axis follows the transmission starting at $S_0 = 0$ and ending at S_A . The length S_A is equal to the length of the transmission l . This parameter needs to be found to calculate the stroke Δx as illustrated in equation 5.1. Equation 5.2 shows the projection of the transmission in the horizontal direction.

$$x_p + L \cos \theta = \int_0^{S_A} \cos(\alpha) dS \quad (5.2)$$

The curvature radius, as illustrated in equation 5.3, can be written in function of a small segment dS of the transmission and the change of the angle $d\alpha$ of that segment.

$$R(s) = \frac{dS}{\sin(d\alpha)} \simeq \frac{dS}{d\alpha} \quad (5.3)$$

The curvature $\kappa = \frac{1}{R}$ is equal to zero at the end of the transmission at point A. A joint allows the transmission to rotate, this means the transmission will not bend at this point so no curvature occurs. The curvature is equal to a value C at the beginning of the transmission at point O. The transmission will bend at point O due to a clamping effect of the damper. The curvature changes linearly in function of the position S on the s -axis in the transmission. This approximation has been made due to the fact that the internal momentum changes linearly in function of S if a force at the end of the transmission is applied. The curvature is directly linked to the internal momentum, $M = EI\kappa$. With all this information the curvature of the transmission can be determined in function of the position in the transmission S on the s -axis

as shown in equation 5.4.

$$R(s) = \frac{dS}{d\alpha} = C \frac{S_A}{S_A - S} \quad (5.4)$$

Solving this equation to α gives equation 5.5.

$$\alpha = \frac{-S^2}{2CS_A} + \frac{S}{C} \quad (5.5)$$

The equation for α obtained in equation 5.5 can be used in equation 5.2 to accomplish equation 5.6.

$$x_P + L \cos \theta = \int_0^{S_A} \cos \left(\frac{-S^2}{2CS_A} + \frac{S}{C} \right) dS \quad (5.6)$$

The procedure can be repeated in the vertical direction to accomplish equation 5.7.

$$y_P + L \sin \theta = \int_0^{S_A} \sin \left(\frac{-S^2}{2CS_A} + \frac{S}{C} \right) dS \quad (5.7)$$

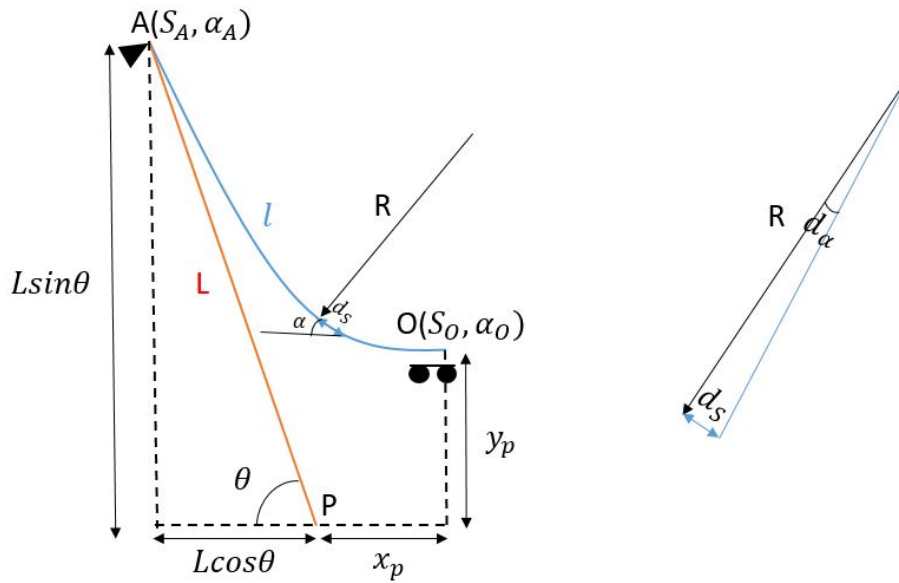


Figure 5.2: The curvature of the transmission.

Equation 5.8 represents a system of two unknown parameters C and S_A and the two equations 5.6 and 5.7. Because the unknown parameter S_A is a boundary of the integral and the difficulty of the analytic solution the system will be solved numerically.

$$\begin{cases} f(C, S_A) \\ g(C, S_A) \end{cases} = \begin{cases} x_P + L \cos \theta - \int_0^{S_A} \cos \left(\frac{-S^2}{2CS_A} + \frac{S}{C} \right) dS \\ y_P + L \sin \theta - \int_0^{S_A} \sin \left(\frac{-S^2}{2CS_A} + \frac{S}{C} \right) dS \end{cases} = \begin{cases} 0 \\ 0 \end{cases} \quad (5.8)$$

5. MATHEMATICAL MODEL

The numerical solution of S_A and C can be found using a jacobi-matrix as represented in equation 5.9.

$$\begin{bmatrix} f(C, S_A) \\ g(C, S_A) \end{bmatrix} = \begin{bmatrix} f(C_i, S_{Ai}) \\ g(C_i, S_{Ai}) \end{bmatrix} + \begin{bmatrix} \frac{df(C_i, S_{Ai})}{dC} & \frac{df(C_i, S_{Ai})}{dS_A} \\ \frac{dg(C_i, S_{Ai})}{dC} & \frac{dg(C_i, S_{Ai})}{dS_A} \end{bmatrix} * \begin{bmatrix} \Delta C \\ \Delta S_A \end{bmatrix} = \begin{bmatrix} 0 \\ 0 \end{bmatrix} \quad (5.9)$$

with:

- $\frac{df(C_i, S_{Ai})}{dC} = \frac{f(C_i + \Delta C', S_{Ai}) - f(C_i, S_{Ai})}{\Delta C'}$
- $\frac{df(C_i, S_{Ai})}{dS_A} = \frac{f(C_i, S_{Ai} + \Delta S'_A) - f(C_i, S_{Ai})}{\Delta S'_A}$
- $\frac{dg(C_i, S_{Ai})}{dC} = \frac{g(C_i + \Delta C', S_{Ai}) - g(C_i, S_{Ai})}{\Delta C'}$
- $\frac{dg(C_i, S_{Ai})}{dS_A} = \frac{g(C_i, S_{Ai} + \Delta S'_A) - g(C_i, S_{Ai})}{\Delta S'_A}$

The system 5.9 needs to be solved to ΔC and ΔS_A . In the first step C_0 and S_{A0} need to be estimated. $\Delta C'$ and $\Delta S'_A$ are small chosen variations to determine the derivative. Important to notice is that these values are not equal to ΔC and ΔS_A . The solution of equation 5.9 with the estimated values for C_0 and S_{A0} gives the first values ΔC and ΔS_A . The next values C_1 and S_{A1} can be calculated using equation 5.10.

$$\begin{aligned} C_1 &= C_0 + \Delta C \\ S_{A1} &= S_{A0} + \Delta S_A \end{aligned} \quad (5.10)$$

This procedure repeats until the values C_i and S_{Ai} , as shown in equation 5.11, for which $f(C_i, S_{Ai})$ and $g(C_i, S_{Ai})$ equal to zero are found.

$$\begin{aligned} C_i &= C_{i-1} + \Delta C \\ S_{Ai} &= S_{Ai-1} + \Delta S_A \end{aligned} \quad (5.11)$$

The final values of C_i and S_{Ai} represent the curvature at $S = 0$ and the length l . The values can be determined for every value of θ . The maximum stroke $\Delta x = l_0 - l$ can be determined by calculating the length $S_{Ai} = l$ at maximum flexion and maximum extension. Figure 5.3 illustrates flexion and extension of the hand [28].

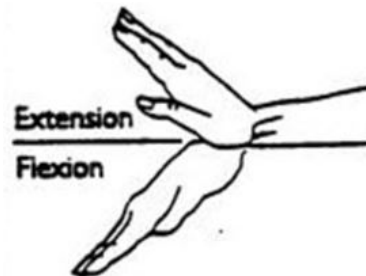


Figure 5.3: A graphical representation of flexion and extension of the hand.

Determination of the length L

Figure 5.4 shows the maximum flexion and extension stroke (left) and the total translation (right) in function of parameter L. The total translation is the distance between the maximal strokes. The numeric values of the other parameters are shown in table 5.1. The parameter L, shown in figure 5.1, can range physically between 30 mm and 80 mm. The total translation in the damper decreases if the length L increases. This is due to the fact that point A in figure 5.1 stays approximately at the same height as the entrance of the damper if L is small. The rotating transmission almost fully transmits into the damper instead of bending. A higher stroke results in a higher damping force, which is desired. For this reasoning the smallest possible length L of 30 mm should be selected. But if the length L is small, the momentum that should counteract the momentum of the tremor is small. For this reason the final length L is taken equal to the average length of about 60 mm.

Parameter	Value
θ_{flex}	$\theta_0 - 35^\circ$
θ_{ext}	$\theta_0 + 55^\circ$
L	(30mm:80mm)
x_P	15 mm
y_P	25 mm
θ_0	$\arcsin(\frac{y_P}{L}) = 30^\circ$

Table 5.1: Values of the other parameters to construct figure 5.4 .

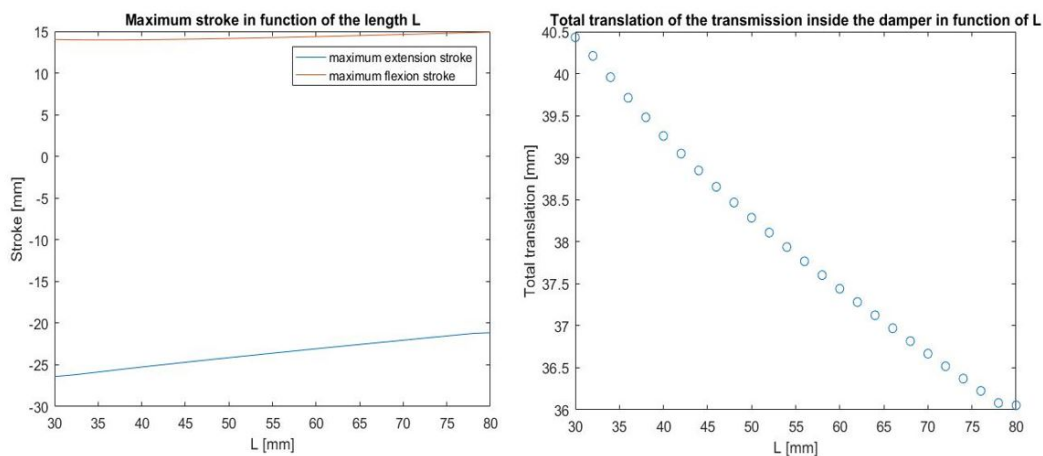


Figure 5.4: The maximum flexion and extension stroke (left) and the total translation (right) in function of parameter L.

Determination of the length x_P

A second parameter that needs to be selected is the horizontal length between the damper entrance and the wrist x_P as shown in figure 5.1. Figure 5.5 shows the maximum flexion and extension stroke inside the damper in function of parameter x_P (left) and the total translation in the damper (right). The numerical values of the other parameters are shown in table 5.2. The maximum extension stroke gives an odd value in the range of $x_P = [5 : 15]$ mm. In this range, the transmission can not bend realistically without interfering with the hand. The total translation increases if the value of parameter x_P increases. For this reason x_P should be taken as big as possible. But the dimensions of the damper are limited and the translation only increases 3mm after a value of $x_P = 25$ mm. For this reason the perfect value for x_P is equal to 25mm.

Parameter	Value
θ_{flex}	$\theta_0 - 35^\circ$
θ_{ext}	$\theta_0 + 55^\circ$
L	55 mm
x_P	[5mm:50mm]
y_P	-25 mm
θ_0	$\arcsin(\frac{y_P}{L}) = 30^\circ$

Table 5.2: Values of the other parameters to construct figure 5.4 .

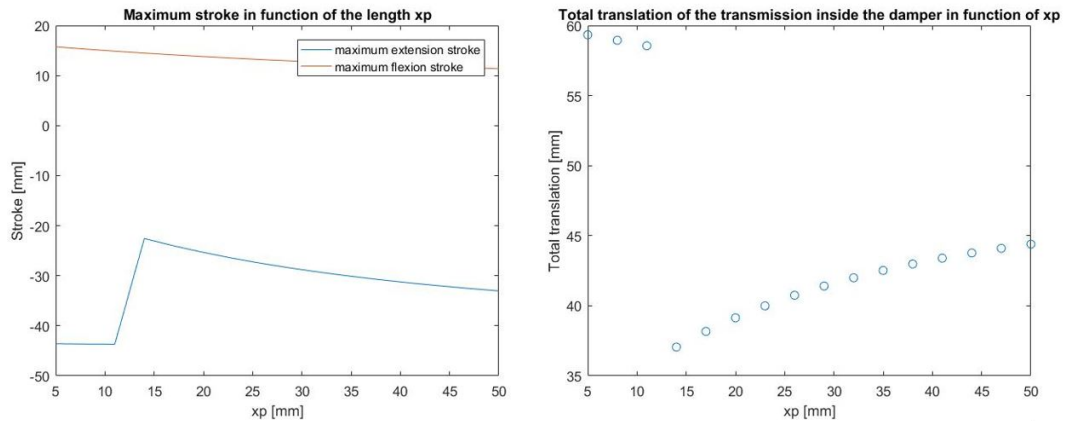


Figure 5.5: The maximum flexion and extension stroke (left) and the total translation (right) in function of parameter x_P .

Determination of the length y_P

The vertical length between the entrance of the damper and the wrist y_P should be taken as small as possible. An important specification of the system is that it needs to be wearable under the clothes. For this reason the height of the system needs to be as small as possible. The smallest possible height is 25 mm. This occurs when the damper is simply attached to

the forearm.

Final results of the stroke

Wearing the wrist brace, the hand has an average maximum extension angle of 55° and a maximum flexion angle of 35° . This means the maximum stroke in both directions differs. Figure 5.6 shows the stroke inside the damper with all the determined parameters. Table 5.3 shows all the values of the parameters of the final damper. Δx_{flex} represents the maximum stroke at a flexion of 35° . Δx_{ext} represents the maximum stroke at an extension of 55° . Δx_{total} is the total translated length within the damper between the maximal extension stroke value and the maximum flexion stroke value. The stroke is quasi linear in function of the angle θ which is ideal for damping characteristics.

Parameter	Value
L	60 mm
x_P	25 mm
y_P	-25 mm
θ_0	$\arcsin(\frac{y_P}{L}) = 24.62^\circ$
θ	$(\theta_0 - 35^\circ : \theta_0 + 55^\circ)$
Δx_{flex}	13.28 mm
Δx_{ext}	27.23 mm
Δx_{total}	40.51 mm

Table 5.3: Values of all the parameters needed for the numerical calculation of maximal extension stroke.

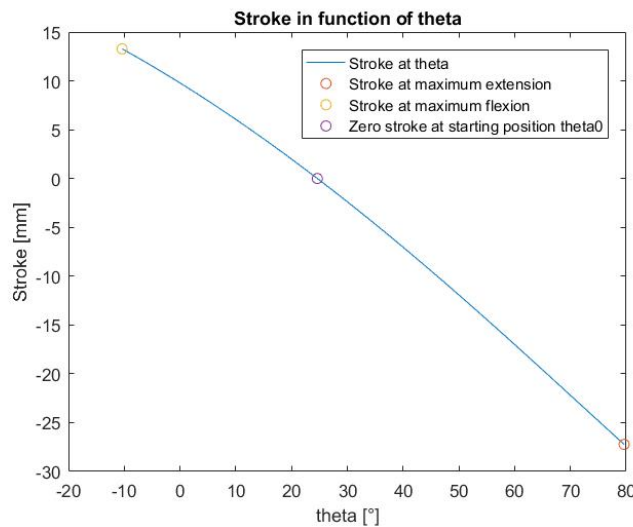


Figure 5.6: The stroke in function of theta with all the determined parameters.

The transmission profile

With the developed mathematical model, the length l of the transmission is known at every value of θ . The mathematical model was set up in function of the s -axis, an axis that follows the transmission. At every point s on the transmission a projection can be made to the x -axis and the y -axis. This procedure can be repeated for a lot of s -values. With this dataset of all the x - and y -coordinates, the profile of the transmission can be determined at every angle θ . Figure 5.7 illustrates the solution of the transmission profile at different θ between the range of maximum flexion and maximum extension. The red lines represent the transmission. The black lines represent the length from the wrist to the attachment point of the transmission and approaches the hand. As can be seen, the transmission never interferes with the hand.

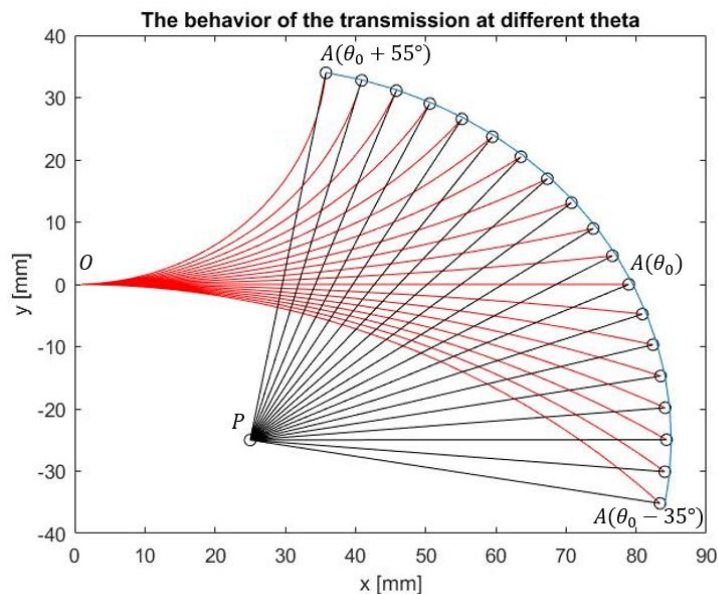


Figure 5.7: The behavior of the transmission at different theta.

5.2 System model

This section determines the full system model. This system model will be converted to a mass-damper-spring model to calculate the equivalent damper constant and the equivalent spring constant. These constants will be used to tune the system to its optimal functionality. In order to set up the system model, all the forces acting on the system need to be known. Figure 5.8 gives a graphical summary of all the forces in the system.

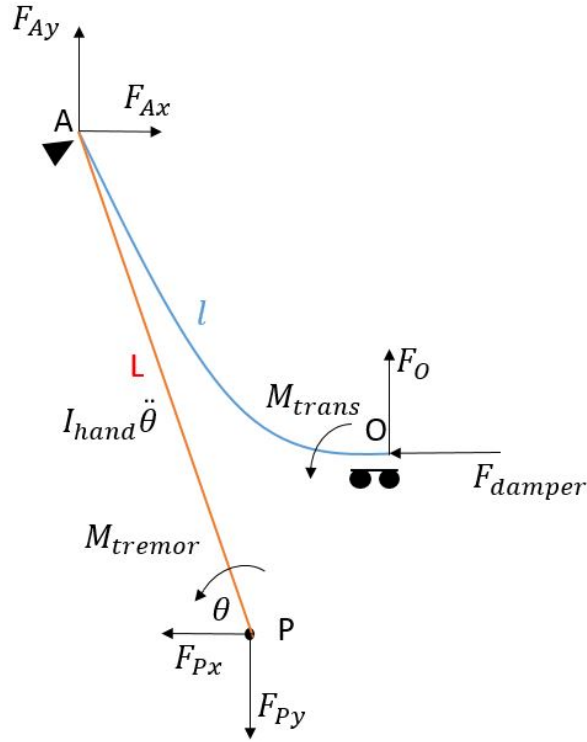


Figure 5.8: A graphical summary of all the forces in the system.

5.2.1 Initial model

At first, the system will be approached with the forearm as the reference. Only the forces on the forearm will be taken into account. These are the forces in point O and point P illustrated in figure 5.8. Equation 5.12 represents the force equilibrium of all the forces acting on the forearm in the horizontal direction. Equation 5.13 represents the same equilibrium but in the vertical direction. At last, equation 5.14 represents the momentum equilibrium.

$$\sum N : F_{Ax} = F_{damper} \quad (5.12)$$

$$\sum V : F_{Py} = F_O \quad (5.13)$$

$$\sum M(P) : I_{hand} \ddot{\theta} = M_{tremor} + M_{trans} + F_O * x_P + F_{damper} * y_P \quad (5.14)$$

- M_{tremor} = known input value
- $M_{trans} = \frac{EI}{\rho(0)}$
- $F_{damper} * y_P = \eta \frac{A}{H} \Delta x * y_P$

with:

E = Young's modulus

I = Moment of inertia

$\rho(0)$ = The curvature radius at $S=0$

η = Dynamic viscosity

A = Damping surface

H = Gap between the damping plates

$\dot{\Delta x}$ = The velocity of the transmission in the damper

The stroke Δx is already determined in section 5.1. The derivative of the stroke to the time represents the velocity inside the damper. The stroke however is formulated in function of θ . Equation 5.15 shows how to derive the derivative to the time.

$$\dot{\Delta x} = \frac{d\Delta x}{dt} = \frac{d\Delta x}{d\theta} \frac{d\theta}{dt} = \frac{d\Delta x}{d\theta} \dot{\theta} \quad (5.15)$$

The force F_O is still unknown. This force can be found by solving the system of the blue beam in figure 5.8. Equations 5.16 to 5.18 represent the equilibrium of the forces in the horizontal direction, the equilibrium of the forces in the vertical direction and the momentum equilibrium.

$$\sum N : F_{Ax} = F_{damper} \quad (5.16)$$

$$\sum V : F_{Ay} = -F_O \quad (5.17)$$

$$\sum M(O) : M_{trans} = -F_O * (x_P + L \cos \theta) + F_{Ax} * (y_P + L \sin \theta) \quad (5.18)$$

From this system of equations the unknown force F_O can be determined as shown in equation 5.19.

$$F_O = \frac{F_{Ax} * (y_P + L \sin \theta) - M_{trans}}{x_P + L \cos \theta} \quad (5.19)$$

The final system model illustrated in equation 5.20 is achieved by filling in all the determined parameters missing in equation 5.14.

$$I_{hand} \ddot{\theta} = M_{tremor} + \frac{EI}{\rho(0)} + \frac{\eta \frac{A}{H} \frac{d\Delta x}{d\theta} \dot{\theta} * (y_P + L \sin \theta) - \frac{EI}{\rho(0)}}{x_P + L \cos \theta} * x_P + \eta \frac{A}{H} \frac{d\Delta x}{d\theta} \dot{\theta} * y_P \quad (5.20)$$

5.2.2 Mass-damper-spring model

Section 5.2.1 determined the system model of the final concept. In order to tune the system for an optimal functionality, the system needs to be approached by a mass-damper-spring model represented in equation 5.21. This approached model can be analyzed using decent bode plots.

$$M_{tremor} = I_{eq} \ddot{\theta} + c_{eq} \dot{\theta} + k_{eq} * \theta \quad (5.21)$$

Linearization

The equivalent values of equation 5.21 can be determined using a linearization around θ_0 . A linearization suggests to derive the system model to $\ddot{\theta}$ to find I_{eq} , to $\dot{\theta}$ to find c_{eq} and to θ itself to find k_{eq} . Equations 5.22 to 5.24 represent these derivatives. The parameter F represents the system model in equation 5.20.

$$I_{eq} = \frac{dF}{d\ddot{\theta}} = I_{hand} \quad (5.22)$$

$$c_{eq} = \frac{dF}{d\dot{\theta}} = \eta \frac{A}{H} \frac{d\Delta x}{d\theta} * \left(\frac{(y_P + L \sin \theta)x_P}{x_P + L \cos \theta} + y_P \right) \quad (5.23)$$

$$k_{eq} = \frac{dF}{d\theta} \quad (5.24)$$

Equation 5.24 is a bit more complex to calculate because all the terms of the equation are dependent on the angle θ except for I_{hand} and M_{tremor} . It is easier to understand if all the terms are linearized separately and afterwards combined back into a final formulation.

The linearization of the first term $\frac{EI}{\rho(0)}$, illustrated in equation 5.25, is quit simple because the term is only varying with θ .

$$\frac{d\left(\frac{EI}{\rho(0)}\right)}{d\theta} = \frac{\frac{EI}{\rho(0)}[\theta_0 + \Delta\theta] - \frac{EI}{\rho(0)}[\theta_0]}{\Delta\theta} \quad (5.25)$$

The linearization of the second term is a bit more complex. The term is varying with parameter θ and $\dot{\theta}$. Equation 5.26 represents the linearization at θ_0 . The first term is equal to zero because $\dot{\theta}_0 = 0$ and the second term also vanishes because $\frac{d\dot{\theta}}{d\theta} = 0$.

$$\frac{d\left(\frac{(y_P + L \sin \theta)\eta \frac{A}{H} x_P \frac{d\Delta x}{d\theta} \dot{\theta}}{x_P + L \cos \theta}\right)}{d\theta} = \frac{d\left(\frac{(y_P + L \sin \theta)\eta \frac{A}{H} x_P \frac{d\Delta x}{d\theta}\right)}{d\theta} [\theta_0] * \dot{\theta}_0 + \frac{(y_P + L \sin \theta_0)\eta \frac{A}{H} x_P \frac{d\Delta x(\theta_0)}{d\theta}}{x_P + L \cos \theta_0} * \frac{d\dot{\theta}}{d\theta} \quad (5.26)$$

The third term is again simple because this term only varies with θ .

$$\frac{d\left(\frac{\frac{EI}{\rho(0)} x_P}{x_P + L \cos \theta}\right)}{d\theta} = \frac{\frac{EI}{\rho(0)} x_P [\theta_0 + \Delta\theta] - \frac{EI}{\rho(0)} x_P [\theta_0]}{\Delta\theta} \quad (5.27)$$

The fourth and last term is again more complex because the term also varies with θ and $\dot{\theta}$. The total equation is equal to zero for the same reason as in the second term.

$$\frac{d\left(\eta * \frac{A}{H} y_P \frac{d\Delta x}{d\theta} \dot{\theta}\right)}{d\theta} = \frac{d\left(\eta * \frac{A}{H} y_P \frac{d\Delta x}{d\theta}\right)}{d\theta} [\theta_0] * \dot{\theta}_0 + \eta * \frac{A}{H} y_P \frac{d\Delta x(\theta_0)}{d\theta} * \frac{d\dot{\theta}}{d\theta} \quad (5.28)$$

Notice that the radius of curvature $\rho(0)$ in the transmission at θ_0 is equal to infinity because their does not occur any bending at this starting position. This simplifies the final equivalent

stiffness to equation 5.29.

$$k_{eq} = \frac{\frac{EI}{\rho(0)} \left(\frac{x_p}{x_p + L \cos \theta} + 1 \right) [\theta_0 + \Delta \theta]}{\Delta \theta} \quad (5.29)$$

Determination of optimal equivalent values

The equivalent values of the desired mass-damper-spring model described in equation 5.21 need to be determined. These values are selected in order to have an optimal functionality for the tremor application. They can be determined by analyzing the bode plot of the transfer function of the mass-damper-spring model. Equation 5.30 represents the transfer function of the system. This equation is found by using a Laplace transformation on the model equation 5.21.

$$\frac{\theta}{M} = \frac{1}{I_{eq}s^2 + c_{eq}s + k_{eq}} \quad (5.30)$$

First the equivalent moment of inertia of the hand $I_{eq} = I_{hand}$ is estimated using average data of the Belgian population. The hand can be approached as a point mass at a certain distance of the wrist. The moment of inertia is equal to the mass multiplied with the squared length. The mass of the hand needs to be estimated. The average weight of the hand is 0.07% of the total weight of the body [21]. The average weight of a Belgian adult man is 79 kg and the average weight of a Belgian adult woman is 66.7 kg [1]. This means the average weight of the Belgian adult population is approximately 73 kg. The length of the wrist to the center of the mass of the hand l is estimated to be 0.07 m.

$$I_{eq} = I_{hand} = m_{averagebody} * 0.007 * l^2 = 0.0025 \text{ kgm}^2$$

The equivalent moment of inertia I_{eq} changes when the individual takes a certain mass in its hand. Figure 5.9 shows the effect of a mass ranging from 0 to 10kg. The important fact to notice is that the cut off frequency decreases with increasing mass. The cut off frequency is the frequency at which the bodeplot decreases significantly, 40dB/dec in a mass-damper-spring model. The bode plot amplitude is graphically represented on a $20 \log_{10} |H|$ -scale. This means if the amplitude decreases with 20dB, the transfer function decreases with factor 10. Or in other words, the necessary momentum needs to increase 10 times to reach the same θ in the system model of equation 5.30. This information concludes that movements at frequencies higher than the cut off frequency are suppressed significantly. So if the mass increases, movements of lower frequencies are already suppressed. To tune the system, it is better to use the smallest I_{eq} where the individual has no mass in his or her hand. This is first of all the most common scenario. But more important, by choosing I_{eq} small, the tremor at lower frequencies should be decently suppressed by choosing an optimal k_{eq} and c_{eq} .

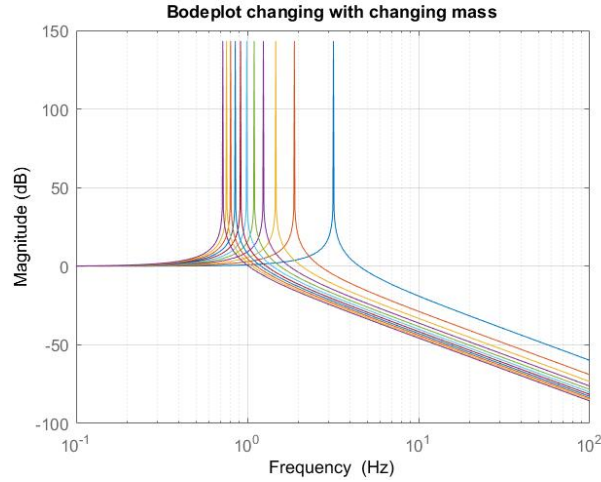


Figure 5.9: The effect of I_{eq} on the transfer function.

The selected I_{eq} is equal to 0.0025 kgm^2 , now the values for k_{eq} and c_{eq} need to be selected. Figure 5.10 shows how the stiffness K_{eq} influences the transfer function. It changes the cut off frequency as discussed in previous paragraph. But it also changes the starting bias of the transfer function. The equivalent stiffness can already suppress the voluntary rotation of the hand if the value of k_{eq} is too high. Figure 2.12 shows how the equivalent damping coefficient c_{eq} influences the transfer function. The damping coefficient is responsible for the smoothening of the resonance peak. The damping coefficient also decreases the transfer function which results in more suppression of the system. Some boundaries need to be chosen to determine the value of k_{eq} . First of all the momentum in the wrist to rotate the hand without any suppression needs to be determined. The hand has a weight of circa $m_{averagebody} * 0.007 = 511 \text{ grams}$. This results in a vertical force of 5.01 N . The length of the wrist to the center of the mass of the hand is estimated to be 0.07 m . The momentum in the wrist is equal to the vertical force times the distance to the wrist, which is 0.35 Nm . The momentum must be multiplied with a factor of 1.2 to compensate for the elastic forces of the skin and muscles and other possible forces. This means the momentum in the wrist M is estimated to be equal to 0.42 Nm . The maximum angle θ to which the hand needs to rotate is equal to the maximum extension angle of 55° or 0.96 rad . This means the voluntary movements, which mostly occur at 1 Hz , should only need a momentum of 0.42 Nm to rotate the hand to 55° . This boundary can be transformed to a decibel boundary for the bode plot:

$$\text{Boundary at } 1\text{Hz: } 20 \log_{10} \left| \frac{\theta}{M} \right| = 20 \log_{10} \left| \frac{0.96 \text{ rad}}{0.42 \text{ Nm}} \right| = 7.18 \text{ dB.}$$

A second boundary is selected based on the tremor characteristic. The tremor amplitude of a patient who suffers from Parkinson's disease has been measured in the previous master project [29]. The measured tremor amplitude was 1.5 cm which is equal to a rotational amplitude of approximately 15° or 0.262 rad . A tremor amplitude of only 1° or 0.017 rad should be acceptable for most of the activities of daily living. The momentum of tremor in the wrist is estimated to be 0.4 Nm [32]. With this knowledge, the second boundary can be determined:

5. MATHEMATICAL MODEL

Boundary at tremor frequency: $20\log_{10}\left|\frac{\theta}{M}\right| = 20\log_{10}\left|\frac{0.017\text{rad}}{0.4\text{Nm}}\right| = -27.43 \text{ dB}$.

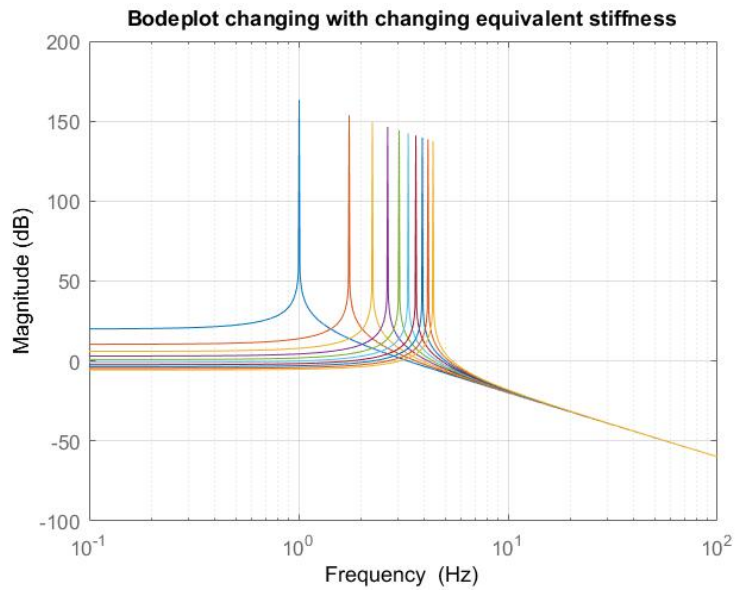


Figure 5.10: The effect of k_{eq} on the transfer function.

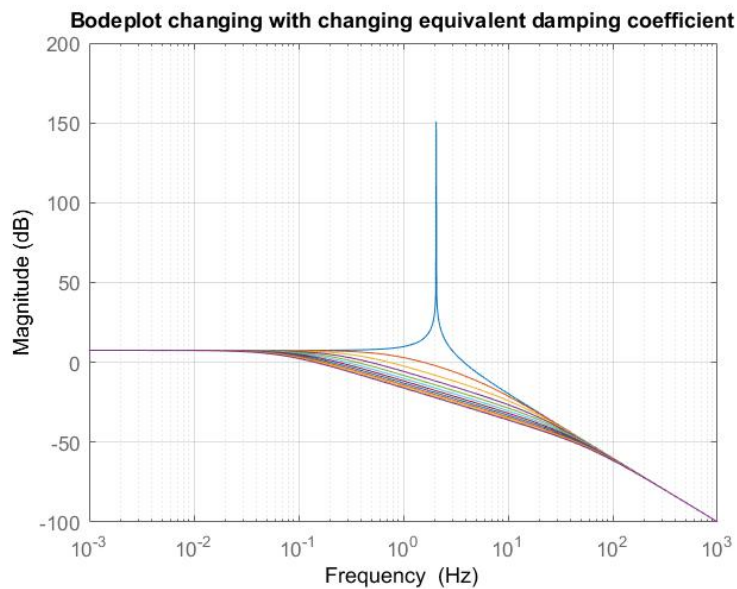


Figure 5.11: The effect of c_{eq} on the transfer function.

This thesis will focus mostly on the suppression of postural tremor and intention tremor. Postural tremor occurs at frequencies between 4 to 12 Hz. Measurements at several patients who suffer from the disease of Parkinson or who have essential tremor show that postural tremor mostly occurs at 6 Hz [18]. This means the hand may only rotate 1° with a momentum of 0.4 Nm at 6 Hz. Intention tremor occurs within a frequency range of 2 to 7 Hz. The same measurements as for the postural tremor show that intention tremor mostly occurs at 4 Hz. This means the hand may only rotate 1° with a momentum of 0.4 Nm at 4 Hz. Figure 5.12 shows the bode plot with the determined k_{eq} and c_{eq} to tune the system for the tremor application. The equivalent stiffness k_{eq} is selected to be 0.4 Nm/rad. This value makes sure the bias of the bode plot is high enough. This way the bode plot is located above boundary 1 for voluntary movements up to 1 Hz. The equivalent damping coefficient varies in a range of 0.04 Ns/m to 1 Ns/m. A damping coefficient of only 0.04 Ns/m is just enough to smoothen the resonance peak. A damping coefficient of 1 Ns/m is enough to achieve boundary 2 at 4 Hz. As can be seen in figure 5.12, the boundaries are unrealistic. The damping coefficient to achieve boundary 2 at 4 Hz already dampens the system to -16 dB at 1 Hz.

$$20\log_{10}|H| = -16\text{dB} \rightarrow H = \frac{\theta}{M} = 0.158 \frac{\text{rad}}{\text{Nm}}$$

This means a momentum of 6.08 Nm is needed to achieve the voluntary rotation of 55° which is unacceptable.

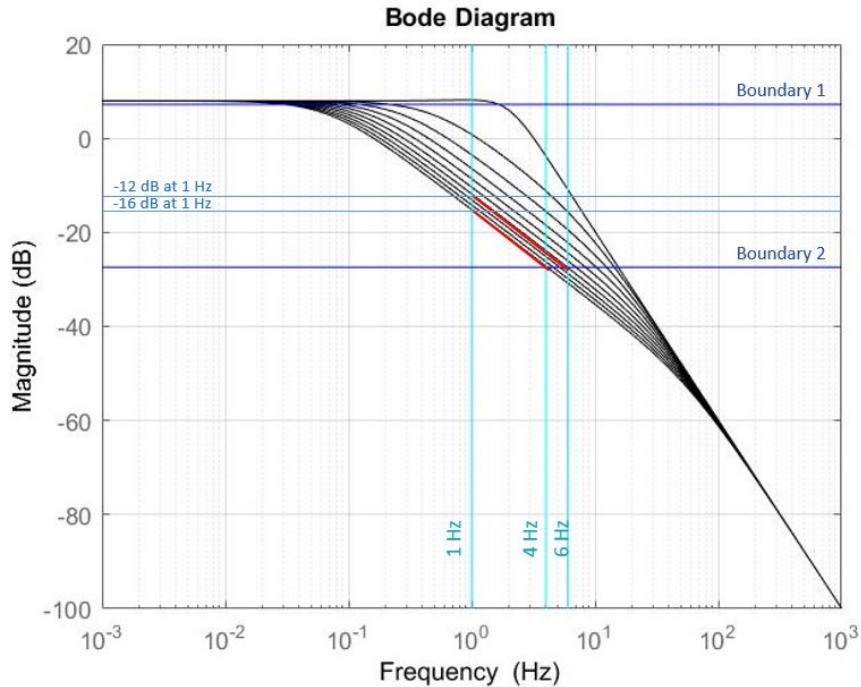


Figure 5.12: The determination of k_{eq} and c_{eq} with the chosen boundaries.

Tremor reduction [%]	Amplitude[°]	Amplitude [rad]	Decibel boundary[dB]
90	15*0.1 = 1.5	0.026	$20\log_{10}\frac{0.026}{0.4} = -23.74$
80	15*0.2 = 3	0.052	$20\log_{10}\frac{0.052}{0.4} = -17.72$
70	15*0.3 = 4.5	0.079	$20\log_{10}\frac{0.079}{0.4} = -14.09$
60	15*0.4 = 6	0.105	$20\log_{10}\frac{0.105}{0.4} = -11.62$
50	15*0.5 = 7.5	0.131	$20\log_{10}\frac{0.131}{0.4} = -9.7$

Table 5.4: Decibel boundaries for certain tremor reductions.

The boundaries need to change in order to make the system work. First off all boundary 1 needs to change. A rotation of 55° almost never occurs in normal activities of daily living. A maximal rotation of 45° or 0.785 rad should suffice for all these activities. The necessary momentum to achieve the rotation of 45° needs to increase. This means the patient will already feel a resistance at voluntary movements. This resistance should stay as small as possible. For this reason, the necessary momentum to rotate the hand should maximally increase with 20%. This results in a new boundary:

$$\text{Boundary at 1 Hz: } 20\log_{10}\left|\frac{\theta}{M}\right| = 20\log_{10}\left|\frac{0.785\text{rad}}{0.42\text{Nm}\cdot 1.20}\right| = 3.85 \text{ dB}$$

Next, the tremor suppression needs to be adjusted. Parkinson disease patients have a tremor of approximately 15° , as said before in this paragraph. A tremor amplitude of only 1° , which is a suppression of more than 90%, is not possible to achieve. The suppression of tremor with 90% should be a goal, but is currently not achieved by the tremor suppression systems described in the literature study. Functional electrical stimulation only achieved a tremor reduction of 50% [13] and 67% +/- 13% [24]. The active system using a DC motor reduced the tremor with maximum 79 % [26]. No tremor reduction records of the Kotovsky and Rosen system and the MRF damper are found. The tremor reduction can be slightly smaller than 90 % in practical applications. A tremor reduction of 80 %, with the initial tremor amplitude of 15° , results in a tremor amplitude of only $15^\circ \cdot 0.2 = 3^\circ$ or 0.052 rad. which results in following bode plot boundary:

$$\text{Boundary at tremor frequency: } 20\log_{10}\left|\frac{\theta}{M}\right| = 20\log_{10}\left|\frac{0.052\text{rad}}{0.4\text{Nm}}\right| = -17.72 \text{ dB}$$

Table 5.4 shows all the decibel boundaries who match with a certain tremor reduction relative to the initial tremor amplitude of 15° . The amplitude represents the maximal rotation of the hand at tremor frequencies.

Figure 5.13 shows the graphical determination of the equivalent constants k_{eq} and c_{eq} . The boundaries determined in table 5.4 are illustrated as well. The final equivalent stiffness k_{eq} is equal to 0.2 Nm/rad. The damping constant varies between 0.04 Ns/m and 1 Ns/m. The smoothening of the resonance peak occurs at 0.04 Ns/m. The damping is big enough to suppress the tremor amplitude to 1° at 4 Hz if the damping coefficient is equal to 1Ns/m.

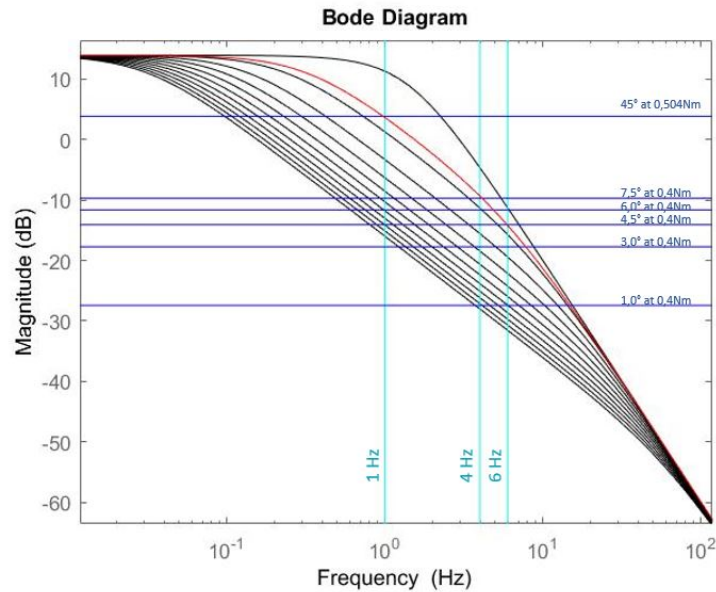


Figure 5.13: The determination of k_{eq} and c_{eq} with the chosen boundaries.

The boundary at 1 Hz, where a momentum of $0.42 \cdot 1.2 = 0.504$ Nm is necessary to rotate the hand with 45° , is approached when the damping coefficient is equal to 0.103 Ns/m. The transfer function at $c_{eq} = 0.103$ Ns/m is represented in figure 5.13 with a red line. The red line crosses the 4 Hz line of intense tremor at approximately -9.7 dB. This results in a tremor amplitude of 7.5° as can be seen in table 5.4. The intense tremor is only reduced by approximately 50%. The red line crosses the 6 Hz line of postural tremor at -14 dB. This results in a tremor amplitude of only 4.5° . This means the postural tremor will be reduced by approximately 70%. Table 5.5 shows the reduced tremor amplitude at all frequencies. Because in reality, pathological tremors occur at frequencies between 3 to 12 Hz. Essential tremor can occur in the full frequency range. Parkinson's disease tremor is limited to frequencies between 4 and 7 Hz. [18]

The tremor momentum is a constant value of 0.4 Nm, this means the tremor amplitude at 0.4 Nm can always be determined from the transfer function H. The tremor amplitude is the maximum angle to which the hand rotates. Figure 5.14 shows how the decibel boundaries for all the different frequencies are determined graphically. The boundary represents the y-value at which the frequency crosses the transfer function with a damping coefficient of 0.103 Ns/m. The reduction of tremor is the reduced tremor amplitude relative to the measured tremor amplitude of 15° of the previous master project.

The damping coefficient needs to increase if for example the tremor needs to reduce to maximal 3° at 5 Hz. By doing this the voluntary movements will need more than 0.504 Nm to achieve a rotation of 45° . This can be acceptable at voluntary activities at frequencies lower than 1 Hz. For this reason the damper is tunable. Also when the individual picks up a

5. MATHEMATICAL MODEL

Frequency [Hz]	Boundary [dB]	H [$\frac{\text{rad}}{\text{Nm}}$]	Amplitude θ [$^\circ$]	Reduction [%]
12	-24.11	0.062	1.43	90.47
11	-22.75	0.072	1.67	88.87
10	-21.32	0.086	1.97	86.87
9	-19.76	0.102	2.34	84.40
8	-18.07	0.125	2.86	80.93
7	-16.23	0.154	3.52	76.53
6	-14.21	0.195	4.47	70.20
5	-11.94	0.253	5.80	61.33
4	-9.62	0.330	7.56	49.60
3	-6.27	0.486	11.13	25.80

Table 5.5: The reduced tremor amplitude at all tremor frequencies.

glass for example. In this case the mass or the equivalent moment of inertia will increase. The bode plot will shift slightly to the right, this means less damping will be needed to obtain a certain reduction of tremor. This phenomena is illustrated in figure 5.15. The figure shows the influence of picking up a mass ranging from 0 to 10 kg. The stiffness is still 0.2 Nm/rad and the damping coefficient is still 0.103 Nm/rad. It is clear that the movements at tremor frequencies are suppressed more, this means less damping is necessary. At 4 Hz the transfer function changes from -9.62 dB (at 0 kg) to -29.79 dB (at 10 kg). This is more than enough suppression. In this case it is better to decrease the damping coefficient because the transfer function is suppressed a lot more at 1 Hz too.

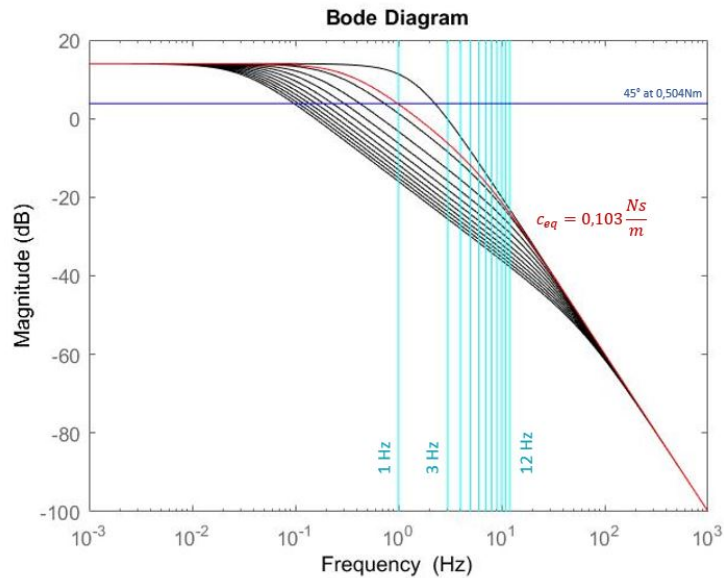


Figure 5.14: The determination of the tremor reduction at all tremor frequencies.

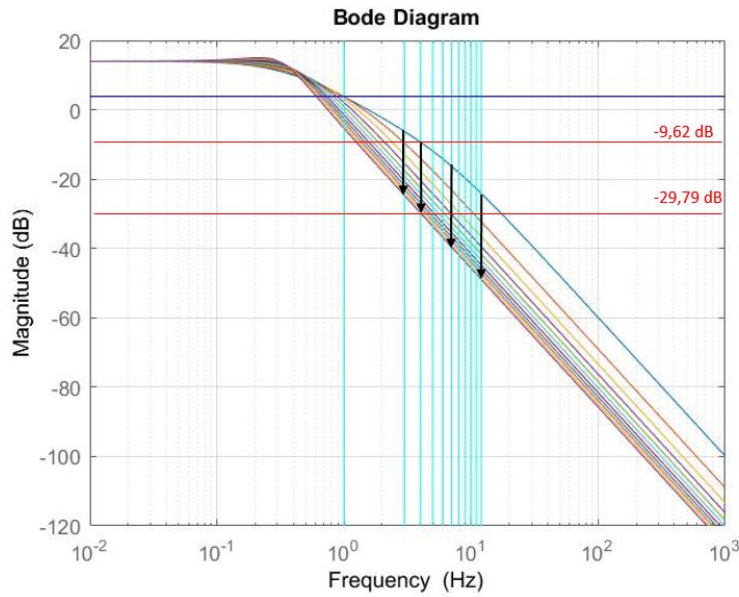


Figure 5.15: The influence on the final system of an external mass.

Determination of the other system parameters

Section 5.2.2 derived the final equations for the equivalent values in function of the system parameters $E, I, \eta, A, H, x_P, L, \theta_0$ and y_P . The parameters L, x_P, y_P and θ_0 are already determined in section 5.1. This section determines the other missing parameters shown in table 5.6.

Symbol	Parameter	Value
η	Dynamic viscosity	20 Pas
E	Young's modulus	210 GPa
I	Moment of inertia	$0.116 * 10^{-12} m^4$
x_P, y_P	Position of the wrist relative to the damper.	0.025m, -0.025m
L	The length from the wrist (P) to the attachment point (A).	0.06m
θ_0	The angle when the hand is in rest.	24.62°
A	The damping surface	$5.85 * 10^{-4} m^2$
H	The gap height between the damping plates.	[9.55 μm : 127.30 μm]

Table 5.6: A summary of all the determined values.

The first missing parameters to determine are the Young's modulus E and the moment of inertia I of the transmission. Equation 5.31 shows the formula of k_{eq} . The only unknown parameters are E and I . Consider a transmission of steel with a Young's modulus E of 210 GPa. Now the equation can be solved numerically to find the last unknown, I . The result is a moment of inertia equal to $0.0280 * 10^{-12} m^4$. The transmission needs to be as wide as possible in order to create a bigger damping surface within the damper. Because the damper

5. MATHEMATICAL MODEL

needs to fit properly on the forearm, a maximum damper width of 20 mm is chosen. For this reason, the maximal width of the transmission is 12 mm.

$$k_{eq} = \frac{\frac{EI}{\rho(0)} x_P}{x_P + L \cos \theta} [\theta_0 + \Delta \theta] - \frac{\frac{EI}{\rho(0)} x_P}{x_P + L \cos \theta} [\theta_0] + \frac{\frac{EI}{\rho(0)} [\theta_0 + \Delta \theta] - \frac{EI}{\rho(0)} [\theta_0]}{\Delta \theta} = 0.2 \frac{\text{Nm}}{\text{rad}} \quad (5.31)$$

Equation 5.32 illustrates the calculation of the final height of the transmission. The final transmission will be 12 mm width and 303 μm high, if made from steel. Calibrated height profiles of steel are available at KULeuven. A steel plate with a height of up to 550 μm was still able to bend fully elastic within the range of maximum flexion and maximum extension. This indicates that the calculated steel transmission can be used for the application.

$$I = \frac{bh^3}{12} = 0.0280 * 10^{-12} \text{m}^4 \rightarrow h = 303 \mu\text{m}. \quad (5.32)$$

Using equation 5.33, the missing parameters η and H can be determined numerically around θ_0 . The gap height H ranges between 17 to 422 μm if the dynamic viscosity is equal to 50 Pas. This range would be ideal in a practical application.

$$c_{eq} = \frac{dF}{d\dot{\theta}} = \eta \frac{A}{H} \frac{d\Delta x}{d\theta} * \left(\frac{(y_P + L \sin \theta) x_P}{x_P + L \cos \theta} + y_P \right) = [0.06 : 0.8] \frac{\text{Ns}}{\text{m}} \quad (5.33)$$

All the design parameters are now determined mathematically, the prototype can be built.

Chapter 6

Final prototype

This chapter describes the final prototype. Section 6.1 describes the final design in detail. The results of the prototype will be discussed in section 6.2. Section 6.3 describes some possible improvements.

6.1 Design

The design consist out of the damper, the transmission and the attachment to the human wrist. The design of the damper is fully explained in section 6.1.1. Section 6.1.2 describes the final design of the transmission. At last, section 6.1.3 describes how the damper is mounted on the forearm. Every section illustrates the link of the design to the mathematical determined parameters.

6.1.1 Design damper

Figure 6.1 and figure 6.2 illustrate the total design of the damper without and with the cover. The damper consists out of four main parts: the oil bath, the cover, the adjusting plate and separation plates. The technical drawings of all the parts are attached in appendix E.

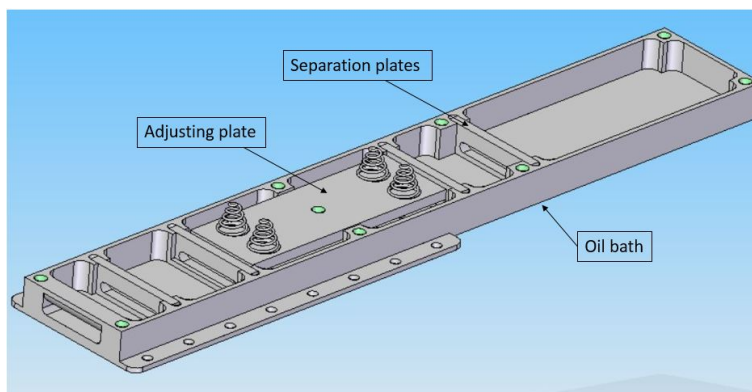


Figure 6.1: The final design of the damper without the cover.

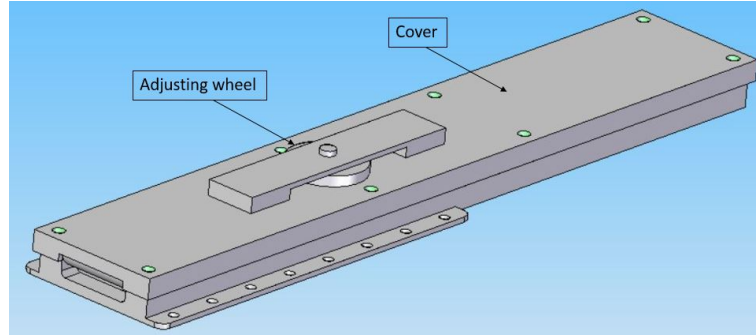


Figure 6.2: The final design of the damper with the cover.

Oil bath

The oil bath is the main part of the damper and contains an oil filled chamber, two sponge chambers and two stroke chambers. The oil filled chamber contains the viscous oil and the adjusting plate. This is where the damping happens. The sponge chambers keep the oil filled chamber water proof. Oil gets attached to the transmission when it moves through the oil filled chamber. The sponges clean the transmission and keep the oil in the chamber. The two stroke chambers are designed to give the transmission free space to move. This way the clothes will not be damaged either. Figure 6.3 illustrates the link to the mathematical model. The strokes determined in section 5.1 are used to design the length of the stroke chambers. The oil chamber is designed to the damping surface of 585 mm^2 .

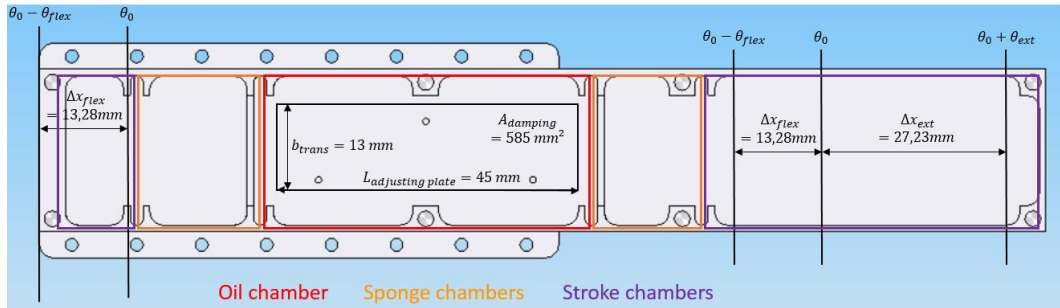


Figure 6.3: The link between the oil bath design and the determined parameters.

Cover

The cover covers the oil bath to keep the damper waterproof. An extra gasket is placed between the cover and the oil bath. The cover is mounted onto the oil bath using M3 screws.

Adjusting plate

The adjusting plate has one M3 threaded hole in the middle of the plate. The adjusting plate is 2 mm thick and an M3 thread has a pitch of $500 \mu\text{m}$. This means the plate contains four windings. An M3 screw goes through this hole. When the M3 screw turns, the adjusting

plate moves up or down. Four conical springs are attached to balance the plate. These springs make sure the adjusting plate stays parallel to the transmission as explained in section 3.2-concept 4. The adjusting plate can regulate the gap height H between 0 and 1 mm. The optimal range of 17 to 422 μm can easily be achieved by the prototype.

Seperation plate

The transmission needs to move through the damper. The separation between the oil filled chamber and the stroke chambers needs to have a groove for the transmission. It is impossible to mill the groove inside the damper. This means separation plates are made which can slide into the right places inside the damper.

Adjusting wheel

The adjusting wheel is attached to the M3 screw which adjusts the height of the adjusting plate. The adjusting wheel increases the radius of the M3 screw. This way the height of the adjusting plate can be controlled more precisely. One turn of the M3 screw is equal to a height regulation of 500 μm . This means the height regulation between 17 and 422 μm can be regulated with almost a full rotation of the screw.

Viscous oil

The viscosity was calculated to be around 50 Pas. The oil used for the damper is Rhodorsil 47V60000 silicone oil given by the department of chemical engineering. The silicone oil has a kinematic viscosity of 60000 centistokes at 25°C. The specific gravity SG of the silicone relative to water is 0.973 at 25°C. This means the density of the silicone oil is equal to 0.973 g/mm^3 . The dynamic viscosity η is equal to the multiplication of the density with the kinematic viscosity. This results in a dynamic viscosity of 58,38 Pas.

Final result of the damper

Picture 6.4 shows all the aluminum parts of the damper. Most of the parts are milled. The oil bath is made with electrical discharge machining.

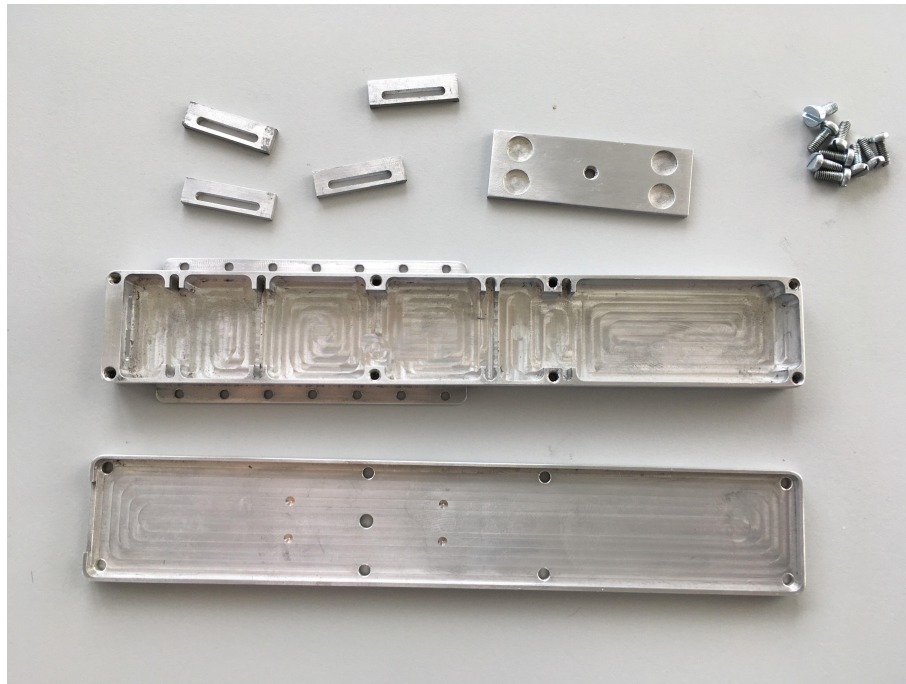


Figure 6.4: The real aluminum damper components.

6.1.2 Design of the transmission

As mentioned in section 5.2.2 - parameters, the transmission is made from steel. The dimensions of the transmission were calculated to be $b=13\text{mm}$ and $h=474\mu\text{m}$ in order to achieve the optimal functionality. The grooves of the separation plates are 2mm, this is the radius of the smallest milling tool available at KULeuven. For this reason, the transmission needs to convert to a thickness of 1.8 mm. Figure 6.5 shows the final design of the transmission. A small groove at the beginning of the transmission makes it possible to attach the transmission to the wrist brace described in section 6.1.3. The real strokes of the transmission are 21 mm at maximal extension and 7 mm at maximal flexion. These strokes are slightly smaller than the determined strokes in section 5.1. This can possibly be explained by extra bending in the transmission due to a friction force at the entrance of the damper.

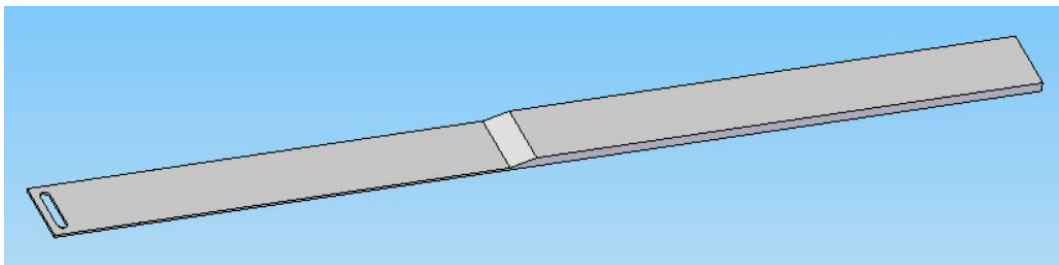


Figure 6.5: The final design of the transmission.

6.1.3 Attachment to the wrist

The damper is attached to the wrist using the bota ortho 501 wrist brace shown in figure 6.6. The wrist brace is breathable and multi-elastic. Silicone pads ensure that the brace is comfortable to wear all day. A removal elastic Velcro tightens the brace around the arm to make sure the damper stays in its position. The wrist brace should minimize the losses due to movements of the skin.



Figure 6.6: The Bota Ortho 501 wrist brace to attach the damper [11].

The damper and the transmission are sewed to the bota wrist brace. Figure 6.7 shows a picture of the damper and the transmission attached to the bota wrist brace. The damper is located at $x_P = 25$ mm in the horizontal direction and $y_P = -25$ mm in the vertical direction to the wrist. These distances were determined in section 5.1



Figure 6.7: Topview and sideview of the final prototype.

6.2 Results

The BAUMER distance sensor, described in section 4.2.1, is used to measure the damping characteristics of the prototype. A spring with a mass attached to it oscillates when an external force is applied. This is a replication of the tremor in the wrist. First the movement profile of the mass is measured without the damper attached to it. Next the spring with the mass is inserted in the wearable orthosis to measure the movement profile again. Figure 6.8 shows the measurement set-up without the orthosis (left) and with the orthosis (right).



Figure 6.8: The test without the orthosis (left) and with the orthosis (right).

The measurements of the distance sensor are sent to the dSPACE control desk to analyze the results. Figure 6.9 shows the result of the test without the orthosis. The amplitude of the oscillation barely changes. Even after 8 seconds the amplitude only decreased with approximately 0.5 mm. Figure 6.10 shows the result with the orthosis. The amplitude is fully suppressed after about 2.5 seconds. This indicates that the wearable orthosis suppresses rotational movements like tremor in the wrist. Only a small change in the response occurs by changing the damping coefficient with the height regulation. In future work, this could be tested better on the test set-up described in chapter 4.

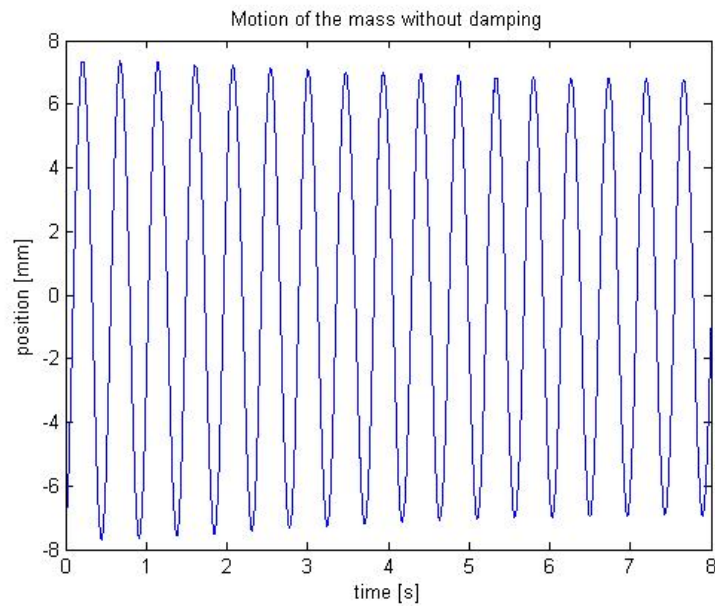


Figure 6.9: The measured movement of the mass without the orthosis.

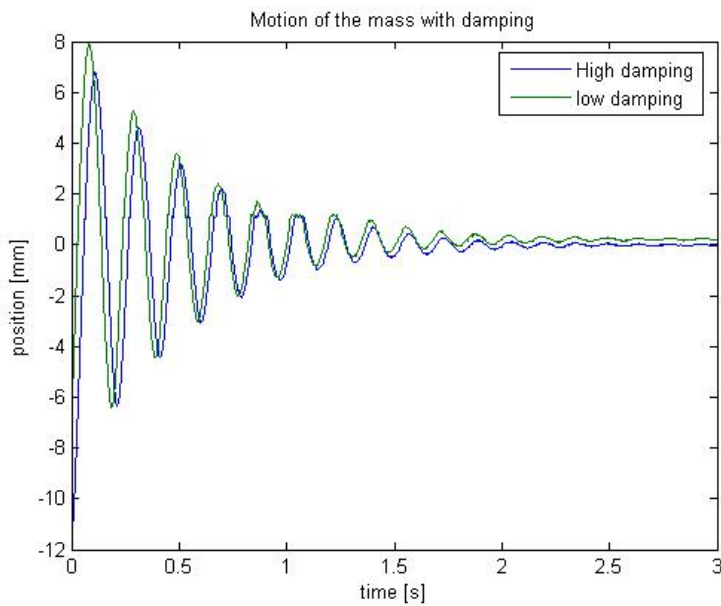


Figure 6.10: The measured movement of the mass with the orthosis.

The orthosis is also tested on Raymond Wuyts. Raymond Wuyts is a patient who suffers from Parkinson's disease. The test is a writing test with and without the orthosis. First he had to write his name and address. Next he had to draw figures. The figures he drew were a sin wave, loops, a spiral and a square spiral. Figure 6.11 shows the difference in writing his

6. FINAL PROTOTYPE

name and address. The left picture shows the writing results without the orthosis. Raymond was able to write almost two lines without tremor, at the end of line two, the tremor starts. He was not able to write his house number at the end of the sentence. He was not able to write the third line at all. The tremor was too severe. The picture in the middle shows the first results with the orthosis. Raymond was able to write all three sentences perfectly. After he wrote the sentences a special phenomena occurred. The tremor in the wrist converted to his elbow. This caused an oscillation of the full forearm. The picture on the right shows the second result with the orthosis. In this test the orthosis was not tightened with the extra Velcro and the damping coefficient was lowered using the height regulation. In this test, the tremor did not seem to convert to the elbow. Raymond was able to write the three sentences without disruptions of tremor.

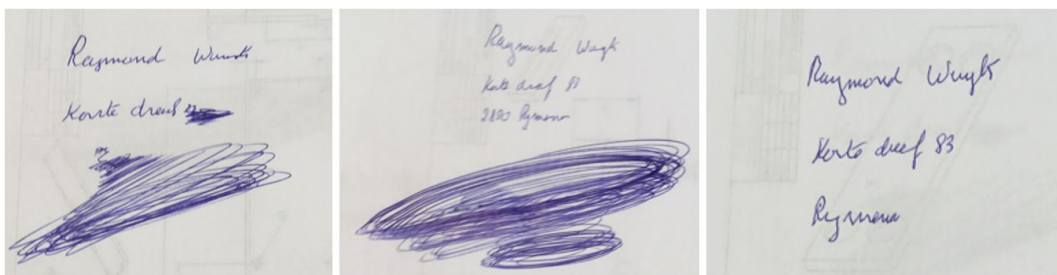


Figure 6.11: Writing the name and adress without the orthosis (left), with the tightened orthosis (middle) and with the non-tightened orthosis with reduced damping (left).

Figure 6.12 shows the difference in drawing figures without (left) and with (right) the orthosis. A tremor started at the end of the sine wave and the loops when Raymond was not wearing the orthosis. The sine wave was drawn perfectly with the orthosis, no tremor occurred at all. The amplitude of the loops decreased, as in the test without the orthosis, but no tremor occurred at the end of the loops. The wearable orthosis did not have a lot of effect on the drawings of the spiral and the squared spiral. This could be because the spirals were not drawn with wrist movements but more with the movement of the fingers. The radius of the spiral decreased with the orthosis due to the damping.

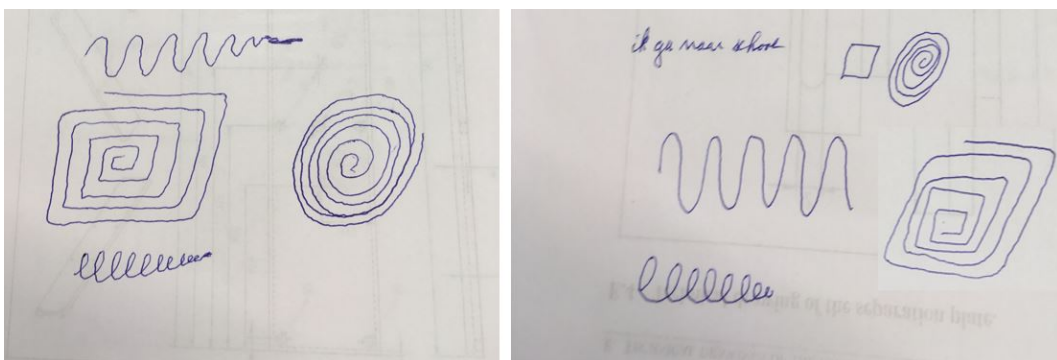


Figure 6.12: Drawing figures without the orthosis (left) and with the orthosis (right).

The full test sheets are attached in appendix F.

6.3 Improvements

This section describes all the possible improvements to optimize the concept.

- There are still many losses due to movements of the wrist brace relative to the forearm. This movements occur due to the elastic character of the skin. A decent brace needs to be build to minimize this losses. This brace should immediately contain the damper to avoid that the damper needs to be sewed to it. The brace should have a decent joint to attach the transmission properly.
- The sponge chambers are a temporary solution to keep the oil in the chamber. The oil in the sponges generates extra damping. A decent method needs to be developed to keep the product water tight. The use of rubber was considered, but is was not used for friction purposes.
- The regulation by hand can be replaced by an automated system. The semi-active dampers were not considered better than this passive system, but the functionality of a semi-active system is much better. For functionality reasons an automated height regulation can be considered. Accelerometers or gyroscopes need to measure the total motion of the hand. A decent tremor estimation algorithm as the adaptive band pass filter can estimate the tremor frequency. The automated height regulation could tune the height to suppress the tremor frequency without suppressing the voluntary movements.
- The transmission can be made from another material as steel. There could be materials with better elasticity characteristics. No time was used to search for other materials as steel.
- The concept only works for the flexion and extension of the hand. The hand is not able to deviate. Deviation of the hand is the rotation to the left or the right. The transmission needs to be redesigned to keep the optimal moment of inertia in the flexion-extension direction but to make movements in the deviation direction also possible.

Chapter 7

Conclusion

The final developed concept is a passive flat plate damper with height regulation. This concept was tested on a test set-up with success. The test set-up indicated a good force behavior with changing height. The final prototype could not be tested to determine if the height regulation of the prototype results in the same force behavior as in the test set-up. In future work, the concept can be fully tested using the test set-up described in chapter 4. Due to time issues, the final prototype was tested using a less complex test set-up. This simplified test, described in section 6.2, indicated that an oscillating hand can be dampened with the orthosis. The prototype was also tested with a writing test by Raymond Wuyts, a Parkinson's disease patient. The final results showed that the orthosis had a positive impact on his writing skills. With the right tuning, the tremor did no longer disturb the writing of sentences. He was also able to write the sentences faster. This indicates that the orthosis is able to reduce tremor in the wrist. The tremor did have the tendency to convert from the wrist to the elbow if the orthosis was tightened too much to the forearm and if the damping coefficient was too high. With a decent fine tuning of the damper, this phenomena seemed to disappear. In future research, the concept can be fully tested with a broad range of Parkinson's disease patients or people who have essential tremor. These patients should execute a broad range of activities of daily living with and without the orthosis. This way the orthosis can be decently characterized by using accelerometers or gyroscopes. One sensor should be placed on the hand and one sensor should be placed on the forearm. This way the tremor in the wrist can be measured at both situations. As said before, the orthosis already had a remarkable impact on the writing skills of the patient and reduces the tremor, but improvements still need to be made. The sponge chambers absorb a lot of the viscous oil, this adds a significant amount of damping to the final system. Another method needs to be used to contain the oil in the oil chamber. The attachment to the wrist with the bota otho 501 wrist brace is not very efficient. The transmission can still move when fully dampened because of the flexibility of this wrist brace. The attachment could be 3D-printed for better results. At last the flexibility of the skin causes some losses of the damping too. Connecting the 3D-printed attachment around the fingers could possibly solve this issue.

Bibliography

- [1] Belgians average in height and weight. <http://www.expatica.com/be/news/Belgians-average-in-height-and-weight>, 3 April 2007.
- [2] Deep brain stimulation. <http://neurosurgery.uthscsa.edu>.
- [3] Myoware muscle sensor. <https://shop.pimoroni.com/products/myoware-muscle-sensor>.
- [4] Othotics. <https://en.wikipedia.org/wiki/Orthotics>, Last edited: 13 May 2017.
- [5] Prolopa 250 bijsluiter. <https://www.medibib.be/producten/prolopa-250-200-mg-50-mg-100-tabletten>.
- [6] Requip modutab 8 mg bijsluiter. <https://www.medibib.be/producten/requip-modutab-8-mg-84-tabletten>.
- [7] Understanding er fluids and their properties. www.smarttec.co.uk.
- [8] Globus pallidus. <https://en.wikipedia.org/wiki/Globuspallidus>, Last edited: 27 May 2017.
- [9] G. F. W. Anne C. Poinier. Pallidotomy for parkinson's disease. <http://www.webmd.com/parkinsons-disease/pallidotomy-posteroventral-pallidotomy-for-parkinsons-disease>, 20 Feb 2015.
- [10] G. F. W. Anne C. Poinier. Thalamotomy for parkinson's disease. <http://www.webmd.com/parkinsons-disease/thalamotomy-for-parkinsons-disease>, 20 Feb 2015.
- [11] D. J. ANTIPUESTO. Electromyography (emg). <http://nursingcrib.com/nursing-notes-reviewer/medical-surgical-nursing/electromyography-emg/>, 7 March 2011.
- [12] Y. Bar-Cohen. *Electroactive polymer (EAP) actuators as artificial muscles: reality, potential, and challenges*, volume 136. SPIE press, 2004.
- [13] J.-S. Brittain, P. Probert-Smith, T. Z. Aziz, and P. Brown. Tremor suppression by rhythmic transcranial current stimulation. *Current Biology*, 23(5):436–440, 2013.
- [14] D. G. Caldwell, G. A. Medrano-Cerda, and M. Goodwin. Control of pneumatic muscle actuators. *System*, 4:20–0, 1995.

- [15] D. Case, B. Taheri, and E. Richer. Design and characterization of a small-scale magnetorheological damper for tremor suppression. *IEEE/ASME Transactions on mechatronics*, 18(1):96–103, 2013.
- [16] J. Caswell. When stroke hits the thalamus. <http://strokeconnection.strokeassociation.org>, 2015.
- [17] A. L. Elaimy, J. J. Demakas, B. J. Arthurs, B. S. Cooke, R. K. Fairbanks, W. T. Lamoreaux, A. R. Mackay, D. R. Greeley, and C. M. Lee. Gamma knife radiosurgery for essential tremor: A case report and review of the literature. *World journal of surgical oncology*, 8(1):20, 2010.
- [18] J. A. Gallego, E. Rocon, J. O. Roa, J. C. Moreno, and J. L. Pons. Real-time estimation of pathological tremor parameters from gyroscope data. *Sensors*, 10(3):2129–2149, 2010.
- [19] G. Grimaldi and M. Manto. Neurological tremor: Sensors, signal processing and emerging applications. *Sensors*, 10(2):1399–1422, 2010.
- [20] M. J. R. Jack Kotovsky, MS. A wearable tremor-suppression orthosis. *Journal of Rehabilitation Research and Development*, 35(4):373–378, 1998.
- [21] R. H. Krishnan, V. Devanandh, A. K. Brahma, and S. Pugazhenthii. Estimation of mass moment of inertia of human body, when bending forward, for the design of a self-transfer robotic facility. *J. Eng. Sci. Technol*, 11(2):166–176, 2016.
- [22] J. Lazarus. Deep brain stimulation. <http://www.parkinson.org/understanding-parkinsons/treatment/surgery-treatment-options/Deep-Brain-Stimulation>.
- [23] R. C. Loureiro, J. M. Belda-Lois, E. R. Lima, J. L. Pons, J. J. Sanchez-Lacuesta, and W. S. Harwin. Upper limb tremor suppression in adl via an orthosis incorporating a controllable double viscous beam actuator. In *Rehabilitation Robotics, 2005. ICORR 2005. 9th International Conference on*, pages 119–122. Ieee, 2005.
- [24] L. P. Maneski, N. Jorgovanović, V. Ilić, S. Došen, T. Keller, M. B. Popović, and D. B. Popović. Electrical stimulation for the suppression of pathological tremor. *Medical & biological engineering & computing*, 49(10):1187, 2011.
- [25] K. A. Mann, F. W. Wernere, and A. K. Palmer. Frequency spectrum analysis of wrist motion for activities of daily living. *Journal of Orthopaedic research*, 7(2):304–306, 1989.
- [26] M. Manto, E. Rocon, J. Pons, J. M. Belda, and S. Camut. Evaluation of a wearable orthosis and an associated algorithm for tremor suppression. *Physiological measurement*, 28(4):415, 2007.
- [27] M. Manto, E. Rocon, J. Pons, J. M. Belda, and S. Camut. Evaluation of a wearable orthosis and an associated algorithm for tremor suppression. *Physiological measurement*, 28(4):415, 2007.

- [28] J. Martin. How biomechanists define movements. *http://jeffygolf.com*, 28 Feb 2012.
- [29] R. S. Mattias Van Den Borre. Starting project to develop an orthotic tremor reduction system: Theoretical approach and proof of principle. 2016.
- [30] R. Nava, M. Ponce, L. Rejon, S. Viquez, and V. Castano. Response time and viscosity of electrorheological fluids. *Smart materials and structures*, 6(1):67, 1997.
- [31] L. Z. Popović, T. B. Šekara, and M. B. Popović. Adaptive band-pass filter (abpf) for tremor extraction from inertial sensor data. *Computer methods and programs in biomedicine*, 99(3):298–305, 2010.
- [32] A. Pruski and H. Knops. Estimation of biomechanical characteristics of tremorous movements based on gyroscopes1. *Assistive Technology: From Virtuality to Reality: AAATE 2005*, 16:138, 2005.
- [33] S. Skaarup, L. Bay, and K. West. Polypyrrole actuators working at 2–30hz. *Synthetic metals*, 157(6):323–326, 2007.
- [34] W. Wen, X. Huang, and P. Sheng. Electrorheological fluids: structures and mechanisms. *Soft Matter*, 4(2):200–210, 2008.

Appendices

Appendix A

Design of experiments

A.1 Framework to determine the friction force

The teflon bars which separate the upper plate from the bottom plate create friction. This friction needs to be subtracted from the measured force to obtain the damping force. The friction between the teflon bar and the steel bottom plate is not a good approximation of the friction force. The viscous oil will act as a lubrication which decreases the friction force. For this reason the teflon bars are greased with the viscous oil. The friction force needs to be measured at different preloads and different velocities to estimate the full friction behavior. Table A.1 shows the framework for this experiment.

Velocity [m/s]	Friction force [N] (preloading 500g)	Friction force [N] (preloading 1kg)	Friction force [N] (preloading 1.5kg)
0.025			
0.05			
0.075			
0.1			
0.125			
0.150			
0.175			

Table A.1: Framework to determine the friction force.

A.2 Framework to determine the relationship between the damping force and the height of the gap

The friction force is determined using the framework described in section A.1. The damping force can now be calculated as the measured force minus the determined friction force. This value can be compared with the theoretical damping force to determine if the inversely linear relationship between the height and the damping force is acceptable. The measurement at each height is repeated three times to minimize the measurement errors. The average values at all the different heights can be used to determine the relationship between the damping force and the height. The velocity needs to be approximately constant. The framework for all the necessary measurements is shown in table A.2.

		Velocity [m/s]	Theoretical force[N]	Measured force [N]
40 micrometer	Measurement 1:			
	Measurement 2:			
	Measurement 3:			
Average:				
60 micrometer	Measurement 1:			
	Measurement 2:			
	Measurement 3:			
Average:				
80 micrometer	Measurement 1:			
	Measurement 2:			
	Measurement 3:			
Average:				
100 micrometer	Measurement 1:			
	Measurement 2:			
	Measurement 3:			
Average:				

Table A.2: Framework to determine the relationship between the damping force and the height of the gap.

Appendix B

Calibration of the sensors

This appendix describes the calibration of the distance sensor and the force sensor used in the test set-up.

B.1 Calibration of the force sensor

This section describes the calibration of the force sensor. A device is used that can measure the mass. The device is attached to the force sensor. If an individual pulls the device with a certain force, the force is displayed as a mass. The voltage of the force sensor is displayed using the simulink program in appendix C. Table B.1 shows all the necessary data for the calibration. The data is collected five times and averaged to minimize the measurement errors.

Newton [N]	Voltage [V]	Calibration factor K [N/V]
30	0.3	100
18	0.15	120
22	1.2	110
26	0.22	118.2
21	0.18	116.7

Table B.1: Measurements for the calibration of the force sensor.

Which gives following final calibration factor:

$$K_{force} = \frac{100+120+110+118.2+116.7}{5} = 113N/V$$

B.2 Calibration of the distance sensor

This section describes the calibration of the distance sensor. The distance sensor always measures relative to its begin position. The begin position can always vary with a couple of millimeters. For this reason the simulink program first measures the begin position as

B. CALIBRATION OF THE SENSORS

a bias. Afterwards the oil bath can move from a known position 1 to a known position 2. The change in voltage in function of the change in distance represents the calibration factor $K_{Distance}$. The calibration factor is always the same, but the distance bias changes every measurement. The calibration factor $K_{Distance}$ is measured four times relative to the begin position and averaged to minimize the measurement errors.

$$Distance = bias + K_{distance} * voltage$$

Distance [mm]	Voltage [V]	$K_{Distance}$
29.76	0	/
40	0.260	39.38
50	0.502	40.31
60	0.754	40.11
70	0.987	40.77

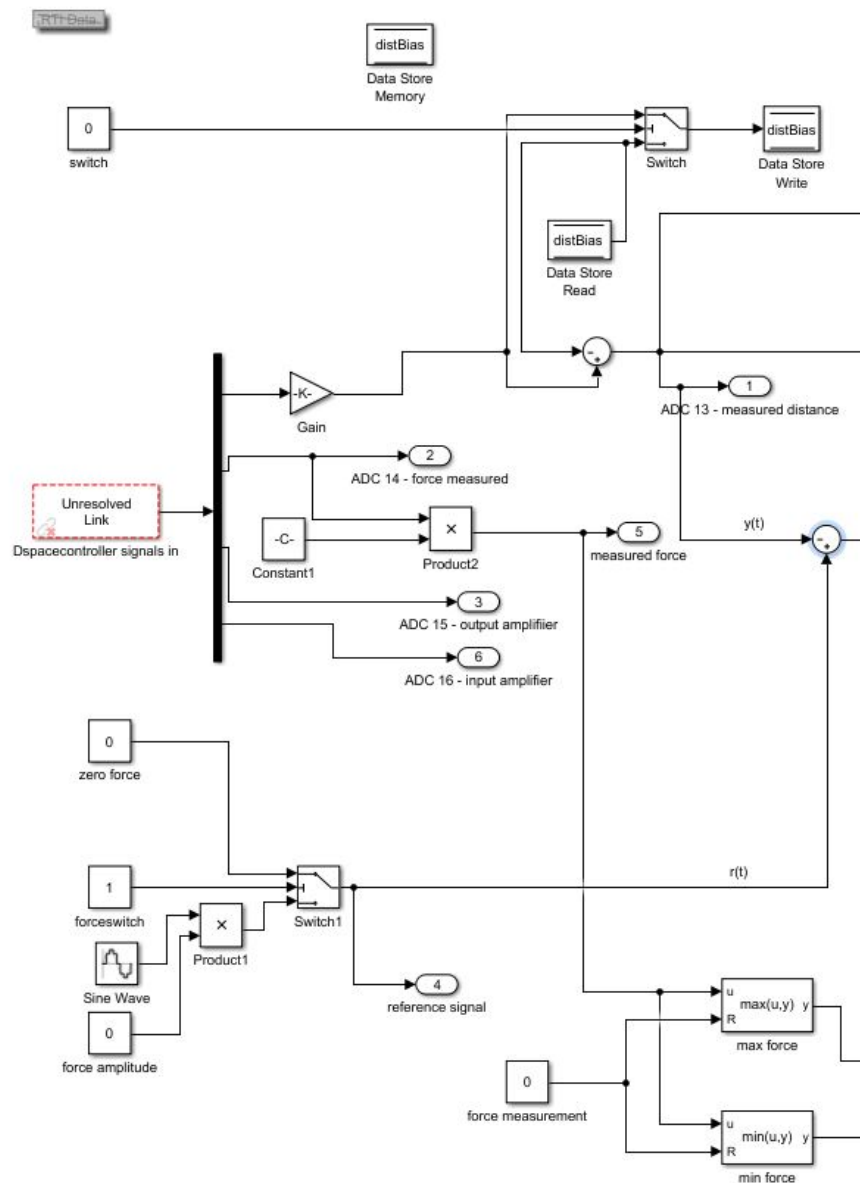
Table B.2: Measurements for the calibration of the distance sensor

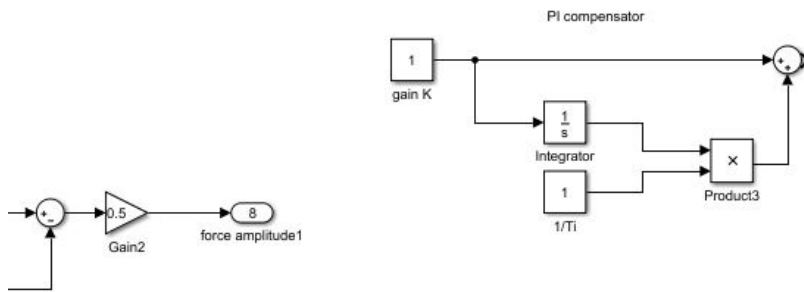
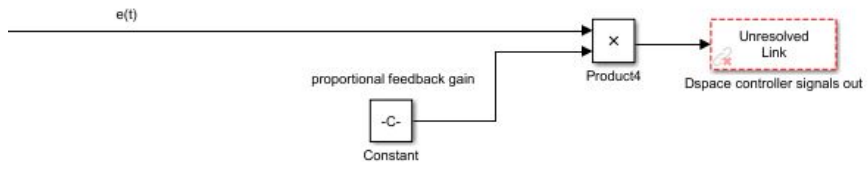
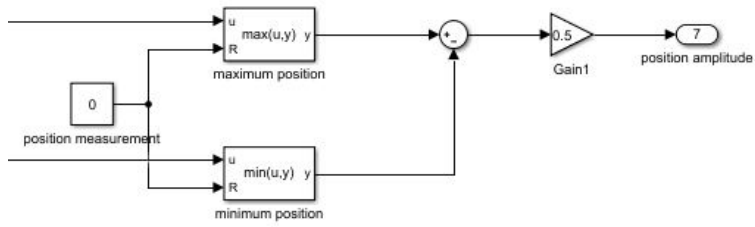
Which gives following final calibration factor:

$$K_{Distance} = \frac{39.38+40.31+40.11+40.77}{4} = 40.14mm/V$$

Appendix C

Simulink program to control the test set-up





Appendix D

Testresults at 60, 80 and 100 micron

D.1 Damping force at 60 micrometer

The dataset at 60 micrometer was too short to make a proper graphical representation. Table D.1 displays the different measurements and theoretical values of the damping force at 60 micron. These values are averaged to minimize measurement errors.

	Velocity [m/s]	Theoretical force [N]	Measured force [N]
Measurement 1	0.163	5.077	5.220
Measurement 2	0.167	5.201	5.427
Measurement 3	0.165	5.139	4.905
Average	0.165	5.139	5.184

Table D.1: Measurements of the damping force at 60 micron.

D.2 Damping force at 80 micrometer

Figure D.1 shows the measured force at a sinusoidal velocity with an amplitude of 0.150 m/s. Figure 4.7 shows the exact friction force without using any interpolation. The friction force is equal to 1.658 N. The friction force needs to be subtracted from the measured force in figure D.1 to obtain the damping force at 80 micrometer.

$$F_{damping} = F_{measured} - F_{friction} = 3.356\text{N} \quad (\text{D.1})$$

The real damping force obtained by equation D.1 can be compared with the theoretical value calculated using formula D.2.

$$F = \frac{v * \eta * A}{H} = 3.504\text{N} \quad (\text{D.2})$$

D. TESTRESULTS AT 60, 80 AND 100 MICRON

$v = 0.150$ m/s Velocity of the oil bath.

$\eta = 1.168$ pa*s Dynamic viscosity of the omala 320 oil.

$A = 0.0016$ m² Contact surface between the plates.

$H = 80$ μ m Height of the gap between the plates.

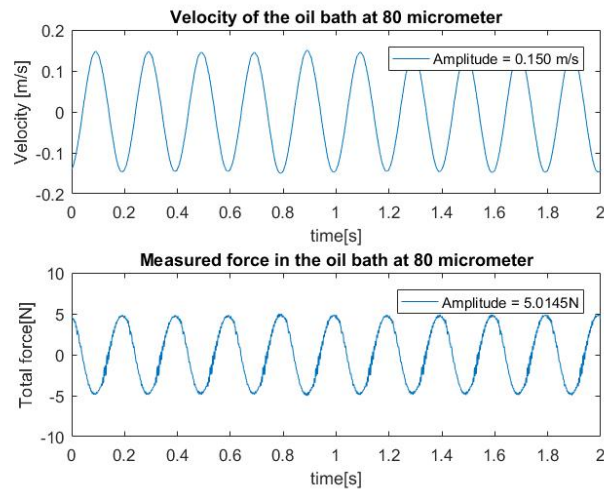


Figure D.1: Velocity and damping force with a gap of 80 micron.

Figure D.2 shows the measured force in function of the velocity. The force seems to be linear in function of the velocity. The coulomb force at a velocity of 0 m/s is difficult to determine graphically due to the deviations. The approximated value of 0.38N as determined in figure 4.7 seems to be in the range of the real value.

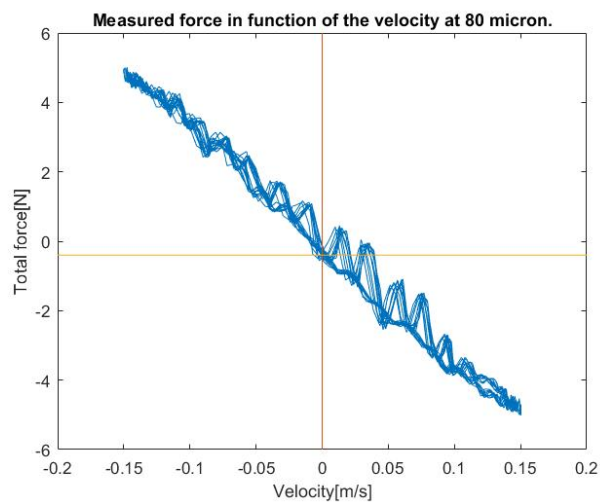


Figure D.2: The measured force in function of the velocity at 80 micron.

The test is repeated three times to minimize the measurement errors. The average value is used to determine the relation between the damping force and the height H of the gap between the plates. Table D.2 shows all the measurements of the three tests and the average values at 80 micrometer.

	Velocity [m/s]	Theoretical force [N]	Measured force [N]
Measurement 1	0.169	3.948	4.346
Measurement 2	0.150	3.504	3.356
Measurement 3	0.163	3.808	3.956
Average	0.161	3.761	3.886

Table D.2: Measurements of the damping force at 80 micron.

D.3 Damping force at 100 micrometer

Figure D.3 shows the measured force at a sinusoidal velocity with an amplitude of 0.177 m/s. The friction force can be determined using figure 4.7 and equals 1.887 newton. Formula D.3 shows how to calculate this friction force from the measurement data of figure 4.7.

$$F_{friction} = \frac{0.177 - 0.150}{0.175 - 0.150} * (1.870 - 1.658) + 1.658 = 1.887N \quad (D.3)$$

The friction force needs to be subtracted from the measured force in figure D.3 to obtain the damping force at 100 micrometer.

$$F_{damping} = F_{measured} - F_{friction} = 3.019N \quad (D.4)$$

The real damping force obtained by equation D.4 can be compared with the theoretical value calculated using formula D.5.

$$F = \frac{v * \eta * A}{H} = 3.308N \quad (D.5)$$

v = 0.177 m/s Velocity of the oil bath.

η = 1.168 pa*s Dynamic viscosity of the omala 320 oil.

A = 0.0016 m² Contact surface between the plates.

H = 100 μ m Height of the gap between the plates.

D. TESTRESULTS AT 60, 80 AND 100 MICRON

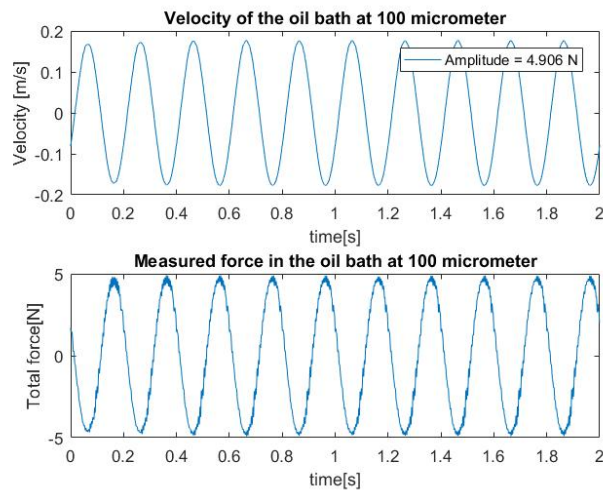


Figure D.3: Velocity and damping force with a gap of 100 micron.

Figure D.4 shows the measured force in function of the velocity. The force seems to be linear in function of the velocity. The coulomb force at a velocity of 0 m/s is difficult to determine graphically due to the deviations. The approximated value of 0.38N as determined in figure 4.7 seems to be in the range of the real value.

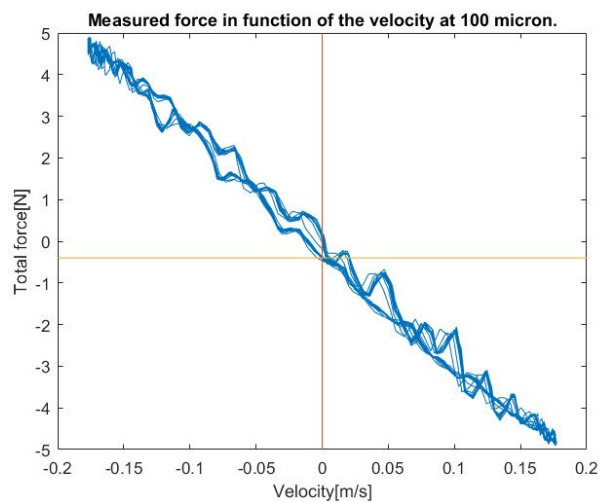


Figure D.4: The measured force in function of the velocity at 100 micron.

The test is repeated three times to minimize the measurement errors. The average value is used to determine the relation between the damping force and the height H of the gap between the plates. Table D.3 shows all the measurements of the three tests and the average values at 100 micrometer.

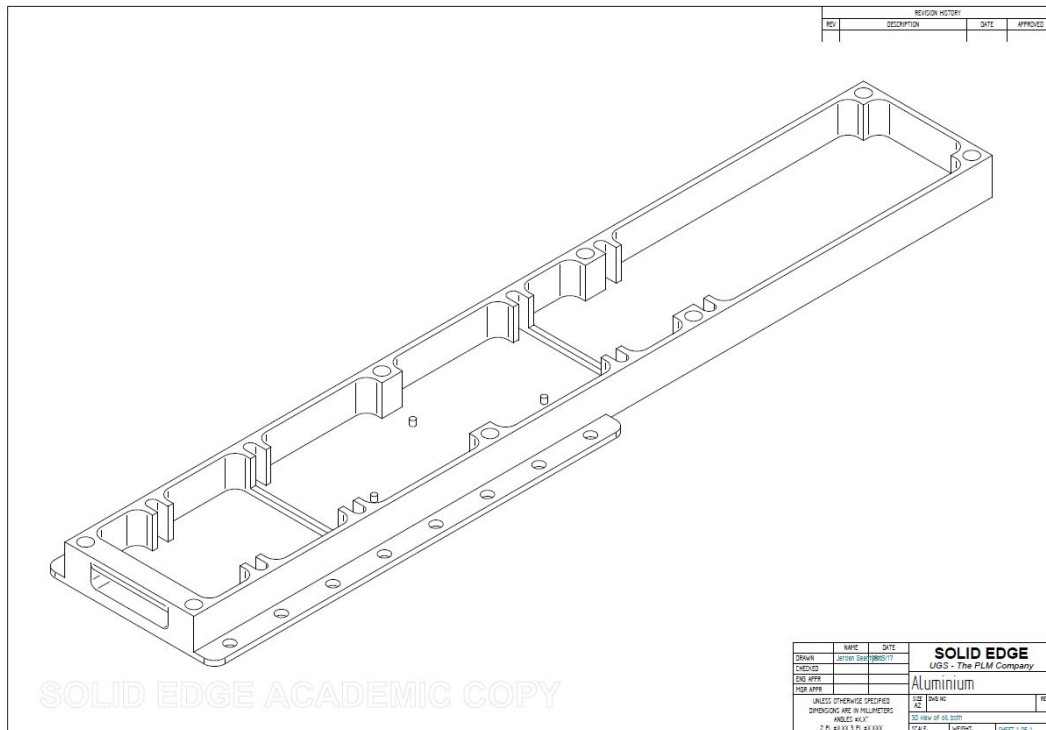
	Velocity [m/s]	Theoretical force [N]	Measured force [N]
Measurement 1	0.164	3.065	3.629
Measurement 2	0.157	2.934	3.259
Measurement 3	0.177	3.308	3.019
Average	0.166	3.102	3.302

Table D.3: Measurements of the damping force at 100 micron.

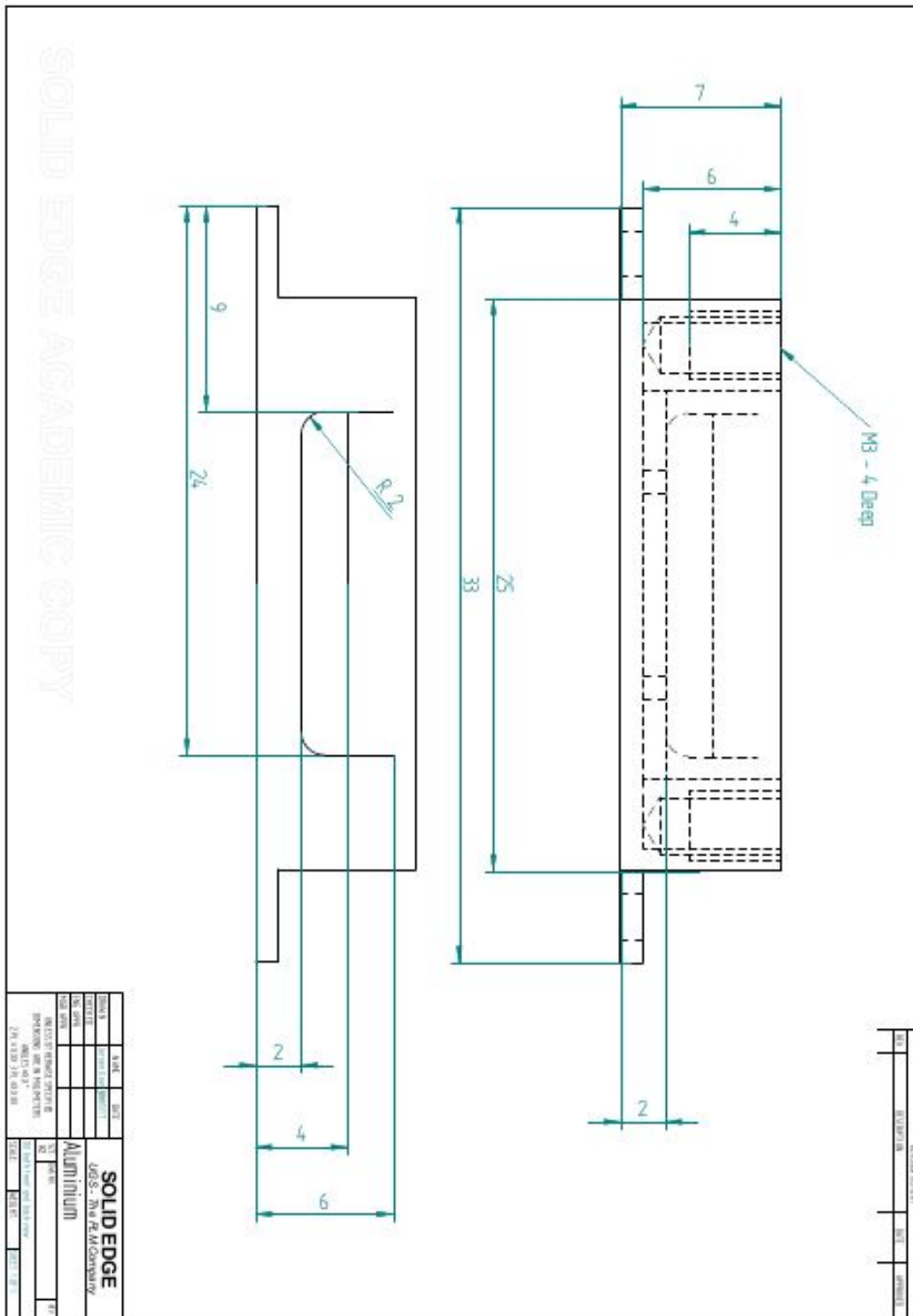
Appendix E

Technical drawings of the final damper components.

E.1 Technical drawings of the oil bath.

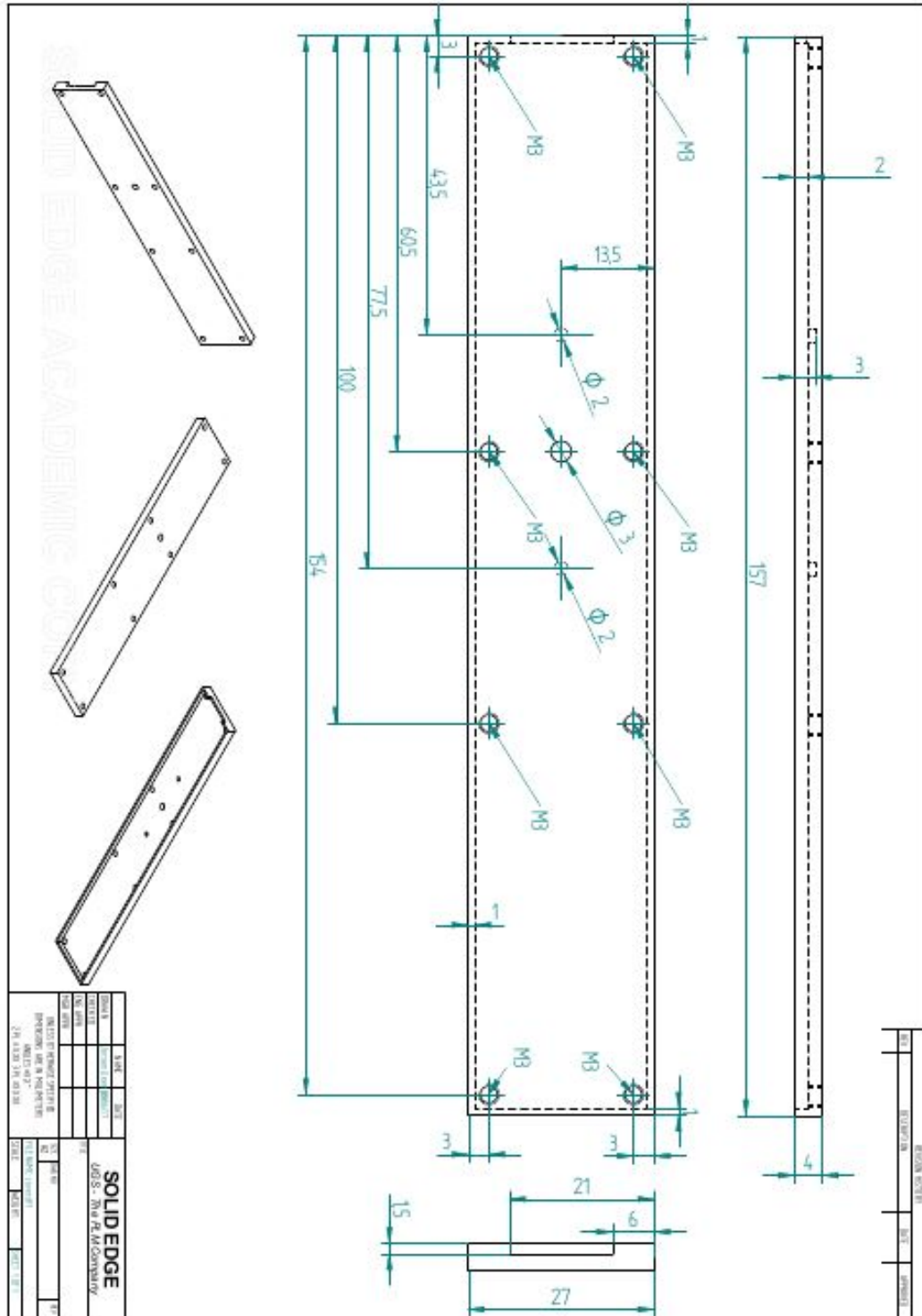


E.1. Technical drawings of the oil bath.



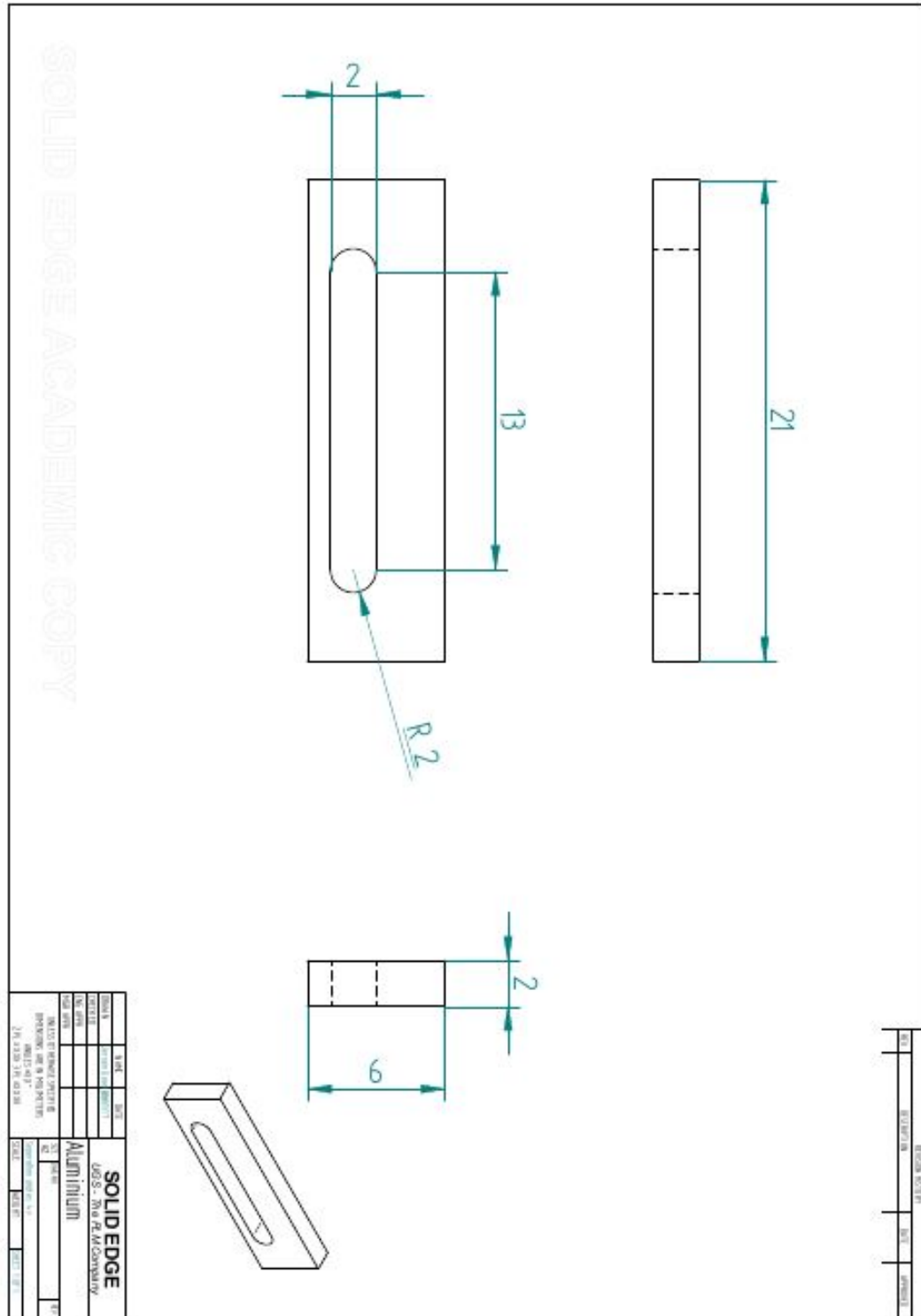
E. TECHNICAL DRAWINGS OF THE FINAL DAMPER COMPONENTS.

E.2 Technical drawing of the cover.



E. TECHNICAL DRAWINGS OF THE FINAL DAMPER COMPONENTS.

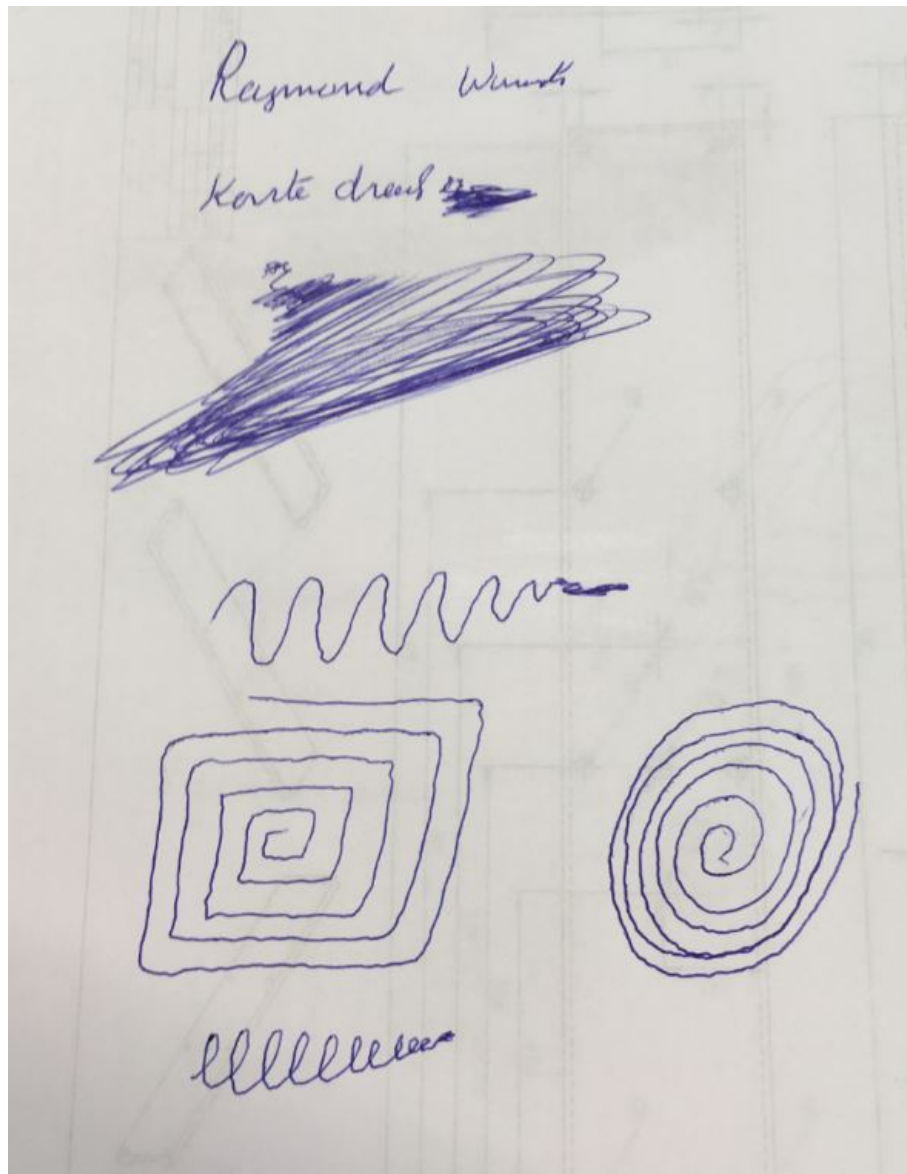
E.4 Technical drawing of the separation plate.



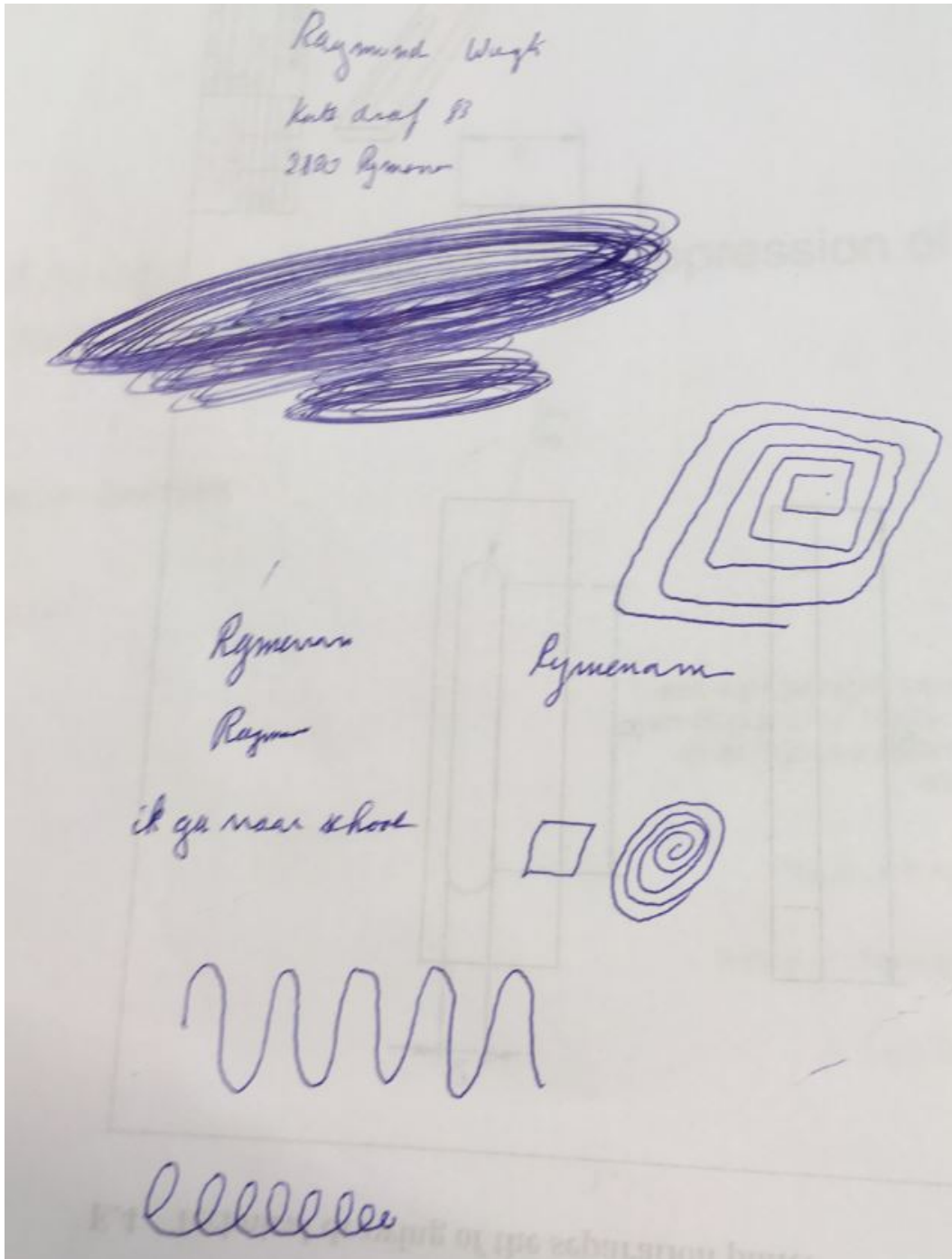
Appendix F

Testresults of the prototype

F.1 Test without the orthosis



F.2 Test with the orthosis at high damping tightened with the velcro strip



F.3 Test with the orthosis at a tuned damping without the velcro strip

